U.PORTO

MESTRADO ONCOLOGIA

ONCOLOGIA LABORATORIAL

Effects and mechanisms of action of marine-derived preussin against the triple negative breast cancer cell line MDA-MB-231 and exploiting 2D and 3D cultures

Rosária Catarino Seabra

M

2022

U.PORTO

Rosária Catarino Seabra. Effects and mechanisms of action of marine-derived preussin against the triple negative breast cancer cell line MDA-MB-231 and exploiting 2D and 3D culturesy

M.ICBAS.2022

Effects and mechanisms of action of marine-derived preussin against the triple negative breast cancer cell line MDA-MB-231 and exploiting 2D and 3D cultures

Rosária Catarino Seabra

INSTITUTO DE CIÊNCIAS BIOMÉDICAS ABEL SALAZAR

Rosária Catarino Seabra

Effects and mechanisms of action of marine-derived preussin against the triple negative breast cancer cell line MDA-MB-231 and exploiting 2D and 3D cultures

Dissertation for the master's degree in Oncology, submitted to the ICBAS - School of Medicine and Biomedical Sciences of the University of Porto

Supervisor – Eduardo Jorge Sousa da Rocha

Category – Full professor

Affiliation – ICBAS - School of Medicine and Biomedical Sciences of the University of Porto

Financial support

This research was supported by the strategic funding UIDB/04423/2020 and UIDP/04423/2020 through national funds provided by FCT – Fundação para a Ciência e Tecnologia to CIIMAR. The Master's degree of Oncology, of the ICBAS – School of Medicine and Biomedical Sciences of the University of Porto, offered additional funding.

Acknowledgments

The journey of developing a dissertation project is not always easy, but several people contributed in different ways to its result. To everyone that gave me their contribution I here express my sincere and deepest gratitude.

First and foremost, to Professor Eduardo Rocha for giving me the opportunity to work on this project, for the trust deposited in my work that allowed me to grow as a professional and as a person, for the guidance, the transmitted knowledge, and the ability to simplify and find a solution to problems that seemed impossible to solve.

To Dr. Fernanda Malhão for all the advice, suggestions, and invaluable efforts to help me in the experimental procedures or the writing of this dissertation, for the patience and support throughout this entire project, for all the knowledge and experience transmitted.

To Professor Alice Ramos, for all the guidance, the readiness to give me insight not only in the experimental procedures but also in the writing of this thesis, and for all the kind words of incentive and strength whenever I needed the most, always reminding me of the value of my work.

To Professor Anake Kijoa for providing the preussin and the insights on its chemistry.

To the team of the Department of Environmental Health of National Institute of Health Dr. Ricardo Jorge (INSA), mainly Doctor Carla Costa, for receiving me for the performance of the comet assay.

To the team of the Immunobiology Group/Host Interaction and response from the Institute for Research and Innovation in Health (i3s), namely Doctor Alexandra Correia, for receiving me and helping me in the execution of the annexin V-PI assay.

To the staff from the Department of Microscopy, especially Dr. Paula Teixeira and Doctor Célia Lopes, for the patience, the given hand whenever needed and for the companionship.

To Pedro for all the patience, support, and strength he gave me in all the moments, both the bad and the good, but most importantly, in the times when I felt too overwhelmed.

To my family for making me who I am today and for all the support. My mom, for all the caring, for always trusting in me. My sister, for all the patience and advice.

To my friends for the understanding, support, and reminder that there is more to life than work.

Declaration of honor

I hereby declare that this dissertation is from my authorship and has not been previously used in other course, or curricular unit of this, or another institution. The references to other authors (affirmations, ideas, thoughts) respect scrupulously the rules of the attribution and are properly indicated throughout the text and in the bibliographic references, according to the norms of referencing. I am aware that the practice of plagiarism and self-plagiarism constitutes an academic offense.

Abstract

Breast cancer accounts for almost one in four cases of cancers in women and represents the leading cause of mortality by cancer in this group. Triple negative breast cancer is an aggressive form of breast cancer with a poor prognosis compared to other subtypes and few therapy choices. New drugs would be particularly welcome to help treat triple negative breast cancer. Preussin is a hydroxypyrrolidine alkaloid that can be isolated from the marine sponge-associated fungi *Aspergillus candidus*. In 2D cell culture models (monolayers), this compound has already been shown to have the potential to reduce cell viability and proliferation and to induce cell death and cell cycle arrest through inhibition of cyclin E-CDK2 kinase. However, more mechanistic data is needed for preussin, and more studies are required to test the compound with *in vitro* models that better mimic the tumors *in vivo*, such as 3D cell culture models (spheroids). Here, we studied the effects of preussin in the triple negative breast cancer cell line, MDA-MB-231, comparing 2D and 3D cell cultures, using ultrastructural analysis, and the MTT, clonogenic, BrdU, annexin V-PI, comet (standard and enzymatic versions) and scratch assays, for viability, long-term survival, proliferation, cell death induction, genotoxicity, and migration analysis, respectively. For 3D cell culture, MDA-MB-231 cells were grown in ultra-low adhesion U bottom plates. We found that preussin decreased cell viability, both in 2D and 3D cell cultures, arising from the impairment of cell proliferation and cell death induction (late apoptosis/necrosis). The preussin effects translated into cellular ultrastructural alterations in 2D and 3D cell cultures. Furthermore, preussin significantly inhibited the migration of MDA-MB-231. Depending on the parameter, preussin effects started at 5 μM and consistently increased in the other concentrations tested (25 and 35 μM). Our data excluded the hypothesis that preussin has genotoxic properties. At last, no conclusions could be drawn from the effects of preussin on MDA-MB-231 long-term survival, and further optimization of the clonogenic assay will be needed. The new data expanded our knowledge of preussin properties while backing prior studies and revealing the preussin potential to be used as a scaffold for developing novel anticancer drugs.

Resumo

O cancro de mama é responsável por um em cada quatro casos de cancro nas mulheres e representa uma das principais causas de morte por cancro, também neste grupo. O cancro da mama do subtipo triplo negativo exibe um comportamento agressivo, tem em geral pior prognóstico do que outros subtipos de cancro da mama e possui poucas opções terapêuticas. O desenvolvimento de novas drogas com propriedades antitumorais representa uma mais-valia para o tratamento desta doença. A preussina é um alcalóide hidroxipirrolidina, que pode ser extraída do fungo *Aspergillus candidus*, por sua vez isolado da esponja marinha *Epipolasis sp.* Este composto já demonstrou a capacidade de reduzir a viabilidade celular e de possuir propriedades antiproliferativas, citotóxicas e de inibição da progressão do ciclo celular de forma dependente da ciclina E-CDK2 quinase, em modelos de cultura 2D. No entanto, é necessário um aprofundamento do estudo da preussina, principalmente em modelos *in vitro*, que melhor representam o comportamento do tumor *in vivo*, como as culturas celulares 3D (esferóides). No presente estudo, avaliámos os efeitos da preussina numa linha celular de cancro de mama triplo negativo (MDA-MB-231). Comparámos a utilização de métodos de cultura 2D e 3D através de análise morfológica, principalmente ao nível ultraestrutural e através dos ensaios de MTT, clonogénico, BrdU, anexina V-PI, cometa (versões alcalinas padrão e enzimática) e ensaio da ferida, para avaliação da viabilidade, sobrevivência a longo prazo, proliferação, indução de morte celular, genotoxicidade e migração, respetivamente. Para obtenção de culturas celulares 3D, cultivámos as células MDA-MB-231 em placas de baixa adesão celular com o fundo em U. Os nossos resultados demonstraram que a preussina tem capacidade de reduzir a viabilidade celular, tanto em modelos de cultura 2D como 3D, em consequência de efeitos antiproliferativos e de indução de morte celular (de necrose e apoptose tardia). Os efeitos da preussina traduziram-se também em alterações morfológicas ultraestruturais, nos dois modelos de cultura testados. A preussina demonstrou ainda a capacidade de inibir a migração celular. Dependendo do parâmetro avaliado, a preussina induziu efeitos a partir de uma concentração de 5 μM, que aumentaram consistentemente nas restantes concentrações testadas (25 e 35 μM). Os nossos dados excluíram a hipótese de indução de genotoxicidade pela preussina. Por fim, não foi possível concluir quais os efeitos da preussina na sobrevivência a longo prazo (pelo ensaio clonogénico), pelo que será necessária a otimização do protocolo. Os novos dados permitiram expandir o nosso conhecimento sobre as propriedades da preussina e simultaneamente corroborar estudos anteriores. Este estudo permitiu assim revelar o potencial da preussina como um modelo para o desenvolvimento de novas drogas com propriedades antitumorais.

Index

Acknowledgments iii

Declaration of honor iv

Abstract v

Resumo vi

Index vii

List of figures x

Abbreviations list xvi

Introduction 1

1. Cancer 1

2. Breast cancer 2

2.1. Epidemiology – incidence, and mortality – sex-specific 2

2.2. Risk factors for breast cancer 4

2.3. Characterization of breast cancer 5

2.4. Triple negative breast cancer 8

3. Potential sources of natural compounds with anti-cancer properties 11

3.1. Fungi 13

3.2. Marine environment as a source of new compounds 14

3.3. Preussin 16

3.4. Development of cancer drugs derived from natural products 18

4. *In vitro* models for investigation and development of anticancer drugs 20

4.1. 2D cell culture 20

4.2. 3D cell culture 21

Objectives 23

Material and Methods 24

1. Cell culture 24

1.1. Subculturing conditions 24

1.2. Trypan blue exclusion assay and determination of cell density 25

1.3. Thawing of frozen cells 25

2. Chemicals and reagents 25
2.1. Stock solutions 26
3. Multicellular aggregates (MCAs) 26
3.1. MCAs obtention 26
3.2. MCAs disaggregation 27
4. Viability assay - MTT assay 27
4.1. MTT in monolayer cell culture 28
4.2. MTT in MCAs 28
5. Clonogenic survival assay 29
5.1. Clonogenic assay in monolayer cell culture 30
5.2. Clonogenic assay in MCAs cell culture 31
6. *In vitro* scratch assay 31
7. Proliferation assay – 5′-bromo-2′-deoxyuridine (BrdU) assay 32
7.1. BrdU assay in monolayer cell culture 33
7.2. BrdU assay in MCAs cell culture 34
8. Comet assay 34
8.1. Single-cell gel electrophoresis 34
8.2. Detection of FPG-sensitive sites 37
9. Annexin V - PI assay 38
10. Morphological analysis 40
10.1. Phase-contrast microscopy and stereomicroscopy 40
10.2. Electron microscopy 40
11. Statistical analysis 41
Results 43
1. Assessment of cell viability – MTT assay 43
1.1. Monolayer cell culture 43
1.2. MCAs 44
2. Analysis of long-term survival – clonogenic assay 45
3. Effects on cell proliferation – 5′-bromo-2′-deoxyuridine (BrdU) assay 48

4. Analysis of cell migration – *In vitro* scratch assay....49
5. Detection of DNA damages – Comet assay....52
6. Induction of apoptosis - Annexin V - PI assay....58
7. Effects on cell morphology....61
7.1. Phase-contrast microscopy and stereomicroscopy....61
7.2. Transmission electron microscopy....64
Discussion....72
Bibliography....86

List of figures

Figure 1 – Estimated number of (**a**) new cancer cases and (**b**) deaths by cancer in both sexes, in 2020, worldwide, and of all ages. Source: GLOBOCAN 2020. Graph Production: Global Cancer Observatory (Ferlay et al., 2020). 2

Figure 2 – Estimated number of (**a**) new cancer cases and (**b**) deaths by cancer in women, in 2020, worldwide, and at all ages. Source: GLOBOCAN 2020. Graph Production: Global Cancer Observatory (Ferlay et al., 2020). 2

Figure 3 – Estimated age-standardized incidence rates of BC in women of all ages in 2020. Source: GLOBOCAN 2020. Graph Production: Global Cancer Observatory (Ferlay et al., 2020).....3

Figure 4 – Chemical structure of (+) – preussin (Buttachon et al., 2018). 16

Figure 5 – Chemical structure of C preussin (Buttachon et al., 2018). 18

Figure 6 – Effects of preussin on cell viability of MDA-MB-231 cells in monolayer cell culture assessed by the MTT assay after 24 h (**a**), 48 h (**b**), or 72 h (**c**) of exposure. Negative control (C) (cells in cell culture medium), solvent control (0 μM of preussin and 0.1% of DMSO), and positive control (cells exposed to 1 μM of Dox) groups were included. The results are expressed as the percentage of cell viability relative to the negative control and are expressed as mean ± SD of n=5. Significant differences, represented with asterisks (* p<0.05; ** p<0.01; **** p<0.0001) were tested by one-way ANOVA, followed by post-hoc Holm-Sidak's multiple comparison test. 44

Figure 7 – Effects of preussin on cell viability in MDA-MB-231 cells, cultured as MCAs, assessed by the MTT assay after 96. Negative control (C) (cells in cell culture medium), solvent control (0 μM of preussin and 0.1% of DMSO), and positive control (cells exposed to 5 μM of Dox) groups were included. The results are expressed as the percentage of cell viability relative to the negative control and are expressed as mean ± SD of n=5. Significant differences, represented with asterisks (* p<0.05; ** p<0.01; **** p<0.0001) were tested by one-way ANOVA, followed by post-hoc Holm-Sidak's multiple comparison test).....45

Figure 8 – Representative images of the colony types obtained for the MDA-MB-231 cell line in the clonogenic assay. Small colonies and composed of densely packed round-like to spindle-shaped cells cells (**a**), Colonies of high diameter, irregularly shaped, with slender cells (**b**), and mixed colonies with spindle-shaped slender cells and round-like to spindle-shaped cells (**c**). After exposure (for 72 h in monolayer cell culture or 96 h in MCAs), 500

viable cells were incubated for 21 days in 6-well plates, for colony formation. The obtained colonies were later stained with crystal violet. Colonies were considered only when composed of 50 cells or more.....46

Figure 9 – Representative effects of preussin on colony formation capability on the MDA-MB-231 cell line, accessed through the clonogenic assay. Cells exposed to preussin in the 2D cell culture model (**a**) or in the 3D cell culture model (**b**). 500 viable cells were re-seeded in 6 well culture plates for 21 days. Colonies were stained with crystal violet, counted (colonies with 50 or more cells), and photographed in an inverted phase-contrast microscope. Cells exposed only to the cell culture medium and to 0.1% of (v/v) of DMSO were added as negative and solvent controls, respectively. Additionally, positive control of 1 μM of Dox in monolayer cell culture (**a**) or 5 μM of Dox in MCAs (**b**), was added. The counted colonies are encircled in orange. 47

Figure 10 – Effects of preussin on long-term survival of MDA-MB-231 cells, cultured in 2D or 3D cell culture models, assessed by the clonogenic assay. After 72 h (monolayer cell culture) or 96 h (MCAs) of exposure, 500 cells were seeded in 6 well plates and incubated for 21 days. Negative control (C) (cells in cell culture medium), and solvent control (0 μM of preussin and 0.1% of DMSO) were included. The results are expressed as the percentage of surviving fraction relative to the negative control and are expressed as mean ± SD of n=5.....48

Figure 11 – Effects of preussin on cell proliferation of MDA-MB-231 cells, cultured as a monolayer and exposed for 72 h (**a**) or cultured as MCAs and exposed for 96 h (**b**), assessed by the BrdU assay. Negative control (C) (cells in cell culture medium), solvent control (0 μM of preussin and 0.1% of DMSO), and positive control (cells exposed to 1 μM (2D cell culture) or 5 μM (3D cell culture models) groups were included. The results are presented as the percentage of cell proliferation relative to the negative control and are expressed as mean ± SD of n=5. Significant differences, represented with asterisks (* $p<0.05$; ** $p<0.01$; *** $p<0.001$; **** $p<0.0001$) were evaluated by one-way ANOVA, followed by post-hoc Holm-Sidak's multiple comparison test. 49

Figure 12 – Representative effects of preussin at 35 or 50 μM on cell migration, accessed through the *in vitro* scratch assay. Cells were seeded in a monolayer with high density, serum-starved for 6 h, scratched with a 100 μl micropipette tip, and exposed to the compounds in culture medium supplemented with 1% FBS. The scratches were photographed in an inverted phase-contrast microscope at 0 h, 24 h, and 48 h of exposure. The cells' front of migration is marked with orange lines. As solvent control, cells were exposed to culture medium with 1% FBS and 0.1% of (v/v) of DMSO. 50

Figure 13 – Representative effects of preussin at 5, 15, and 25 μM on cell migration accessed through the *in vitro* scratch assay. Cells were seeded in a monolayer at a high density, serum-starved for 6 h, scratched, and exposed to the compounds in culture medium supplemented with 1% FBS. The scratches were photographed in an inverted phase-contrast microscope at 0 h, 24 h, 48 h, and 72 h of exposure. The cells' front of migration is marked with orange lines. As solvent control, cells were exposed to culture medium with 1% FBS and 0.1% of (v/v) of DMSO.....51

Figure 14 – Effects of preussin on cell migration of MDA-MB-231 cells cultured as a monolayer, after 24 h (**a**), 48 h (**b**), or 96 h (**c**) of exposure, accessed through the *in vitro* scratch assay. Negative control (C) (cells in DMEM supplemented with 1 % FBS), solvent control (0 μM of preussin and 0.1% of DMSO), and intern control (IC) (cells exposed to DMEM supplemented with 10 % FBS). The results are expressed as the percentage of cell migration and are expressed as mean ± SD of n=5 (three replicates per experiment). Significant differences, represented with asterisks (* $p<0.05$; ** $p<0.01$; *** $p<0.001$) were evaluated by one-way ANOVA, followed by post-hoc Holm-Sidak's multiple comparison test. 52

Figure 15 – Effects of preussin on cell viability in MDA-MB-231 cells, cultured as MCAs, assessed by the MTT assay after 24 h. Negative control (C) (cells in cell culture medium), solvent control (0 μM of preussin and 0.1% of DMSO), and positive control (cells exposed to 5 μM of Dox) groups were included. The results are expressed as the percentage of cell viability, relative to the negative control, and are expressed as mean ± SD of n=5. 53

Figure 16 – Effects of preussin at 25 and 35 μM on cell viability of MDA-MB-231 cells cultured in 2D (**a** and **b**) or 3D (**c** and **d**) cell culture model after 2 h (**a** and **c**) or 24 h (**b** and **d**) of exposure. Cell viability was accessed through the trypan blue exclusion assay using an automated cell counter CountessTM. Negative control (C) with cells in culture medium, solvent control (0 μM of preussin and 0.1% of DMSO) of cells exposed to 0.1% (v/v) of DMSO, and positive control for the enzymatic version of comet assay with cells exposed to 4.5 mM of $KBrO_3$, groups were included. The results are expressed as mean ± SD of the percentage of cell viability from n=5. 54

Figure 17 – Representative images of the analysis of comets from MDA-MB-231 cells, using the Comet Assay IV™ software. The blue line indicates the beginning of the head, the green line represents the middle of the head, and the pink line shows the end of the comet's tail. Comets with low levels of DNA damage, with the DNA distributed in a rounded shape, with no or a small tail, a nucleoid (**a**). Comets with higher levels of DNA damage, with a well-defined head and a tail constituted of damaged DNA (**b**). 54

Figure 18 – Representative images of the standard version of comet assay in MDA-MB-231 cells treated with preussin at 25 μM or 35 μM, after 24 h of exposure, either cultured in a 2D or 3D cell culture model. As solvent control, cells were exposed to 0.1% of (v/v) of DMSO and for the positive control, nucleoids from a negative control group were exposed to 50 μM of H_2O_2. Samples were analyzed with the Comet Assay IV™. 55

Figure 19 – Genotoxic effects (induction of strand breaks) of preussin at 25 and 35 μM on MDA-MB-231 cells cultured in a 2D cell culture model, after 2 h (**a**) or 24 h (**b**) of exposure or cultured in a 3D cell culture model and exposed for 2 h (**c**) or 24 h (**d**), measured through the standard version of the comet assay. Negative control (C) with cells exposed only to the cell culture medium, solvent control (0 μM of preussin) of cells exposed to 0.1% (v/v) of DMSO, and positive control of nucleoids exposed to 50 μM of H_2O_2 in PBS, groups were selected. The results were measured as the percentage of DNA in the comet's tail. The results are expressed as mean ± SD of n=5 (from 50 comets per gel and 2 gels per condition). Significant differences from the negative control group, represented with asterisks **** p<0.0001) were evaluated by one-way ANOVA, followed by post-hoc Holm-Sidak's multiple comparison test. 56

Figure 20 – Representative images of the enzymatic version of the SCGE assay, using the FPG enzyme, in MDA-MB-231 cells treated with preussin at 25 μM or 35 μM, after 24 h of exposure, cultured in a 2D or 3D cell culture model. As SC, cells were exposed to 0.1% (v/v) of DMSO, and for the positive control, nucleoids from a negative control group were exposed to 4.5 mM of $KBrO_3$. Samples were analyzed with the Comet Assay IV™. 57

Figure 21 – Genotoxic effects (FPG sensitive sites) of preussin at 25 and 35 μM on MDA-MB-231 cells cultured in a 2D cell culture model after 2 h (**a**) or 24 h (**b**) of exposure or cultured in a 3D cell culture model and exposed for 2 h (**c**) or 24 h (**d**). Negative control (C) (cells exposed only to cell culture medium), solvent control (0 μM of preussin) (cells exposed to 0.1% (v/v) DMSO), and positive control (cells exposed for 1 h to 4.5 mM of $KBrO_3$), groups were selected. The results were measured as the percentage of DNA in the tail of the comet and calculated by subtracting the percentage of DNA damage from the non-FPG enzyme-treated samples from the FPG enzyme-treated samples. The results are expressed as mean ± SD of n=5 (from 50 comets per gel and 2 gels per condition). Significant differences, represented with asterisks **** p<0.0001) were evaluated by one-way ANOVA, followed by post-hoc Holm-Sidak's multiple comparison test. 57

Figure 22 – Representative images of flow cytometry gating strategy used in the Annexin V-FITC/PI double staining of MDA-MB-231 cells, cultured in 3D and 2D cell culture models, to evaluate the induction of early apoptosis and late apoptosis/necrosis. Gating for the

isolation of MDA-MB-231 cells and exclusion of cellular debris (**a**), and for selecting single cells and excluding aggregated cells (**b**). The gated cells were distinguished based on the PI/Annexin V staining: Q1 + Q2 (Annexin$^{+ \text{ or } -}$/ PI^{+}) represented the cells in necrosis/late apoptosis; Q3 (Annexin^{+}/ PI^{-}) represented the cells in early apoptosis; Q4 (Annexin^{-}/ PI) represented the living cells (**c**). SCC: side-scattered light; FSC: forward-scattered light; H: height; A: area; PI: propidium iodide.....58

Figure 23 – Effects of preussin at 25 and 35 μM, in the induction of cell death (late apoptosis/necrosis), and early apoptosis, on MDA-MB-231 cells cultured in 2D (**a**) or 3D (**b**) cell culture models, respectively exposed for 72 h or 96 h. Early apoptosis, and late apoptosis/necrosis induction, were accessed by Annexin V-FITC/PI double staining followed by flow cytometry and analysis with the FlowJo™ software. Negative control (C) with cells exposed only to cell culture medium), solvent control (Preussin at 0 μM) of cells exposed to 0.1% (v/v) DMSO, and positive control where cells were exposed to Dox (at 1 μM in 2D cell culture and 5 μM in 3D cell culture) groups were added. The results were measured as the percentage of cells in each stage, either alive, in early apoptosis, or in late apoptosis/necrosis. The results are expressed as mean ± SD of n=5. Differences in comparison with the negative control group, in each cell state, were evaluated by one-way ANOVA, followed by post-hoc Holm-Sidak's multiple comparison test (in the early apoptotic and late apoptotic/necrotic cells groups) or Brown-Forsythe and Welch ANOVA tests (in the alive cells groups). Statistically significant differences are represented with asterisks (* $p<0.05$; ** $p<0.01$; **** $p<0.0001$).....60

Figure 24 – Representative effects of preussin on cell morphology, in cells cultured in a monolayer cell culture model, and photographed in an inverted phase-contrast microscope. Cells were exposed to preussin at 5, 15, 25, 35, or 50 μM, during 24, 48 h, and 72 h. Cells exposed only to cell culture medium, to 0.1% of DMSO or 1 μM of Dox, were included as negative, solvent, and positive control groups, respectively.....62

Figure 25 – Schematic representation of the shape of the MDA-MB-231 cell line obtained MCAs.....63

Figure 26 – Representative effects of preussin on MCAs morphology and photographed in the dark field of a stereomicroscope. MCAs were exposed to preussin at 5, 15, 25, 35, or 50 μM, for 96 h. Cells exposed only to cell culture medium, to 0.1% of DMSO or 5 μM of Dox, were included as negative, solvent, and positive control groups, respectively. 63

Figure 27 – Representative images of TEM analysis of MDA-MB-231 cells cultured as a monolayer. Cells were exposed for 72 h only to DMEM, in the negative control (**a** and **b**), or

to 0.1 % (v/v) DMSO, in the solvent control (**c** and **d**). Black arrowheads: membranes blebs; White arrowheads: slender finger-like structures; C: dilated cisternae; Ld: lipid droplets; Mb: multivesicular bodies; Mi: mitochondria; N: nucleus; Nu: nucleolus; ReR: rough endoplasmic reticulum; Vc: vesicles. 65

Figure 28 – Representative images of TEM analysis of preussin exposed MDA-MB-231 cells cultured as a monolayer. Cells were exposed for 72 h to several preussin concentrations: 5 μM (**a**), 15 μM (**b** and **c**), 25 μM (**d**), and 35 μM (**e** and **f**). Black arrowheads: membranes blebs; White arrowheads: slender finger-like structures; C: dilated cisternae; Dv: degenerative vesicles; Ld: lipid droplets; Mb: multivesicular bodies; Mdb: multivesicular electron-dense bodies; Mi: mitochondria; N: nucleus; ReR: rough endoplasmic reticulum; Vc: vesicles. 66

Figure 29 – Representative images of semithin sections (**a**, **b**, and **c**) and TEM (**d**, **e**, **f**, and **g**) analysis of MDA-MB-231 MCAs. The MCAs were exposed for 96 h only to DMEM in the negative control (**a** - **e**), or to 0.1 % (v/v) DMSO, in the solvent control group (**f** and **g**). Asterisk: electron-dense amorph material; black arrows: electron-dense slightly granular material; black arrowheads: membranes blebs; white arrowheads: finger-like structures; Ld: lipid droplets; Lu: lumen-like structures; Mdb: multivesicular dense bodies; Mi: mitochondria; N: nucleus; Nec: necro-apoptotic core NC: necrotic cells; Nu: nucleolus; ReR: rough endoplasmic reticulum; Vc: vesicles. 68

Figure 30 – Representative images of TEM analysis of preussin-exposed MDA-MB-231 MCAs. The MCAs were exposed for 96 h to preussin at a concentration of: 5 μM (**a**), 15 μM (**b**), 25 μM (**c** and **d**), and 35 μM (**e** and **f**). Asterisk: electron-dense amorph material; black arrows: electron-dense, slightly granular material; black arrowheads: membranes blebs; white arrowheads: microvilli-like structures; Dv: degenerative vesicles; G: Golgi complex; Ld: lipid droplets; Lu: lumen-like structures; Mb: multivesicular bodies; Mdb: multivesicular dense bodies; Mi: mitochondria; N: nucleus; Nc: necrotic cells; Nu: nucleolus; Vc: vesicles. 70

Abbreviations list

%tDNA – Percentage of DNA in the comet tail

2D – Two dimensional

3D – Three dimensional

A – Absorbance

ATCC – American Tissue Culture Collection

AP – Apurinic or apyrimidinic

BSA – Bovine serum albumin

BC – Breast cancer

BrdU – 5′-bromo-2′-deoxyuridine

CDK2 – Cyclin dependent kinase 2

Cells % – Percentage of cells

Dox – Doxorubicin

DMEM – Dulbecco's Modified Eagle Medium

DMSO – Dimethyl sulfoxide

ECM – Extracellular matrix

EDTA – Ethylenediamine tetraacetic acid

EGFR – Epidermal growth factor receptor

EMA – European Medicines Agency

ER – Estrogen receptor

FDA – Food and Drug Administration

FBS – Fetal Bovine Serum

FPG – Formamidopyrimidine DNA Glycosylase

H_2O_2 – Hydrogen peroxide

HER2 – Human epidermal growth factor receptor 2

IC_{50} – Half-maximal inhibitory concentration

IHC – Immunohistochemistry

$KBrO_3$ – Potassium bromate

MCA – Multicellular aggregates

ML – HDI – Medium and low human development index

MTT – 3-(4,5-dimethylthiazol-2-yl)-2,5-diphenyltetrazolium bromide

n=5 – Five independent experiments

NMR – Nuclear magnetic resonance

NP – Natural product

P53 – Protein 53

PBS – Phosphate-buffered saline

PD-1 – Programmed death 1

PD-L1 – Programmed death ligand 1

Pen/strep – Penicillin/streptomycin

PGR – Progesterone receptor

PI – Propidium iodide

SCGE – Single-cell gel electrophoresis

SD – Standard deviation

TNBC – Triple negative breast cancer

TE – Tris-EDTA

USA – United States of America

VH-HDI – Very high and high human development index

Introduction

1. Cancer

Almost one and half decades before, it was estimated that by 2020 the number of new cancer cases worldwide would reach 16.5 million per year (Bray & Møller, 2006). In fact, according to data from GLOBOCAN, in 2020, this number was higher than predicted, with approximately 19.3 million new cases of cancer diagnosed worldwide (10.1 million in men and 9.2 million in women). Cancer represents one of the leading causes of mortality, accounting for almost 10 million deaths in 2020 (5.5 million deaths in males and 4.4 million in females). Both the number of new cancer patients and cancer-related deaths were higher in men than in women. Asia is estimated to account for most cancer cases and related deaths worldwide, with 49.3% and 58,3% of cases, respectively. In turn, Europe is the second continent with higher incidence and mortality associated with cancer, representing 22.8% of cancer cases and 19.6% of cancer-related deaths worldwide. It is important to mention that the incidence and cancer-associated mortality may be partially explained by the difference in population distribution, which is much greater in Asia, accounting for 59.5% of the worldwide population. In contrast, Europe only represents 9.7% of the population. Furthermore, in the American continent, the total cancer cases and deaths represent 20.9% and 14.2%, respectively, while Africa has an incidence of 5.7% and a mortality of 7.2% (Ferlay et al., 2020).

In 2020, it was estimated by GLOBOCAN 2020 that breast cancer (BC) was the most incident type of cancer, followed by lung cancer, with over 2 million diagnosed new cases of cancer worldwide (Figure 1a). Colorectum, prostate, and stomach cancers were the following most common types of cancer, with more than 1 million new cases each (Figure 1a). As for mortality, in 2020, GLOBOCAN estimated that the types of cancer with the highest mortality rates were, first, lung, with more than 1.5 million deaths, followed by colorectum, liver, stomach, and BC (Figure 1b) (Ferlay et al., 2020; Sung et al., 2021).

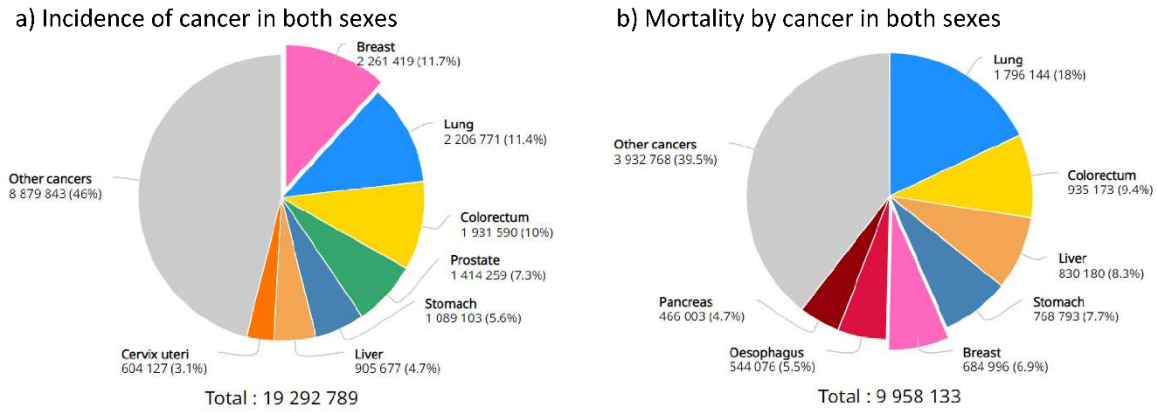

Figure 1 – Estimated number of (**a**) new cancer cases and (**b**) deaths by cancer in both sexes, in 2020, worldwide, and of all ages. Source: GLOBOCAN 2020. Graph Production: Global Cancer Observatory (Ferlay et al., 2020).

2. Breast cancer

2.1. Epidemiology – incidence, and mortality – sex-specific

BC represents the type of cancer with the highest incidence in both sexes. Nonetheless, this occurs because BC accounts for the most diagnosed type of cancer in women worldwide, representing approximately 99% of all cases, accounting for almost one in four cases of cancer in women (Figure 2a) (Konduri et al., 2020; Miranda et al., 2021; Siegel et al., 2018).

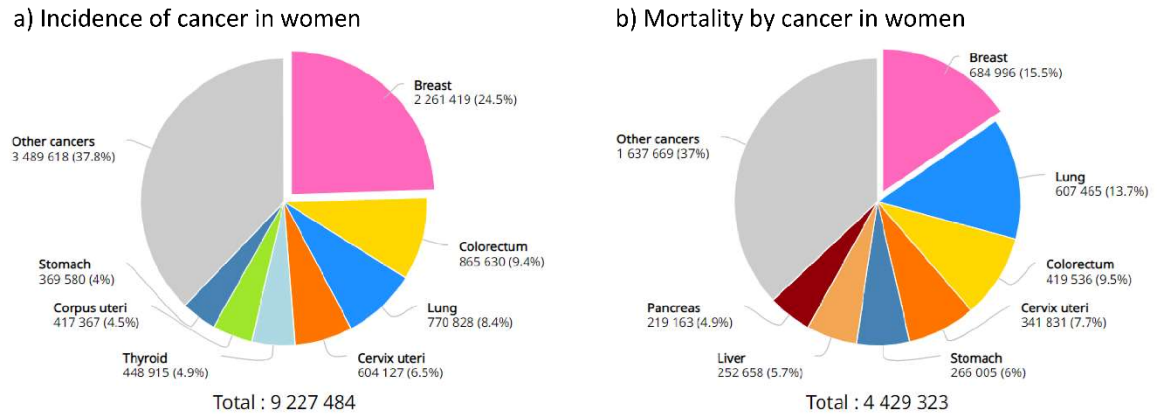

Figure 2 – Estimated number of (**a**) new cancer cases and (**b**) deaths by cancer in women, in 2020, worldwide, and at all ages. Source: GLOBOCAN 2020. Graph Production: Global Cancer Observatory (Ferlay et al., 2020).

Incidence of BC varies based, not only on sex, but also on age, racial, ethnic, geographic levels, and socioeconomic status. The incidence rates of BC differ according to the country's income. In low and middle-income countries, the incidence of BC was similar for pre-

and postmenopausal women. In high-income countries, BC incidence was higher in postmenopausal women (Heer et al., 2020). Furthermore, the age-specific incidence rate pattern of BC varies with the molecular pattern of BC. Estrogen receptor (ER) positive and human epidermal growth factor receptor 2 (HER2) negative BC has its peak incidence in women between 75 and 79 years old. In triple negative BC (TNBC), the incidence peak occurs before the age of 70. As for the HER2-positive BCs, the incidence rates vary less abruptly compared to BC with different molecular patterns (Brinton et al., 2018; Howlader et al., 2014).

BC represents the first or second type of cancer with higher incidence in women, in almost every country. Nonetheless, cancer incidence rates largely vary among regions, being greater in Australia, North America, and northern and western Europe, and lower in almost all the countries of the African and Asian continents (Figure 3). Additionally, the incidence of BC is substantially higher in countries with very high and high human development index (VH-HDI), than in countries with medium and low human development index (ML-HDI) countries (Lei et al., 2021; Sung et al., 2021). In VH-HDI countries, BC is more frequently diagnosed at earlier stages of the disease (stage I or II). The high registry of BC cases may be attributed to the increased detection through BC screening programs. Failure to have a screening system results in underdiagnosis. Nonetheless, the higher registry of BC cases may also be associated with higher exposure to risk factors related to lifestyle, women's reproductive history (including lower fertility), menopausal hormone therapy and oral contraceptives intake, as well as population growth and aging (Lei et al., 2021; Sung et al., 2021; Torre et al., 2017). ML-HDI countries have a lower incidence of BC than VH-HDI countries, but it is diagnosed in the later stages of the disease (stage III or IV) (Sung et al., 2021; Torre et al., 2017).

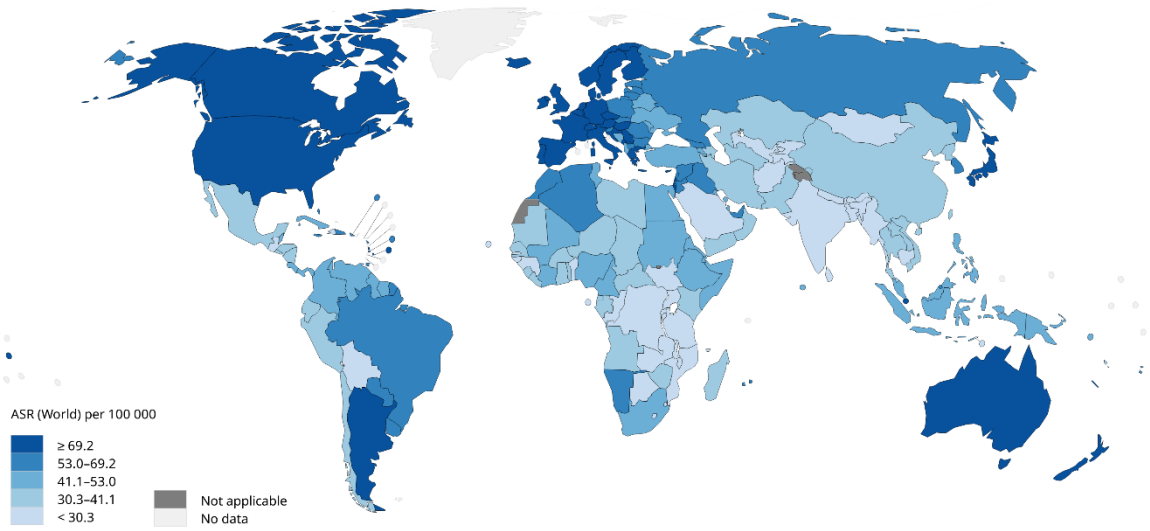

Figure 3 – Estimated age-standardized incidence rates of BC in women of all ages in 2020. Source: GLOBOCAN 2020. Graph Production: Global Cancer Observatory (Ferlay et al., 2020).

BC only represents the fifth cancer with higher mortality in both sexes. Still, it is the leading cause of mortality by cancer in women, accounting for almost 685 thousand deaths worldwide, in this group (Figure 2b) (Ferlay et al., 2020). Despite the higher incidence rates of BC in women from VH-HDI countries, mortality rates in women from ML-HDI countries are higher (Lei et al., 2021; Sung et al., 2021). The higher mortality rates may be associated with the later stages of diagnosis of BC tumors but also limited access to treatment (Brinton et al., 2014; Sung et al., 2021; Torre et al., 2017).

A decrease in BC mortality rates have been observed in developed countries since the late 80s and early 90 (Siegel et al., 2022; Wojtyla et al., 2021). But disparities in BC's incidence and mortality rates from different racial, socioeconomic, and geographic groups still arise, even within the same country. In the United States of America (USA), black women have around 41% higher mortality associated with BC, than white women, even though incidence rates of BC are slightly higher (about 4%) in the latter group (Siegel et al., 2022).

2.2. Risk factors for breast cancer

BC is a multifactorial disease with several known modifiable and non-modifiable risk factors. One of the main non-modifiable risk factors is genetic sex. As already described, BC occurs predominantly in women while extremely rare in men. This difference in incidence based on sex appears as a consequence of breast cell stimulation by sex hormones, namely via ER and progesterone receptor (PGR) in women (Łukasiewicz et al., 2021).

Age is also a non-modifiable risk factor, with BC incidence rates varying in a different pattern in women above or below 50 years old, with a greater risk of developing BC at older ages. Indeed, most of the cases, over 75%, occur after the age of 50. Furthermore, the BC incidence rates pattern varies with age, being associated mainly with menopausal status and, consequently, hormonal status (Brinton et al., 2018; Howlader et al., 2014; Łukasiewicz et al., 2021).

Race also represents a non-modifiable risk factor, dependent on the BC subtype. White women show a higher incidence of BC than women from other races. In its turn, black women show a higher incidence of the TNBC cancer subtype (Howlader et al., 2014)

BC incidence is also affected by reproductive factors. Between these, it is possible to mention the menstrual cycle where early menarche and late age at menopause are associated with higher risk. Furthermore, women who underwent bilateral oophorectomy show a decreased risk. As to the reproductive history, nullipara women and the late age of first birth

are associated with a higher risk. In its turn, breastfeeding is associated with a decrease in the risk of developing BC. The exogenous hormone intake represents an additional modifiable risk, including hormonal birth control, and more markedly, menopausal hormone therapy which displays an accepted known risk due the estrogen-progestin intake (Lei et al., 2021; Sung et al., 2021; Torre et al., 2017).

Other modifiable risk factors such as lifestyle patterns, physical inactivity, higher body mass index, exposure to ionizing radiation, and non-modifiable risk factors, including personal history of previous BC and higher mammographic density, also represent relevant risk factors for the development of BC. Family history of BC also represents a significant risk factor with an increased risk inversely correlated with the age of the diagnosed family member (higher risk at younger ages) and positively associated with the number of affected relatives and the existence of bilateral disease (Brinton et al., 2018).

Another highly relevant risk factor is genetic susceptibility due to germline mutations, mainly in high penetrance genes but also in medium and low penetrance genes. BRCA1 and BRCA2 gene mutations are the main mutations that confer an elevated risk for BC (Antoniou et al., 2003; Mavaddat et al., 2013; Thompson, 2002). Other high penetrance genes associated with several syndromes are also described in BC, including protein 53 (P53) gene mutation in Li-Fraumeni syndrome, PTEN gene mutation in Cowden syndrome, STK11 gene mutation in Peutz-Jeghers syndrome, CDH1 gene mutation in Hereditary Diffuse Gastric Cancer syndrome(Børresen-Dale & Anne-Lise, 2003; Fusco et al., 2020; Kaurah et al., 2002; Mcgarrity et al., 2001). Germline mutations in moderate to low penetrance genes such as PALB2 gene mutation associated with Fanconi anemia syndrome, ATM gene mutation associated with ataxia-telangiectasia, the CHEK2, and BARD1 gene mutations, among others, correlate with a moderate risk of BC development (Cybulski et al., 2011; Gatti et al., 1999; Hu et al., 2020; Weber-Lassalle et al., 2019; Yang et al., 2020).

2.3. Characterization of breast cancer

BC has a large molecular and histologic heterogeneity, with varying biological and morphologic characteristics. These features translate into different clinical behavior and response to treatments. Traditionally, BC diagnosis is based on the histologic characteristics and the tumor, lymph node, and metastasis (TNM) stages. The histological analysis comprises the pathological growth pattern (either the tumor cell type, architectural characteristic, secretion, and immunohistochemical profile), histologic differentiation, and the immunophenotype

(based on the expression of ER, progesterone receptor (PGR), and HER2 gene amplification). In its turn, the TNM classification evaluates the tumor size, nodal status, and the existence of distant metastasis (Cardoso et al., 2019; Łukasiewicz et al., 2021).

BC can also be characterized based on its molecular characteristics. According to the molecular profile, BC can be classified into four main accepted intrinsic subtypes, luminal A, luminal B, HER2-enriched, and basal-like (Cardoso et al., 2019; Perou et al., 2000). These BC intrinsic subtypes allow for substantial prognostic information in the outcome and behavior of the disease but also aid in therapeutic decisions on whether the patients will benefit or not from a certain therapy. The classification of BC into intrinsic subtypes, through the usage of molecular techniques, gives more precise information on the prognosis and predictive behavior of the tumor (Caan et al., 2014; Ohnstad et al., 2017; Parker et al., 2009; Prat et al., 2015, 2021). Nonetheless, in clinical practice, the European Society for Medical Oncology recommends the classification of BC into surrogate intrinsic BC subtypes: Luminal A-like, Luminal B-like (either HER2 positive or negative), HER2 positive (non-luminal), and TNBCs, comparable to the luminal A, luminal B, HER2-enriched and basal-like BC intrinsic subtypes, respectively (Table 1) (Allison et al., 2019; Cardoso et al., 2019). Besides the four major described subtypes in the latest WHO classification of BC, two other minor subtypes, such as the normal breast-like (that arises as a controversial subtype) and the claudin-low, have also been distinguished (Allison et al., 2019; Badve et al., 2011; Tang & Tse, 2016; Weigelt et al., 2010).

The alternative, clinicopathologically surrogate classification of BC subtypes can be assessed based on the expression of three main biomarkers: ER, PGR, and HER2 amplification or overexpression, and an additional biomarker to give information on proliferation status, the Ki67 (Table 1). Since they are less expensive and readily available techniques, the expression status of the abovementioned biomarkers should be assessed through anatomopathological techniques, either immunohistochemistry (IHC) or in situ hybridization. The recommendation is the assessment of ER, PGR, and Ki67 status through IHC. HER2 status (gene amplification) should be classified preferably by in situ hybridization, or in the alternative, HER2 overexpression can be assessed by IHC, with confirmation through *in situ* hybridization for the unclear IHC score (Cardoso et al., 2019; Coates et al., 2015; Park et al., 2018). The usage of these four biological markers allows the definition of clinicopathological BC groups with significance in prognostic and therapeutic decisions.

The luminal A-like subtype of BC is characterized by the high expression of ER and PGR, the lack of amplification/overexpression of HER2, and a low expression of proliferation bi-

omarkers. Furthermore, this subtype of BC should also be characterized by a low-risk molecular signature, whenever these techniques are available (Cardoso et al., 2019; Goldhirsch et al., 2013). The luminal B-like subtype can be distinguished into two more specific subtypes, either HER2 positive or negative. In both subtypes, it is observed the expression of ER, but a different pattern of expression of HER2, PGR, and Ki67. In the luminal B-like HER2 negative subtype, the lack of HER2 amplification/overexpression is observed, with simultaneous high Ki67 and/or low PGR expression (Cardoso et al., 2019; Goldhirsch et al., 2013). Additionally, a high-risk molecular signature is also observed and should be evaluated whenever these techniques are available. In turn, the luminal B-like HER2 positive subtype, besides the ER expression, has HER2 amplification/overexpression and variable proliferative fraction and PGR expression (Cardoso et al., 2019; Goldhirsch et al., 2013). The HER2 positive non-luminal subtype of BC is characterized by HER2 gene amplification but lacks expression of ER and PGR. For last, in the TNBC is observed lack of expression of ER, PGR, and no amplification of the HER2 gene (Table 1) (Cardoso et al., 2019; Goldhirsch et al., 2013).

Table 1 – Surrogate definitions of intrinsic BC subtypes

Intrinsic subtype		Luminal A	Luminal B		HER2-enriched	Basal-like
Clinico-pathological surrogate definition	Subtype	Luminal A-like	Luminal B-like (HER2 –)	Luminal B-like (HER2 +)	HER2 + (non-luminal)	TNBC
	Biomarkers status	ER + HER2 – Ki67 low PGR high	ER + HER2 – At least one: Ki67 high or PGR -/low	ER + HER2 + Any Ki67 Any PGR	HER2 + ER – PGR –	ER – PGR – HER2 –

Adapted from Cardoso et al., 2019

"+" - positive

"–"- negative

"HER2+" - HER2 overexpressed or amplified

BC clinicopathological surrogate subtypes, assessed through IHC expression, are not always concordant with the intrinsic BC subtypes, resulting in over or under-treatment of certain BC subtypes (Park et al., 2018).

The different subtypes of BC have different incidence rates, prognoses, and, consequently, different types of recommended therapies. In fact, the subtypes of BC that express hormone receptors (ER or/and PGR), luminal A and B-like subtypes, are the most common types of BC (Cardoso et al., 2019; Howlader et al., 2014; Yersal & Barutca, 2014). The luminal A-

like represents the subtypes of BC with higher incidence but also better prognosis, having a high response to endocrine therapy. In the luminal B-like, chemotherapy with or without anti-HER2 therapy (depending on the tumor HER2 status), mainly with trastuzumab or dual blockade with trastuzumab/pertuzumab (in the HER2 positive cases), followed by endocrine therapy is the recommended (Neo)-adjuvant systemic treatment in the majority of cases of these subtypes of BC (Cardoso et al., 2019; Yersal & Barutca, 2014).

The HER2 positive (non-luminal) subtype has a poor prognosis, especially when untreated, due to its aggressive clinical behavior, with poor metastasis and recurrence outcomes. With the development of targeted molecular therapies and anti-HER2 agents, the HER2-positive BCs achieve a better prognosis with significant improvement in the time to disease progression, tumor objective response rate, and survival time of patients with metastatic BC tumors (Brown et al., 2008; Cardoso et al., 2019; Howlader et al., 2014; J. Wang & Xu, 2019).

Similarly to the untreated HER2 positive (non-luminal) subtype of BC, the TNBC also has a highly aggressive nature and poor prognosis. Nonetheless, the therapeutic options are reduced to chemotherapy due to the lack of molecular targets (ER, PGR, and HER2), contrary to the other BC subtypes (Cardoso et al., 2019; Garrido-Castro et al., 2019).

2.4. Triple negative breast cancer

The TNBC accounts for more than 10% of all the BCs, and is associated with early age of onset and, as already mentioned, poor prognosis (Bauer et al., 2007; Dent et al., 2007; Howlader et al., 2014). Furthermore, TNBC incidence across different ethnic and racial groups is also variable. Non-Hispanic Black women have a higher incidence of TNBC, 1.8 to 2 times more likely to develop TNBC than women from other ethnicities. Hispanic women also have a slightly higher risk of developing TNBC, with a 1.2 to 1.3 times higher risk (Bauer et al., 2007; Harris et al., 2006; Howlader et al., 2014).

TNBC's poor prognosis is associated with a more advanced stage at diagnosis, when compared to other subtypes of BC, earlier and higher rates of recurrence, high rates of invasion, low overall and breast cancer-specific survival, rapid disease progression, and a short survival rate following the first metastatic event (Badve et al., 2011; Bauer et al., 2007; Dent et al., 2007; Harris et al., 2006).

Women with TNBC have higher early recurrence (metastatic and local) rates, with most metastatic and local recurrence occurring within the first three years after diagnosis. TNBC also displays higher metastatic recurrence rates than other subtypes of BC, since almost

34% of women with TNBC experience distant recurrence, whereas, in other subtypes of BC, the proportion drops to 20.4%. Furthermore, the risk of death rates and BC-related death were 1.7 and 1.8 times higher in women with TNBC than with non-TNBCs, with a decrease in overall survival (Dent et al., 2007; Harris et al., 2006).

Due to the lack of molecular targets (ER, PGR, and HER2), the TNBC has limited therapeutic options, with chemotherapy (mainly with regimens of anthracyclines and taxanes, used preferably sequentially) as the only recommended adjuvant treatment option for early, locally advanced and metastatic BC cases (Allison et al., 2019; Cardoso et al., 2018, 2019; Garrido-Castro et al., 2019; Senkus et al., 2015).

TNBC is a heterogeneous disease with a high mutation burden and a varying gene expression classification depending on the method used. Through gene expression, besides basal-like BC intrinsic subtype, TNBC may also comprise all the other BC intrinsic subtypes, HER2 overexpression, luminal A or B, or the less accepted, normal-like (whose definition is somewhat controversial and that is defined by some authors as arising from an artifact of inadequate sampling, with cross-contamination with normal breast tissues) and claudin-low subtypes (Allison et al., 2019; Badve et al., 2011; Bastien et al., 2012; Prat et al., 2015; Tang & Tse, 2016; Weigelt et al., 2010).

Further molecular subclassification can be obtained based on the TNBC molecular characteristics. Lehmann et al. (2011) subclassified the TNBC into six subtypes based on gene expression: basal-like 1 or 2, mesenchymal, mesenchymal stem-like, luminal androgen receptor (AR), and immunomodulatory. Burstein et al. (2015) distinguished four TNBC subtypes through RNA and DNA fingerprinting analysis: luminal AR, mesenchymal, and basal-like immune-suppressed or immune-activated. Nonetheless, there is still no consensus on a clinically relevant and prognostic classification (Allison et al., 2019).

Most of TNBCs have a basal-like phenotype, with as little as 56% to about 80.6% of TNBCs showing a basal-like intrinsic BC subtype gene expression pattern, depending on the method used to identify the basal-like subtype, followed by the HER2-enriched (7.8% to 9.1%), Luminal B (3.2% to 4.4%) and Luminal A (1.6 to 2.2%) (Ahn et al., 2016; Bastien et al., 2012; Bertucci et al., 2008; Prat et al., 2013; Rody et al., 2011). The inverse is also observed, where most basal-like BC subtypes have a TNBC phenotype (ER, PGR, and HER2 negative), in an overlap of 68.5 % to 81 %. (Bastien et al., 2012; Bertucci et al., 2008; Prat et al., 2013).

Basal-like BC intrinsic subtype characterization is not yet wholly defined since there is not a consensual definition with therapeutic and prognostic value, varying whether it is assessed through IHC biological markers expression or by gene expression molecular profiling (Badve et al., 2011; Cheang et al., 2008; Lehmann et al., 2011). Overall, basal-like BC is characterized by a high expression of basal epithelial markers, such as keratins 5, 6, 14, and 17, laminin, integrin β 4, epidermal growth factor receptor (EGFR), and P-cadherin. This subtype of BC may also be associated with a high expression of proliferation-related genes such as MKI67, intermediate expression of HER2 genes, and very low expression of luminal genes (Cheang et al., 2008; Perou et al., 2000; The Cancer Genome Atlas Network, 2012; Yersal & Barutca, 2014).

Basal-like has one of the highest overall mutation rates. Basal-like BC often arbor mutations in tumor suppressor genes, mainly the protein 53 (P53) gene (occurring in 80% of the cases), less frequently in the PIK3CA (occurring in 9% of the cases), and in the BC gene 1 (BRCA1). Basal-like BC, as well as TNBCs are frequently associated with BRCA1 mutations. In fact, about 75% of women with BC carrying a BRCA1 mutation, had basal-like or TNBC subtype of BC. In women between 30 and 34 years old with TNBC, the probability of being a BRCA1 mutation carrier is 26.5% whereas for other subtypes of BC the BRCA1 mutation incidence is substantially lower, about 5%. Alterations in the PI3K/AKT pathway are also described in basal-like BC, with the above-mentioned *PIK3CA* mutation, but also AKT*3* amplification, and PTEN mutation or loss (Alluri & Newman, 2014; Lakhani et al., 2002; The Cancer Genome Atlas Network, 2012).

A subset of TNBCs also display a claudin-low phenotype in a variable range between 1.5 and 14%, and that is usually associated with a poor prognosis (Prat et al., 2010; Rody et al., 2011). Its identification often falls into the normal-like and basal-like categories. Claudin-low BC is oftentimes characterized by a low expression of tight junction encoding genes, such as claudin 3, 4, and 7, E-cadherin, and occludin. This subtype of BC also shows higher expression of epithelial-to-mesenchymal transition genes, and stem cell markers, but low luminal and proliferation-associated genes (Prat et al., 2010).

Claudin-low BCs, present high levels of immune cell infiltration, and programmed death ligand 1 (PD-L1) expression. Furthermore, this subtype of BC is associated with a low mutational burden but usually displays mutations in the P53 gene and genes related to the PI3K/AKT pathway as well as amplification of KRAS and BRAF and loss of NF1 (Fougner et al., 2020; Rädler et al., 2021). The claudin-low BC subtype is poorly understood. Fougner et al. (2020) proposed an alternative method to identify this subtype of BC by redefining it

as a phenotype that may be expressed by the other intrinsic BC subtypes, and not an individual intrinsic subtype of BC.

New target therapies with Poly-ADP-Ribose-Polymerase inhibitors for BC with BRCA mutations, programmed death 1 (PD-1) and PD-L1 inhibitors for PD-L1 positive TNBCs, antibody-drug conjugates for targeted drug delivery, and AKT inhibitors, are currently being tested and developed. But chemotherapy still represents the standard treatment approach for all TNBC cancers (Cardoso et al., 2019; Lyons, 2019).

Due to TNBC characteristics, chemotherapy-associated toxicity, the development of drug resistance, and early onset of metastasis, the search for compounds aimed at different therapeutic targets or that potentiate the existing established drugs with minimal or at least decreased toxicity towards normal cells has become a priority, to overcome the poor prognosis associated with this disease (Hulst et al., 2022; Kapałczyńska et al., 2016).

3. Potential sources of natural compounds with anti-cancer properties

Due to nature's chemical diversity, the natural environment represents an important and vast source of new bioactive molecules (Harvey, 2008; Newman & Cragg, 2020; Wright, 2019). As stated by Atanasov et al. (2021) “Natural products (NPs) are structurally ‘optimized’ by evolution to serve particular biological functions”. This evolutionary history confers them a unique and structural complexity, wide scaffold diversity, different mechanisms of action, and, in this way, a wide range of biological activities, giving them a valuable therapeutic potential (Atanasov et al., 2021; Newman & Cragg, 2020; G. D. Wright, 2019). Additionally, natural and NP-derived therapeutic agents, as well as compounds used as models for the development of analogs with higher efficacy, can be obtained from very different sources, such as plants, microorganisms (bacteria and fungi), and animals, both from terrestrial and marine environments (Cragg & Pezzuto, 2016; Harvey, 2008; Newman & Cragg, 2020).

NPs are currently used for treating a broad spectrum of diseases, serving as antibacterial, anticancer, antifungal, antiviral, antiparasitic, and immunosuppressive drugs, to name a few (Harvey, 2008; Newman & Cragg, 2020). Pharmacotherapeutics of natural origin can be obtained as biological macromolecules, unaltered NPs, or molecules from which derivatives with pharmacotherapeutic properties can be produced. Furthermore, many of the already developed pharmaceutical compounds result from drugs obtained through semisynthetic modifications of NPs, totally synthesized compounds with a pharmacophore from NPs, or consist of synthetic products that mimic the natural compounds' mode of action. In fact, in

the last four decades, from the 1881 developed drugs (excluding biological effectively identical agents to drugs previously approved and including vaccines), about 41.8% of the developed drugs came from natural origin, either biological macromolecules, unaltered NPs, botanical drugs, or derivatives of NPs. About 14.5 % consisted of synthesized drugs with a pharmacophore from NPs, and only 36.2 % consisted of totally synthesized products (Newman & Cragg, 2020).

A large portion of the approved pharmaceutical agents with origin in NPs is used as antibiotics or as anticancer drugs. In the field of cancer, the panorama is not very different from what was described for the pharmacotherapeutics of natural origin or derived from them. NPs represent around 47.7 % of all approved anticancer therapeutic agents (a total of 237 anticancer drugs, excluding vaccines), either by the Food and Drug Administration (FDA) or the European Medicines Agency (EMA), and other similar organizations around the world. Furthermore, synthesized compounds with a pharmacophore derived from NPs represent 24.5%, and purely synthetic compounds only represent 27.4% (Newman & Cragg, 2020). Some of the most commonly used chemotherapeutic agents are of natural origin. For example, taxanes and anthracyclines, recommended in treating TNBC, consist mainly of NPs, or NP derivatives (Cardoso et al., 2019; Newman & Cragg, 2020).

Taxanes are mitotic inhibitors used in cancer treatment and include paclitaxel, cabazitaxel, and docetaxel. Paclitaxel, the first approved taxane, is an NP initially extracted from the bark of the Pacific yew (Cui et al., 2021; Newman & Cragg, 2020; Ojima et al., 2016). Cabazitaxel and docetaxel are NP derivatives (semisynthetic drugs) whose precursor was extracted from the bark of the yew tree (Cui et al., 2021; Newman & Cragg, 2020).

In the group of anthracyclines used in cancer treatments, it is possible to distinguish the NPs daunorubicin, first isolated from the bacteria *Streptomyces peucetius, and* doxorubicin (Dox) initially isolated from a mutant variant of the daunorubicin producing *Streptomyces peucetius* strain. Furthermore, some NP derivatives of semisynthetic anthracyclines are also used in the treatment of cancer including, epirubicin, idarubicin, pirarubicin, and valrubicin (Hulst et al., 2022; Newman & Cragg, 2020). In fact, NPs have a great potential to be used either as chemotherapeutic agents or as adjuvants when used concomitantly with already established therapeutic regimens to improve their effectiveness or reduce the adverse effects of the drug and the adjuvant (de Oliveira Júnior et al., 2018; Dehelean et al., 2021; Lin et al., 2019).

Plants represent the primary source of bioactive compounds used as therapeutic agents, and it is estimated that only 15% of the plant species have been studied for their potential use in developing new therapeutic drugs. These numbers are even more accentuated in

the study of microorganisms, where it is estimated that less than 1% have been discovered, even though they represent around 90% of all the natural diversity (Mathur & Hoskins, 2017; Süntar, 2020).

Using microorganisms as a source for new potential therapeutic compounds is an attractive option compared to other organisms, such as plants, since they are generally less time-consuming and more cost-effective to culture and maintain (Atanasov et al., 2021; How et al., 2021). Even though many microorganisms are difficult to maintain outside their natural environment, some strains allow for easier genetic manipulation, are easily cultured and maintained, and enabled the production of high quantities of the bioactive NPs. Fungi, for example, are usually easy to grow outside their natural environments, can be grown in bio-reactors in great quantities, stored for large periods, and consequently allow an excellent availability of bioactive compounds. Even for microorganisms that are not easily maintained in culture, it is possible to clone and express biosynthetic gene clusters of NPs in well characterized, and easy-to-culture microorganisms' strains (Atanasov et al., 2021; How et al., 2021).

3.1. Fungi

Fungi represent the second group of organisms with higher species diversity, right after the insects. Various studies estimate that the number of fungi species ranges between 1.5 million to 12 million species worldwide. Of these fungi species, it seems that only 7% have been described, of which only 5% have been cultivated in the laboratory; when considering the hypothesis with the lowest number of estimated fungi species (1.5 million) (Ramírez-Rendon et al., 2022; B. Wu et al., 2019).

Fungi are a very resourceful yet poorly explored source of bioactive compounds. These microorganisms have always represented an important source of therapeutic agents, starting with the discovery of penicillin, the first developed antibiotic, obtained by Alexander Fleming from the *Penicillium notatum* (Gaynes, 2017; Sanchez & Demain, 2017). Further, their relevance in drug development continued with the discovery of some fungi species capable of producing the wide used anticancer anthracycline paclitaxel or other metabolites already in use in the treatment of cancer, such as camptothecins, podophyllotoxins, and the vinca alkaloids (Cragg & Pezzuto, 2016; How et al., 2021; Ramírez-Rendon et al., 2022).

Some other fungi metabolites and their analogs showed promising results in the treatment of cancer and therefore are currently under phase I, II, or III clinical trials, including plinabulin

and fingolimod, based on the search on https://clinicaltrials.gov (ClinicalTrials.Gov.; How et al., 2021)

3.2. Marine environment as a source of new compounds

The scope of nature as a source of new compounds is widened even more with the search for new molecules in the marine environment (Jiménez, 2018; G. D. Wright, 2019). Oceans cover around 70% of the earth's surface. Nonetheless, the marine environment is still understudied, with more than 95% of the deep ocean yet to be explored (Jiménez, 2018). Oceans represent a rich and resourceful environment with a great diversity of physical conditions such as salinity, hydrostatic pressure, temperature, oxygen levels, and light that translates into a wide diversity of habitats and ecosystems. The great variety of physical and ecological conditions results in broad biodiversity, representing around 95% of the world's biosphere (Altmann, 2017; Ameen et al., 2021; Deshmukh et al., 2018; Jimenez et al., 2018). In fact, 34 out of 35 of the already identified animal phyla exist in the marine environment, 8 of which are only described in the aquatic environments (Altmann, 2017). To thrive and proliferate in these environments characterized by extreme conditions, organisms, including microorganisms, need to adapt to these conditions. One of these adaptative mechanisms is the production of bioactive molecules, many of which may present relevant potential in the treatment of various diseases, including cancer (Ameen et al., 2021; Deshmukh et al., 2018; Jimenez et al., 2018).

The research of new compounds with origin in the marine environment dates back to the '50s with the discovery of spongothymidine and spongouridine, two nucleosides that, about 10 years later, would give rise to important advances in the development of chemotherapeutic drugs and that later lead to the development of cytarabine, considered the first marine-derived drug (Jimenez et al., 2018; Varijakzhan et al., 2021). By now, several drugs with origin in marine organisms have been approved for the treatment of cancer, such as cytarabine, trabectedin, eribulin mesylate, nelarabine, lurbinectedin, and the antibody-drug conjugates (ADC) brentuximab vedotin, enfortumab vedotin, polatuzumab vedotin, belantamab mafodotin and, more recently, and tisotumab vedotin (Cragg & Pezzuto, 2016; Papon et al., 2022). Furthermore, plitidepsin was already approved in Australia, and disitamab vedotin in China (Deeks, 2021; Dyshlovoy & Honecker, 2019).

Furthermore, other marine-derived compounds, such as plinabulin, marizomib, plocabulin, AGS-16C3F, tisotumab vedotin, ladiratuzumab vedotin, telisotuzumab vedotin, enapotamab vedotin, cofetuzumab pelidotin, to name a few, are currently undergoing phase I, II, or III, clinical trials (Papon et al., 2022).

3.2.1. Marine-derived fungi – diversity and potential

The biodiversity in the marine environment includes algae, invertebrates (such as marine sponges), vertebrates, and a myriad of microorganisms (including fungi, archaea, and bacteria) that represent important sources of bioactive compounds (Wali et al., 2019).

Marine-derived fungi may englobe the marine obligate (fungi that only proliferate in the marine environment) and the facultative (fungi with origin in the terrestrial environment but that adapt to the marine environment). However, the distinction between these two is not always easy (Ameen et al., 2021). In the marine environment, besides its isolation from water and sediments, marine-derived fungi have also been found in symbiotic interactions, associated with host macroorganisms such as algae, mangroves, corals, and marine animals such as sea cucumber, snails, and sponges (Cragg & Pezzuto, 2016; Deshmukh et al., 2018).

The marine sponges are important sources of bioactive compounds, some of which were approved for cancer treatment, as described above (Papon et al., 2022; Varijakzhan et al., 2021; L. Wu et al., 2021). The marine sponges are filter feeders. The water passes through the sponge pores (ostia), and the amoebocyte cells engulf the water's existing particulates. In this filtration process, some microorganisms may be phagocytized by the sponge, but others remain in the sponges' mesohyl (the inner sponge cell lining). These microorganisms can then develop symbiotic interactions with the sponge, enrolling in its physiological processes, including nutrition, skeleton stabilization, metabolite production, and chemical defense (Debbab et al., 2011; Varijakzhan et al., 2021). Thus, it is worth noting that some of the bioactive substances discovered in sponges, mostly secondary metabolites, are created by the sponge's symbiotic microorganisms rather than by the sponge itself (Varijakzhan et al., 2021).

Although the sponges' microorganism's population density is highly variable, about 40% of the sponge volume may be comprised of microorganisms (Debbab et al., 2011; Varijakzhan et al., 2021). The diverse conditions (including the symbiotic interactions with other organisms) to which the marine-derived fungi are subjected lead to the development of unique metabolic pathways that may, in turn, lead to the development of a wide variety of natural products with potential pharmaceutical proprieties, including anticancer drugs (Ameen et

al., 2021; Deshmukh et al., 2018; Jimenez et al., 2018; Saeed et al., 2021; Varijakzhan et al., 2021). However, despite the many compounds isolated from marine-derived fungi, none has been approved yet to treat human diseases (Ameen et al., 2021; Saeed et al., 2021).

Plinabulin, for example, is a derivative from the NP diketopiperazine halimide isolated from the fungus *Aspergillus sp.* (from marine and terrestrial sources) and the NP phenylahistin isolated from the terrestrial fungi *Aspergillus ustus* (Blayney et al., 2022; How et al., 2021; Jiménez, 2018). Plinabulin is a microtubule destabilizing agent that is currently being evaluated in several phase I, II, or III clinical trials, according to data from https://clinicaltrials.gov (*ClinicalTrials.Gov*, n.d.).

Overall, fungi, and especially marine-derived fungi symbionts, represent an exciting source of bioactive compounds with unique structures with high potential pharmacological proprieties, including anticancer proprieties that deserve further investigation.

3.3. Preussin

Preussin, or (+)-preussin, as also known, is a hydroxypyrrolidine alkaloid (Figure 4) that was initially extracted from the fermentation broths of *Aspergillus ochraceus* (Schwartz et al., 1988) and later from *Preussia* sp. (Johnson et al., 1989). More recently, preussin was also isolated from cultures of *Aspergillus candidus* (KUFA 0062), found in association with the marine sponge *Epipolasis sp.*, captured from the Similan Island National Park's coral reef, in Phang-Nga province, Southern Thailand (Buttachon et al., 2018). Furthermore, various authors have described different methods for its synthesis (Arévalo-García, 2014; Basler et al., 2005; Beier & Schaumann, 1997; Buchman et al., 2016; Draper & Britton, 2010; Hausherr et al., 2019; P. Q. Huang et al., 2015; Kanazawa et al., 1986; Khandare et al., 2020; Lee et al., 2000; Mao et al., 2018; McGrane & Livinghouse, 1993; Okue et al., 2002; Raghavan & Rasheed, 2003; Rong et al., 2017; Veeresa & Datta, 1998).

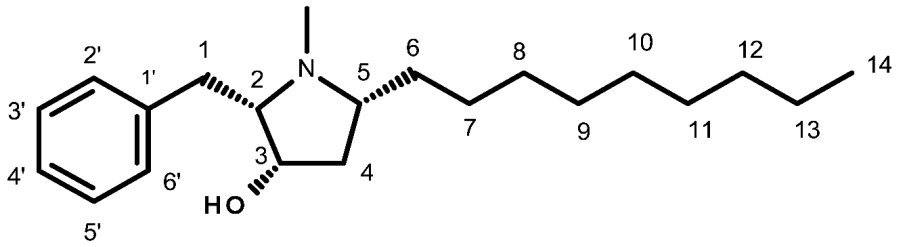

Figure 4 – Chemical structure of (+) – preussin (Buttachon et al., 2018).

Different preussins have been identified and isolated from natural sources. Besides the one simply-called preussin, it has already been shown the isolation of preussin B, extracted from *Simplicillium lanosoniveum*; preussin C, isolated from the marine sponge-associated *Aspergillus candidus* and *Aspergillus flocculosus*, and the preussins D to K, obtained from the fermentation broths of the marine sponge-associated *Aspergillus flocculosus* (Buttachon et al., 2018; Fukuda et al., 2014; Gu et al., 2018).

Although there is little bibliography about preussin and its isomers, the (+)-preussin is the most described and seems to have a wider diversity of biological activities. This preussin has shown antifungal activities both against filamentous and yeast forms of fungi (Johnson et al., 1989; Kasahara et al., 1997; Schwartz et al., 1988). It was also suggested to have a bacteriostatic and bactericidal action against gram-positive bacteria, with the capability to inhibit methicillin and vancomycin-resistant bacteria strains (Buttachon et al., 2018), and even shown to exhibit antiviral proprieties (Goss Kinzy et al., 2002).

Several authors have also shown preussin to present cytotoxic proprieties (Achenbach et al., 2000; Buttachon et al., 2018; Malhão et al., 2019). Achenbach et al. (2000) showed that synthetic preussin could decrease cell survival of several human cancer cell lines with a half-maximal inhibitory concentration (IC_{50}) between 1.2 and 4.5 μM in HL-60 (promyelocytic leukemia), HeLa (cervical carcinoma), A549 (lung adenocarcinoma), MCF-7 (breast carcinoma), lines PC-3, DU-145, and LNCaP (prostate carcinoma) and MeWo (melanoma) cell lines. Recently, Buttachon et al. (2018) demonstrated that preussin, extracted from the marine sponge-associated *Aspergillus candidus*, decreased cell viability with a variable IC_{50} between 12.3 μM and 74.1 μM. This study included the HT29 (colorectal adenocarcinoma), HCT116 (colorectal carcinoma), A375 (melanoma), HepG2 (hepatocellular carcinoma), A549 (lung cancer), T98G (glioblastoma astrocytoma), MCF-7, and U251 (glioblastoma multiforme), human cell lines, here described from the most sensitive to the less sensitive to preussin (lower to the highest IC_{50}) (Buttachon et al., 2018). Malhão et al. (2019) demonstrated that this marine fungi-derived preussin decreased cell viability below 50% in the human BC MCF-7, and SKBR3 cell lines, at a concentration of 50 μM, for cells cultured in monolayer. Nonetheless, at this concentration, preussin decreased cell viability in all tested BC cell lines (MCF-7, MDA-MB-231, and SKBR3) and in the non-tumoral breast cell line, MCF12A (Malhão et al., 2019). Furthermore, in a three-dimensional (3D) cell culture model, preussin decreased cell viability at 50 or 100 μM for MCF-7, SKBR3, MDA-MB-231, and MCF-12-A, depending on the used proxies (either lactate dehydrogenase release, MTT or resazurin conversion assays). It is important to note that in the 3D cell culture model, 50 or 100 μM were the only tested concentrations (Malhão et al., 2019).

Preussin has also been shown to induce apoptosis in HL-60 cell line through caspase 8, and cytochrome c-caspase 9 pathways, with the activation of caspases 3 and 8, and the release of cytochrome c, respectively (Achenbach et al., 2000), and to increase the expression of caspase 3 in MCF-7, SKBR3, MDA-MB-231 and, MCF-12-A cell lines (Malhão et al., 2019). This compound was also shown to decrease cell proliferation in MCF-7, SKBR3, MDA-MB-231, and MCF-12-A cell lines both in monolayer and 3D cell cultures (respectively 25 and 50 μM), with MDA-MB-231 cell line showing higher resistance than the other cell lines in monolayer culture (Malhão et al., 2019). Preussin also promoted cell cycle arrest through the G1 phase preventing the progression into the S phase by inhibiting cyclin E kinase (CDK2-cyclin E) in A549 cells and HL-60 cells (Achenbach et al., 2000), despite not being observed in fission yeast cells (Okue et al., 2002). Cell cycle arrest caused by exposure to preussin was also observed in 3Y1 normal rat fibroblast (Kasahara et al., 1997). Furthermore, preussin has also been shown to be a DNA-damaging agent in *Saccharomyces cerevisiae* yeast (Overhand & Hecht, 1994).

The diversity of preussin biological activities has been attributed to some of its molecular characteristics. When comparing preussin and preussin C, Buttachon et al. (2018) emphasized the importance of the N-methyl group on the pyrrolidine ring (present in the (+) – preussin (Figure 4) but not observed for the preussin C (Figure 5)), for the preussin antifungal and cytotoxic proprieties.

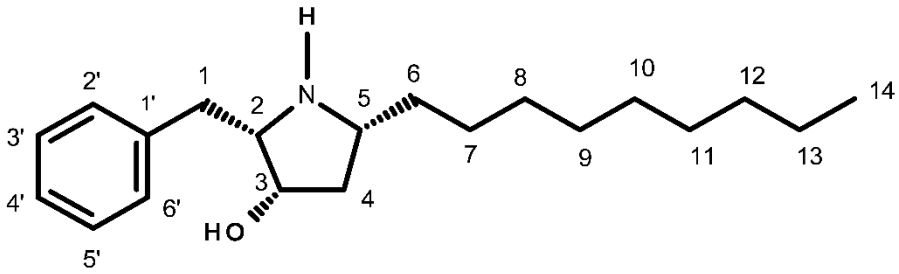

Figure 5 – Chemical structure of C preussin (Buttachon et al., 2018).

3.4. Development of cancer drugs derived from natural products

According to the FDA, drug development comprises 5 steps. First, the discovery and development of new compounds, followed by preclinical research (with *in vitro* and *in vivo* models), clinical research, review of all data available to decide on the approval of the drug, and if and after approval, drugs are monitored on its safety (U.S. Food and Drug Administration (FDA), 2018).

Traditionally, the discovery and development of anticancer drugs derived from NPs consist first in the obtention of crude extracts from an organism. After extraction, the crude extract

is tested on its pharmacological activities. If promising, it undergoes the next step: fractioning the crude extract until pure bioactive compounds are isolated. Nonetheless, impurities may be present in the extracted and isolated NPs, resulting in altered behavior. With this in mind, an advanced purity analysis is recommended before further studies. The process of isolation involves biological screening and may need multiple rounds of fractioning. The isolated bioactive compounds are later identified based on phenotypic assays and characterized on their molecular mechanism of action. This is a laborious and time-consuming process. Furthermore, this process may be impaired due to the incapability of culturing the organism outside its natural habitat, the inability of the organism to produce determined NPs out of its habitat, or the quantity they produce may not be enough for its identification and classification and, later on, for preclinical studies (Atanasov et al., 2021).

Nonetheless, new drug discovery and development advances overcame or at least allowed for the diminishing of NPs' drug discovery limitations. These may include developing new culturing methods that mimic the natural environment and in situ analysis, with the incubation of the microorganism in the environment from which it was collected. New methods for extraction, dereplication, and pre-fractioning of the crude extracts may also represent other methods of circumventing the investigation of NPs for developing new therapeutical drugs. For example, the crude extract fractioning can be optimized so that the sub-fraction contains NPs with characteristics of pharmacological relevant compounds, such as moderate hydrophilicity. Also, metabolomic analysis, through nuclear magnetic resonance (NMR) spectroscopy, high-resolution mass spectrometry, and liquid chromatography for isomer separation, allows for the analysis of several metabolites simultaneously and its rigorous characterization (Atanasov et al., 2021).

Some approaches allow for the obtention of NPs, and NP hybrids, analogs, and derived scaffolds leading to the production of compounds with higher biological activities, selectivity, and better pharmacokinetic proprieties. Microorganism genetic manipulation and cloning of NPs biosynthetic gene clusters into other, more easily cultured and better-characterized, microorganisms allow the increase in the NPs yields and/or the production of NPs analogs with higher biological pharmacological relevant proprieties (Atanasov et al., 2021; Patra et al., 2018; Press et al., 2019)

In addition to genetic manipulation, these techniques may include biosynthetic engineering with manipulation of the organism's biosynthetic pathways, derivatization of isolated NPs, or the semisynthesis of NP analogs (Atanasov et al., 2021; Patra et al., 2018). Even compounds that display relevant pharmacological proprieties still display some challenges that may reduce their therapeutic effects, such as limited plasma solubility and biodistribution,

low dissolution and absorption, high instability, rate of degradation during storage, and rate of excretion, resulting in lower bioavailability and pharmacological activity with poor pharmacokinetic properties (Atanasov et al., 2021; Beck et al., 2017; Large et al., 2021; Mitchell et al., 2021).

Several approaches allow for the diminishing of these drawbacks. These may include the usage of delivery systems such as liposomes, polymeric and inorganic nanoparticles, and antibody-drug conjugates (Mitchell et al., 2021; Patra et al., 2018). These techniques allow for drug delivery with higher therapeutic efficacy, selectivity with tissue-targeting capabilities, reduced systemic toxicity, and lower drug toxicity compared to free drug administration. Further, these drug delivery systems enable higher maximum tolerated doses and efficient bioavailability (Beck et al., 2017; Large et al., 2021; Mitchell et al., 2021).

4. *In vitro* models for investigation and development of anticancer drugs

Cell culture represents an indispensable model, used as the first approach in drug discovery, development, and characterization. Cell culture has low cost-effectivity, allows for the obtention of consistent and reproducible results, and the possibility of performing a high number of replicates, thereby diminishing the usage of animal models (Edmondson et al., 2014; Freshney, 2010).

4.1. 2D cell culture

Most *in vitro* studies with cells have used the two-dimensional (2D) culture method, in which the cells grow in a monolayer and adherent to a solid substrate (Kapałczyńska et al., 2016). Despite its advantages, such as the simplicity of methods, and the low costs associated with maintaining the cell cultures and performing research tests, cultures with adherent cells have disadvantages that limit their use and the conclusions drawn from them (Habanjar et al., 2021; Kapałczyńska et al., 2016)016). The disposition of the cells as a monolayer translates into their homogeneous exposure to the cell culture medium, resulting in a similar availability of oxygen and nutrients to the cultured cells. Further, the disposition of the cells also influences the cell morphological characteristics resulting in an altered cell structure, more elongated and flattened. It also influences the cell-cell interactions and cell junctions, which are decreased in the 2D cell culture model. These altered characteristics result in modified signaling pathways, which translate into altered cell metabolism, differentiation and

proliferation rates, viability, cell invasion, transcriptional and apoptotic patterns, and sensitivity to different compounds, not mimicking the tissue and tumor structure, behavior and microenvironment complexity found *in vivo* (Białkowska et al., 2020; Duval et al., 2017; Habanjar et al., 2021; Jensen & Teng, 2020; Kapałczyńska et al., 2016; Langhans, 2018).

4.2. 3D cell culture

Three-dimensional (3D) cell culture consists on the obtention of multicellular aggregates (MCA), also called spheroids. Various methods have already been described for the obtention of 3D cell cultures. These may include cell culture in scaffold-free environments or scaffold structures from natural and synthetic origin, and either grown in scaffold 3D structures or in substrates that mimic the extracellular matrix (ECM) (Habanjar et al., 2021; Lv et al., 2017).

The scaffold-free methods of 3D cell culture are tendentially less expensive and characterized by high throughput and easily obtention protocols. These may include: a) pellet culture, where cells are concentrated by centrifugation, and the pellet is resuspended in culture medium for spheroid formation; b) hanging drop, in which a drop of cell suspension is placed on the lid of a culture plate which is turned upside-down, and the formation of spheroids is induced by gravity and cell culture medium surface tension; c) microwell-based non-adhesive agarose scaffolds, in which cells are seeded in agarose molds and spinner culture, forcing cells to aggregate by continuous agitation; d) liquid overlay technique, where cells are seeded in low attachment plates which are coated with non-adhesive materials such as agarose or pHEMA, forcing cells to aggregate (Fang & Eglen, 2017; Froehlich et al., 2016; Habanjar et al., 2021; Lv et al., 2017). In this last technique, the spheroid formation may be improved using rounded or v-shaped bottom plates. (Langhans, 2018).

3D cell culture techniques allow for the obtention of dynamic structures, the spheroids, that are classically composed of: a) an outer layer of cells with a high rate of proliferation, which have more access to nutrients and oxygen from the cell culture medium; b) an intermediate layer with senescent cells; and c) a necrotic center, were cells have lower availability of oxygen and nutrient levels. Due to its 3D structure, with varying availability of nutrients and oxygen, this cell culture model mimics the *in vivo* tumor and tissue biochemical, morphological, and physiological conditions (Costa et al., 2016; Habanjar et al., 2021). In fact, when cultured in a 3D cell culture model, tumoral cells prevenient from patients better maintained their pattern of expression of caspase 3 and ki67, when comparing the cells cultured in 3D or 2D cell culture models (Imamura et al., 2015). Nonetheless, it is important to mention

that the spheroid's characteristics, including the spheroid morphology, the cell's pattern of distribution in different stages of cell proliferation and death (necrosis or apoptosis), and cell cohesion, are influenced by the method of obtention, as well as the cells in culture (Malhão et al., 2022).

Despite allowing to overcome the already mentioned disadvantages of 2D cell cultures, 3D cell cultures are more laborious, expensive and require more precise work (for culture uniformization) when compared to the 2D cell culture (Habanjar et al., 2021; Langhans, 2018)

Due to its tridimensionality, the 3D cell culture shows important features for anti-cancer drug discovery and development, including the capability to mimic tumor *in vivo* characteristics such as cell morphology, gene expression, cell surface receptors organization, drug resistance, hypoxia, migration, proliferation, differentiation, dormancy, and anti-apoptotic patterns, as well as the cell-cell interaction and the tumor microenvironment including cell-ECM interactions (Fontoura et al., 2020; Habanjar et al., 2021; Langhans, 2018).

Objectives

This study aimed to explore and expand the *in vitro* anticancer proprieties of the bioactive compound preussin, purified from marine sponge-associated fungi, in the TNBC cell line MDA-MB-231 while comparatively investigating 2D and 3D *in vitro* cell culture models.

The following specific objectives were set, using preussin as the compound of primary interest and Dox as a reference drug when comparing the 2D and 3D models:

1. Optimize assays for conducting drug screening in 3D cultures of MDA-MB-231 cells;
2. Select the lowest concentrations of preussin that induced a reduction of cell viability in the MDA-MB-231 cell line, either cultured in 2D or 3D models;
3. Evaluate the preussin antiproliferative, long-term survival, genotoxic, and cytotoxic (distinguishing between apoptosis and necrosis) effects, considering the pre-identified concentrations, in 2D and 3D cell culture models;
4. Describe the stereomicroscopy and ultrastructural alterations induced by preussin in both types of culture models and also using the pre-identified concentrations;
5. Evaluate the effects of preussin in cell migration at low concentrations of preussin in a 2D cell culture model.

Material and Methods

1. Cell culture

The MDA-MD-231 cell line was purchased from American Tissue Culture Collection (ATCC). Cells were maintained as monolayer cell cultures in Dulbecco's Modified Eagle's Medium (DMEM) with high glucose, without glutamine, and phenol red supplemented with 10% fetal bovine serum (FBS) and 1% penicillin/streptomycin (pen/strep). The maintenance was made in T25 cm^2 (with 5 ml of DMEM) and T75 cm^2 (with 15 ml of DMEM) culture flasks (Orange Scientific, Braine-l'Alleud, Belgium) in an MCO 19AIC humidified incubation chamber (Sanyo, Osaka, Japan) at 37°C and 5% CO_2. Cells were regularly observed under an inverted phase-contrast CKX41 microscope (Olympus, Tokyo, Japan), and the medium was replaced every two to three days. When about 80%-90% confluence was reached, cells were in their logarithmic phase and were harvested and subcultured (as described in section 1.1. Subculturing conditions). Cell suspensions with the desired cell density were obtained from the subcultures to perform different assays, either as monolayers or 3D cell cultures (MCAs).

1.1. Subculturing conditions

Cells were washed twice with phosphate-buffered saline (PBS) [pH 7.2-7.4], detached with 0.25 % Trypsin 0.02 % ethylenediaminetetraacetic acid (EDTA) (1 ml for cells cultured in T25 cm^2 flasks or 3 ml of for cells cultured in T 75 cm^2 flasks) at 37°C for 3-5 min. When cells became rounded-shaped and started to detach, the action of trypsin was stopped by adding supplemented DMEM in a proportion higher than 1:2 (v/v) (2 ml of DMEM in T25 cm^2 flasks and 6 ml of DMEM in T75 cm^2 flasks). This process of disaggregation was helped by mechanical shearing. After trypsinization, cells were centrifuged at 280 g in a 416 centrifuge (Gyrozen, Gimpo, Korea), the supernatant removed, and cells were resuspended again in DMEM (1 ml for T25 cm^2 flasks cultured cells or 3 ml for T75 cm^2 flasks cultured cells). The cell density and viability of the obtained cell suspension were accessed through the trypan blue exclusion assay (see section 1.2. Trypan blue exclusion assay and determination of cell density). Finally, cell suspensions with the desired concentrations were prepared according to the assay that was being performed. Subcultures were obtained by seeding approximately 200 µl of cell suspension in 5 ml of supplemented DMEM in T25 cm^2 flasks or 1 ml of cell suspension in 15 ml of supplemented DMEM in T75 cm^2 flasks. The final volume was adjusted to obtain the desired concentration for seeding. When the cultured cells reached passage 35, new cell cultures were obtained from frozen cells.

1.2. Trypan blue exclusion assay and determination of cell density

The trypan blue exclusion method was used to determine cell density and viability of cell suspensions. In this assay, cells are mixed with trypan blue. Viable cells show impermeability to the dye (appear bright under a microscope), and the non-viable cells that do not have cell membrane integrity are permeable to the dye (appear blue under a microscope (Freshney, 2010). To perform this assay, 20 µl of cell suspension were added to an equal volume of 0.1% trypan blue (w/v) in PBS. Immediately, 10 µl were loaded into a Neubauer chamber and the number of live and dead cells was counted. Cell density and viability were calculated according to the following equations:

$$\textbf{Cell density}\ (\text{nº cells/ml}) = \text{average number of cells} \times 2\ (\text{dilution factor}) \times 10^4\ (\text{conversion factor for Neubauer chamber})$$

$$\textbf{Cell viability}\ (\%) = \frac{\text{nº of viable cells}}{\text{nº of total cells}} \times 100$$

1.3. Thawing of frozen cells

New cell cultures were obtained from cells frozen in DMEM supplemented with 10% FBS, 1% pen/strep, and 10% dimethyl sulfoxide (DMSO) at -80 °C. The 1 ml aliquots of frozen cells were thawed to 37°C by adding supplemented DMEM, previously heated, and seeded in a T75 cm^2 flasks with 15 ml of supplemented cell culture medium and incubated at the standard incubation conditions (37°C and 5% CO_2). After 24h, the cell culture medium was exchanged to remove the DMSO present in the culture.

2. Chemicals and reagents

Dox (D1515), FBS, collagenase from *Clostridium histolyticum*, 3-(4,5-dimethylthiazol-2-yl)-2,5-diphenyltetrazolium bromide (MTT), low melting point (LMP) agarose, normal melting point (NMP) agarose, and potassium bromate ($KBrO_3$) were purchased from Sigma Aldrich (Missouri, USA). DMEM (with high glucose, without glutamine, and phenol red) and DMSO were acquired from VWR Chemicals (Ohio, USA). FBS, trypsin/EDTA, and pen/strep were obtained from Biochrom KG (Berlin, Germany). Trypan blue, crystal violet, methylene blue, azure II, glutaraldehyde solution, and hydrogen peroxide (H_2O_2) were obtained from Merck (Darmstadt, Germany). SyberGold™ from Thermo Fisher Scientific (Massachusetts, USA), the FPG enzyme from New England Biolabs (Barcelona, Spain), BrdU assay kit from Roche

(Basel, Switzerland), and FITC-conjugated Annexin V, Annexin V buffer, and propidium iodide (PI) from BioLegend (California, USA).

Preussin was isolated from the marine sponge *Epipolasis* sp. associated fungi *Aspergillus candidus* KUFA 0062 (collected from the coral reef of Similan Island National Park in Phang-Nga province of Southern Thailand). The preussin process of isolation and purification has been described by Buttachon et al. (2018).

2.1. Stock solutions

Preussin (10 mM), Dox (20 mM), and SyberGold™ (1000x) were prepared as stock solutions in DMSO and, MTT (5 mg/ml) was prepared in sterile PBS. The solutions were kept in aliquots at -20 °C and freshly diluted right before use.

For each experiment, dilutions (work solutions) of the stock solutions of Dox and preussin were freshly prepared, before use, using a cell culture medium with a final concentration of 0.1% of DMSO. Right before use, preussin was diluted to a concentration of 50 µM from which were obtained the other final preussin concentrations of 35 µM, 25 µM, 15, and 5 µM. Dox was used as a positive control and prepared to a final concentration of 1 µM (for monolayer culture exposure) or 5 µM (for MCAs exposure). As a negative control, cells were only exposed to the cell culture medium (DMEM); as solvent control, cells were exposed to DMEM with 0.1% DMSO. Additional control groups were added depending on the assay that was being performed.

3. Multicellular aggregates (MCAs)

3.1. MCAs obtention

To obtain MDA-MB-231 MCAs, 200 µl of cell suspension at $4x10^5$ cells/ml were seeded in 96-well ultra-low attachment plates (Corning, New York, USA) and incubated at 37 °C, with 5% CO_2 for 72 h. MCAs were then exposed to preussin at the desired concentrations according to the assay that was being performed.

3.2. MCAs disaggregation

To execute this study, certain tests required the MCAs disaggregation to obtain cell suspensions following the exposure period. MCAs trypsinization is a delicate process since it implies high cell manipulation, which may cause cell damage or even cell loss (especially when transferring MCAs to 1.5 ml tubes and washing them with PBS). Several protocols were experimented to evaluate the adequate method that induced less damage in the cells. After being obtained, three MCAs were transferred to 1.5 ml tubes, washed gently two times with warm PBS, and centrifuged in a Microstar 12 centrifuge (VWR, Pennsylvania, USA) at 280 g for 5 min between washes. After washing with PBS, the MCAs were incubated with 100 µl of the disaggregation solution for 5 min, with or without mechanical disaggregation. The tested disaggregation solutions were: a) 20mM EDTA with 2% DMSO; b) 20 mM EDTA with 10% DMSO; c) 1 mg of collagenase in 2ml HBSS; d) trypsin-EDTA (Mandujano-Tinoco et al., 2013; Vincent-Hubert et al., 2011). In the trypsin-EDTA condition, 100 µl of the disaggregation solution was used, and then 300 µl supplemented medium was added to stop trypsinization. MCAs viability was assessed by trypan blue assay, as described above.

4. Viability assay - MTT assay

MTT assay is a viability assay where MTT, a yellow tetrazolium salt, can be absorbed and then metabolized by the cell into formazan, a purple water-insoluble compound (Meerloo et al., 2011; Präbst et al., 2017). This reaction depends on an electron donor such as NADH, NADPH, succinate, or pyruvate and is carried out by mitochondrial or cytoplasmic enzymes such as dehydrogenases, oxidoreductases, oxidases, and peroxidases. Some reduction molecules such as glutathione, ascorbic acid, and coenzyme A may also reduce MTT to formazan through non-enzymatic reactions (Präbst et al., 2017). Mitochondrial enzymatic activity is constant in most viable cells. Subsequently, the conversion of MTT into formazan crystals allows the usage of MTT as a colorimetric assay with which it is possible to measure the increase or decrease in the number of viable cells. In this way, it is possible to infer a compound's effect on cell proliferation and cytotoxicity activity by quantifying cellular metabolic activity (Meerloo et al., 2011; Präbst et al., 2017). Since formazan is obtained intracellularly as needle-like crystals, it causes cell disruption, making unfeasible its usage in further studies, and it also causes the need for a step of solubilization of these crystals for homogenous reading of the formazan. Additionally, all procedures should be performed under low light conditions since MTT is degraded by light (Meerloo et al., 2011; Präbst et al., 2017).

4.1. MTT in monolayer cell culture

The MTT assay was used to evaluate the effects of preussin in MDA-MB-231 cells, as previously tested by Malhão et al. (2019). MDA-MB-231 cells were seeded at a density of 5 x10^4 cells/ml, 100 µl of cell suspension per well in 96-multiwell culture plates (Orange Scientific, Belgium) and incubated at 37°C and 5% CO_2 for 24 h to allow cell adhesion. Cells were then exposed to preussin at concentrations of 5, 15, 25, 35, and 50 µM and incubated for 24, 48, and 72 h in the incubation chamber under the same conditions. Negative control, solvent control, and positive control groups were also added. Simultaneously, an additional blank control group was included in which exposure and control solutions were added to wells without cells. This procedure allowed the obtention of background A measurements. After the defined exposure time, 10 µl of MTT solution in PBS were added to each well and incubated for 3 h, protected from light in the incubation chamber. After MTT metabolization, the medium was completely removed, and the formed formazan crystals were dissolved by adding to each well 100 µl of DMSO/ethanol solution (in the proportion of 1:1) (v/v), and the plates were agitated for 15 min in a plate shaker. Absorbance (A) was read in the Multiskan™ GO Microplate Spectrophotometer (Thermo Fisher Scientific, Massachusetts, USA) at 570 nm. Data was analyzed first by subtracting the background of each condition (mean of the A of the blank of each exposure condition) from the mean A of the cells of each exposure condition, followed by the calculation of the percentage of cell viability in relation to the control, as described by Malhão et al. (2019):

Mean A (without background) = mean A of exposed cells - mean A of the blank

$$\textbf{Cell viability}\ (\%) = \frac{\text{mean A (without background) sample at 570 nm}}{\text{mean A (without background) control at 570 nm}} \times 100$$

The values of measured A should be proportional to the number of viable cells in the culture. MTT assay was performed in five independent experiments (n=5), using triplicates per exposure condition.

4.2. MTT in MCAs

To evaluate the cytotoxic effects of preussin in MDA-MB-231 MCAs, a modified version of the MTT assay was implemented in monolayer cell culture (Malhão et al., 2019). MCAs were obtained as described previously (sub-section 3.1. MCAs obtention) and were exposed to preussin at 25, 35, and 50 or Dox at 5 µM (positive control) for 96 h. Following the

assessment of preussin's induced decrease in the MCAs viability at 96 h of exposure, the concentrations of 25 and 35 µM were selected for evaluation of its proprieties through other proxies. Accordingly, the effects of preussin on cell viability were also assessed through the MTT assay at 24 h of exposure to later perform the comet assay (to explore the preussin induced genotoxicity). Following the defined period of exposure with preussin, 15 µl of MTT were added to each well and incubated for 4 h. After this time, MCAs were carefully transferred from the ULA-rounded bottom plate into a flat-bottomed culture plate with a 1000 µl micropipette tip. To diminish the damage and cell loss that this process could cause, the end of the 1000 µl micropipette tip was cut to augment the tip diameter. The excess of the medium was carefully removed with a 100 µl micropipette tip. Formazan crystals were solubilized by adding 150 µl of DMSO to each well and by agitating in a plate shaker for 20 min. In MCAs, DMSO was used alone to solubilize the formazan crystal since it allowed better and easier solubilization of these crystals than the usage of a solution of DMSO/ethanol (as it was used in monolayer cell culture). The results were also expressed as a percentage of cell viability already described in the 2D cell culture MTT assay. The MTT assay in MCAs was performed in five independent assays, using triplicates for each exposure condition.

5. Clonogenic survival assay

Clonogenic survival assay is a long-term survival assay with which it is possible to measure the long-term effects of a compound in cell survival by evaluating its long-term cytostatic effects either by cell cycle arrest or DNA synthesis inhibition (Freshney, 2005; Sumantran, 2011). The principle of this assay is based on the capability of a single cell to originate a viable colony. In this way, cells from cell suspensions are seeded at low density to obtain isolated cells from which representative colonies may form. By counting the number of colonies formed, it is possible to assess alterations in cell survival considering the cells' regenerative capacity by allowing cells with reversible damages and cells resistant to drugs to proliferate. Generally, colonies should be considered if they have more than 50 cells (Freshney, 2005). Despite its advantages, the clonogenic assay does not account for cell-to-cell interaction since the cells are seeded at a low density (Freshney, 2005; Sumantran, 2011). The clonogenic survival assay was utilized here to assess the long-term cytostatic effects of preussin, as previously described (Ramos et al., 2019).

5.1. Clonogenic assay in monolayer cell culture

MDA-MB-231 cells were seeded in 24-well plates (Orange Scientific, Braine-l'Alleud, Belgium) at a density of 1 x10^5 cells/ml, 500 µl per well, and incubated for 24 h at 37°C e 5% CO_2 for cell adhesion. After this period, cells were initially exposed to preussin at a concentration of 35 and 50 µM. Based on the obtained results, it was later decided to lower the used concentrations of preussin in this assay. In this way, in subsequent assays, cells were exposed to preussin at a concentration of 5, 15, 25, and 35 µM. Simultaneously, negative control (DMEM), solvent control (0.1 % DMSO), and positive control (1 µM of Dox) groups were added.

After 72 h of exposure, cells were carefully washed twice with PBS and harvested by trypsinization with 150 µl of trypsin/EDTA for 3 min at 37°C and 5% CO_2. When cells became round-shaped, trypsinization was stopped by adding 300 µl of supplemented cell culture medium, and cells were carefully resuspended for cell suspension homogenization. Living cells were counted with trypan blue in the Neubauer chamber as previously described, and serial dilutions of the cell suspension were performed to obtain a final dilution of 250 cells/ml. Then 2 ml of cell suspension were seeded in 6-multiwell culture plates (500 cells/ well). Five hundred cells in 2 ml of cell suspension (Orange Scientific, Braine-l'Alleud, Belgium) were incubated for 21 days at 37°C and 5% CO_2. The number of cells initially seeded was 200 cells per well. Nonetheless, based on the obtained results, the protocol was optimized to 500 cells per well. Also, the incubation time was raised from 10 days to 21 days. Furthermore, to assure adequate humidity, which would lead to less medium evaporation, cells seeded in the 6-multiwell culture plates, were incubated inside a small plastic with a humidified paper towel. After 21 days of incubation, cells were washed with PBS and fixed *in situ* for 15 min at 37°C with 4% (w/v) paraformaldehyde in PBS (stored as aliquots at -20 °C and, just before use, it was thawed at room temperature and heated to 37 °C). Cells were then stained with crystal violet at 0.05% (w/v) in PBS for 30 min at room temperature, washed, and air-dried. Colonies with more than 50 cells were observed and counted in an SZX10 stereomicroscope (Olympus, Tokyo, Japan). Plating efficiency (PE) and surviving fraction (SF) were calculated as follows (Ramos et al., 2019):

$$\textbf{PE} = \frac{\text{nº of colonies counted}}{\text{nº of seeded cells}} \qquad \textbf{SF}\ (\%) = \frac{\text{PE of treated cells}}{\text{PE of control}} \times 100$$

This assay was performed in 5 independent experiments.

5.2. Clonogenic assay in MCAs cell culture

Three MDA-MB-231 MCAs were exposed to preussin at a concentration of 5, 15, 25, or 35 µM. In the positive control group, cells were exposed to 5 µM of Dox. Negative control and solvent control groups were also included. After 96 h of exposure, MCAs were disaggregated as described previously (section 5.1 - Clonogenic assay in monolayer cell culture), and through serial dilutions we obtained a cell suspension of 250 cells/ml. As it has already been described for the monolayer cell culture, 2 ml of the obtained cell suspension were seeded in 6 well plates and incubated for 21 days at 37°C and 5% CO_2. After, the colonies were washed twice with PBS, fixed with 4% paraformaldehyde in PBS, and stained with 0.05% (w/v) crystal violet in PBS. The colonies with more than 50 cells were counted, and the PE and PF were calculated, as reported in the mentioned section 5.1. Five independent assays were performed.

6. *In vitro* scratch assay

In vitro scratch assay or cell wound-healing assay is used to measure cell migration in monolayer cultures. In this assay, a scratch is made in a confluent cell monolayer, and it is later observed at different time points to evaluate the scratch closure (Cory, 2011).

To evaluate the effects of preussin on the ability of MDA-MB-231 cells to migrate, cell culture conditions had to be initially determined. In this way, a gradient of seeding densities (2.5 x10^5 cells/ml, 3 x10^5 cells/ml, 5 x10^5 cells/ml, 10 x10^5 cells/ml, and 20 x10^5 cells/ml in 500 µl per well, in 24-well plates) were tested. The seeding density of 2.5 x10^5 cells/ml allowed the obtention of a confluent uniform monolayer without cell crowding. To establish a reference point, a line was drawn in the center of each well with a permanent marker, and cells were seeded at the chosen density and incubated at 37°C and 5% CO_2. After cell adhesion (24 h of incubation), cells were starved for 6 h with serum-free media for cell cycle synchronization (Sharma et al., 2020). Scratching the monolayer cell culture causes cell rupture that leads to the release of mitogenic stimuli, which in turn promotes cell migration. This period of cell starvation with the serum-free medium before scratching minimizes the cells' endogenous migration (Cory, 2011).

After starvation, a scratch was made with one flowing single movement with a 100 µl micropipette tip, in a vertical position and guided by a ruler, to assure that the scratch was a straight line, had a uniform width, and that the scratches of the different exposure conditions had similar dimensions to minimize variability. After scratching, cell debris and suspended

cells were immediately removed by washing two times with PBS so the motility-released stimuli could be quickly (Cory, 2011). Cells were then exposed for 72 h to preussin at 35, and 50 μM, prepared in serum-reduced cell culture medium (DMEM) with 1% FBS (v/v), to reduce proliferation stimuli, and with 1% penicillin/streptomycin (v/v) (Ozman et al., 2021). As a negative control, cells were exposed only to the serum-reduced cell culture medium, as solvent control cells were exposed to 0.1% DMSO (v/v) in the serum-reduced cell culture medium, and intern control cells were exposed to DMEM with 10% FBS. After getting the first results, the preussin concentrations were diminished to 5, 15, and 25 μM.

Two different fields of each scratch were photographed using the inverted phase-contrast microscope CKX41 microscope with an objective lens of 2x amplification and coupled with an M5DC-CYL camera (Pixellink, New York, USA) at time points of 0 h, 24 h, 48 h, and 72 h. This assay was performed in 5 independent experiments with 3 replicates per condition. MDA-MB-231 cell migration was assessed, with free Fiji software (version 1.53c, National Institute of Health, Maryland, USA), at different time exposures. The acquired images were initially converted into binary images. Then, a region of interest of the scratch was selected by cropping the image laterally, by selecting the central 2/3 of the image (assessed by the Grid function of the Fiji software) and at the front of migration (horizontal line at a point with high cell density). The cropping limits were obtained by drawing a rectangle, and the area of interest was obtained by cropping the image through the selected limits of the rectangle. The area of the region of interest of the scratch was obtained with the function of “Area fraction” which allowed the exclusion of the cells present in the middle of the scratch.

The percentage of migration was evaluated as described by (Ramos et al., 2019):

$$\textbf{Migration}\ (\%) = \frac{\text{wound area at 0 h - wound area at 24, 48, or 72 h}}{\text{wound area at 0 h}} \times 100$$

The assay was performed as five independent assays with triplicates per exposure condition.

7. Proliferation assay – 5′-bromo-2′-deoxyuridine (BrdU) assay

To evaluate preussin effects on cell proliferation, BrdU assay was performed with the Cell Proliferation ELISA, BrdU (colorimetric) kit (Roche, Switzerland), both in monolayer and MCAs cell culture as described by the manufacturer with some modifications, mainly for 3D cell culture, as described by Malhão et al. (2019).

The BrdU assay allows for indirect detection of cell proliferation by measuring the incorporation of BrdU into the newly synthesized DNA. BrdU is a pyrimidine analog that, in proliferating cells, during cell division, will be incorporated into the DNA in substitution for thymidine. The incorporated BrdU can later be detected through ELISA techniques using anti-BrdU antibodies. In this way, the number of proliferating cells in the sample should be proportional to the quantified incorporated BrdU (Gauthier et al., 2003).

7.1. BrdU assay in monolayer cell culture

To perform the BrdU assay in MDA-MB-231 cells in 2D cell culture, 100 µl of cell suspension at a density of 5 x10^4 cells/ml were seeded in 96-multiwell culture plates and incubated at 37°C and 5% CO_2 for 24 h, for cell adhesion. After adhesion, the cells were exposed to 25 or 35 µM of preussin and incubated at standard conditions for 72 h. Negative control, solvent control, and positive control groups were also added. An additional blank control group in which the solutions of exposure and control groups were added to wells without cells, to obtain background A measurements.

After exposure, DNA was labeled by incorporation of BrdU, by adding 10 µl of BrdU labeling reagent to each well (final concentration of 10 µM) and incubating cells for 2 h at 37°C and 5% CO_2. After removing the labeling medium, the cells were dried for 1h at 60 ºC and stored at 4 ºC overnight. The following day, the cell DNA was denatured with 200 µl of FixDenat reagent for 30 minutes at room temperature. The denaturing reagent was removed, and 100 µl/well of working solution of the monoclonal antibody mouse anti-BrdU conjugated with peroxidase (1:100 dilution) was added to each well and incubated at room temperature for 90 min, for detection of BrdU incorporation into cellular DNA. Furthermore, the wells were washed 3 times with 200 µl/well of washing solution (1x PBS) and incubated with tetramethylbenzidine substrate solution at room temperature for 30 min, for later photometric detection. At last, the A was measured at 370 and 492 nm with the microplate reader Multiskan™ GO Microplate Spectrophotometer. The developed color, and consequently the measured A should directly correlate to the amount of synthesized DNA and, in this way, to the number of proliferating cells. The percentage of cell proliferation was calculated, first by obtaining the difference between the measured A at 370 nm and the measured A at 492 nm, from each well, followed by subtraction of the mean A of the blank groups to the mean A of the exposed cells. At last, cell proliferation was calculated in relation to the control group through the following equation:

$$\textbf{Cell proliferation}\ (\%) = \frac{\text{A of sample}}{\text{A of control}} \times 100$$

7.2. BrdU assay in MCAs cell culture

The BrdU assay in MCAs was performed with modifications to the protocol described for monolayer cell culture.

As described before (3.1 MCAs obtention), MCAs were obtained and later exposed to preussin at 25 or 35 µM and incubated at 37°C and 5% CO_2 for 96 h. Negative control, solvent control, and positive control groups were also added and incubated in the same conditions. A blank control group was added, in which the solutions of exposure and control groups were added to wells without cells to obtain background A measurements. After exposure, 100 µl out of a total of 200 µl of medium were removed from each well (to have a final volume of 100 µl of the medium in each well), and 10 µl of BrdU labeling reagent were added to a final concentration of 10 µM. The MCAs were incubated for 4 h at 37°C and 5% CO_2, for DNA incorporation of pyrimidine. The MCAs were then transferred to a flat-bottom 96 well plate, carefully removing all the exceeding culture medium. The following steps followed the described for the monolayer cell culture (7.1 BrdU assay in monolayer cell culture). After drying at 60 °C for 1h and incubated overnight at 4 °C, the cells' DNA was denatured by incubating the MCAs with 10 µl of Fix Denat reagent, followed by incubation with 100 µl anti-BrdU-POD working solution for BrdU incorporation detection. At last, MCAs were incubated with Substrate Solution, and the A was measured at 370 and 492 nm, by photometric detection, with the microplate reader Multiskan™ GO Microplate Spectrophotometer Proliferation in exposed groups was calculated in relation to the control group as was described above (3.1 MCAs obtention).

8. Comet assay

8.1. Single-cell gel electrophoresis

The standard comet assay or alkaline single-cell gel electrophoresis (SCGE) is used to evaluate DNA damage and genotoxic effects of compounds in single cells. This assay detects strand breaks (double and single-strand breaks) and alkali-labile sites (Collins et al., 2008).

After embedding cells in a thin agarose gel, performing cell lysis and histone removal, it is possible to obtain structures occupied by DNA and with similar shape and size to the nucleus, called the nucleoids. DNA is organized as a supercoiled structure around histones to form nucleosomes. After histone removal, the nucleosomal organization is destroyed, but the negatively charged supercoiled structure of DNA is maintained. When DNA strand breaks are present, the loops of supercoiled DNA are relaxed. Therefore, when subjected to an electrophoretic field, the DNA migrates from the cathode towards the anode through the agarose gel, giving an image resembling a comet. After DNA staining, comets are observed under a fluorescence microscope and 100 comets are randomly selected to evaluate the % of DNA contained in the comet tail (Azqueta & Collins, 2013). The greater the % of DNA detected in the comet tail, the higher the number of relaxed DNA loops caused by the presence of strand breaks and, consequently, the higher the level of DNA damage.

Before performing the comet assay, the exposure conditions were evaluated for cell viability at 24 h of exposure through the MTT assay; as already described in section 4 - Viability assay - MTT assay, both for monolayer and MCAs cell culture (sub-sections 5.1 and 4.2, respectively). Since the tested conditions had viability higher than 70%, the comet assay was executed. The obtained results are the outcome of 5 independent experiments (triplicates were performed), each executed on different days.

The genotoxicity effects of preussin were also evaluated at 2 h and 24 h of exposure, by the alkaline version of the comet assay as described by Malhão et al. (2021), both in monolayer and MCAs.

In monolayer cell culture, 1×10^5 cells/ml were seeded in a volume of 500 µl, in 24 well plates. These cells were incubated at 37°C and 5% CO_2 for 24 h, for cell adhesion. MCAs were acquired as described in the sub-section 3.1 MCAs obtention. After that, monolayer and MCAs were exposed to preussin at 25 and 35 µM, for 2h and 24h at 37°C and 5% CO_2. Simultaneously, negative control (cells treated with medium) and solvent control (cells treated with 0.1% DMSO) groups were performed. The positive control (cells treated with H_2O_2 for alkaline) was also included, as described below.

After 2 and 24 h of exposure, cells were washed 2 times with PBS and trypsinized as described above in sub-section “5.1 Clonogenic assay in monolayer cell culture”, for the monolayer cell culture, and in sub-section “3.2 MCAs disaggregation”, for the MCAs. After trypsinization, cells were immediately transferred into an ice bath to avoid cellular repair (Collins et al., 2008). The cell density and viability of each condition, both in monolayer and MCAs,

were evaluated with the trypan blue exclusion assay using an automated cell counter Countess™ (Invitrogen, Massachusetts, USA). Then, approximately 3 × 10^4 cells per condition (the equivalent of 5 ×10^3 cells per gel) were collected in 1.5 ml tubes, centrifuged at 1500 g for 10 s in a MicroStar12 centrifuge (VWR, Pennsylvania, USA), and immediately transferred to ice protected from light. The supernatant was completely removed, and the cells were gently resuspended in 470 µl of LMP agarose at 0.5% (w/v) in PBS, pre-heated to 37 °C (Note: LMP agarose was kept in 2 ml aliquots at 4 °C and each aliquot was heated only once to avoid alteration in LMP agarose concentration caused by evaporation). From this cell suspension, 70 µl were pipetted into 1% (w/v) NMP agarose-coated microscope slides. The slides were previously prepared by dipping conventional microscope slides in liquid NMP agarose at 1% (w/v), let dry for 24 h at room temperature, and stored protected from dust. After dispensing the cell suspension in LMP agarose into the slide, a 22 x 22 mm coverslip was immediately placed on top, and the slide was transferred to a cold horizontal surface to obtain the gel. Per experimental condition, 3 slides (with 2 gels each) were performed (one to be kept in a lysis solution, the other in buffer F, and the last to incubate with FPG). To be used as a positive control for the alkaline standard version of SCGE, two additional slides from the negative control conditions (2D or 3D cell culture) were also collected. The slides were kept horizontally at 4 °C for 10 min, for complete gel solidification. After this time, the coverslips were carefully removed by sliding them through the gel. At this stage, to obtain the positive control of the alkaline SCGE, 2 gels of the same slide, with cells from the control conditions (from 2D or 3D cell culture) were either exposed to cold 50 µM of H_2O_2 in PBS or PBS, for 5 min on ice protected from light and later washed with cold PBS.

For cell lysis and, consequently, DNA release, all the slides were treated with a lysis solution [2.5 M NaCl, 100 mM Na_2EDTA, 10 mM Tris Base, at pH 10, with 1 % (v/v) Triton X-100 added right before use] for 1 h at 4 °C in the dark. The positive control and exposure groups slides were incubated separately in lysis solution to avoid DNA damage caused by H_2O_2 residues. After lysis, all the slides were washed with distilled water and in cold electrophoresis buffer [0.3 M NaOH and 1 mM Na_2EDTA, pH>13]. For DNA unwinding, the slides were transferred into the electrophoresis chamber and incubated in the electrophoresis buffer for 40 min at 4 °C protected from light. Later, the electrophoresis of the gel-embedded bodies, nucleoids, was taken at 21 V (1 V/cm) for 20 min at 4 °C, protected from light. The slides were washed with distilled water three times for 5 min each and then dehydrated in absolute ethanol three times for 5 min each. After dehydration, they were left to dry at room temperature.

Right before analysis, the slides were stained for 30 min with a freshly thawed aliquot of SyberGold™ staining solution, at a final dilution of 1X in Tris-EDTA (TE) Buffer [10 mM Tris-HCl and 1 mM EDTA, pH 7.5], under slight agitation and protected from light. Slides were washed with deionized and left to dry at room temperature, also in the dark, and analyzed with a Motic BA410 ELITE microscope, attached to an epi-fluorescence illuminator Motic MXH-100 power supply for HG 100W, with 100x magnification (Filter Set: Exciter D480/30x, Emitter D535/40nm, Dichroic 505DCLP) (Motic, Kowloon, Hong Kong). For each condition, 100 non-overlapping, randomly selected comets were evaluated from duplicated gels (50 from each gel), avoiding the comets from the edge of the gels. For comet analysis and image capture, Comet Assay IV™ software (Instem PLC, Staffordshire, United Kingdom) was used, and the cell DNA damage was measured through the percentage of DNA in the comet tail (% tDNA). The results are expressed as % tDNA of five independent assays, each performed on different days.

8.2. Detection of FPG-sensitive sites

Cells quickly repair single-strand breaks. Therefore, they may represent less relevant DNA damage than other types of DNA damage that can be mutagenic and have higher effects on viability and genetic stability. For this reason, other types of DNA damage, such as adducts, cross-links, and oxidized and alkylated bases, should also be evaluated. Accordingly, lesion-specific enzymes, like the formamidopyrimidine DNA glycosylase (FPG), may be used. FPG enzyme allows the detection of DNA oxidative damage through the detection of FPG-sensitive sites. FPG enzyme has the capability to remove oxidized purines (like 8-oxo-7,8-dihydroguanine or formamidopyrimidines) and adducts of ring-opened N7 guanine formed by alkylating agents. This removal of oxidized purines by the FPG in the enzymatic version of the comet assay results in (abasic) apurinic or apyrimidinic (AP) sites in DNA. These abasic sites are converted into DNA strand breaks, by the activity of an AP lyase enzyme or by incubating the nucleoids in the highly alkaline electrophoresis buffer (Azqueta & Collins, 2013).

The genotoxicity effects of preussin were also evaluated by the enzymatic version of comet assay at 2 h and 24 h of exposure, as described by the FPG supplier, both in monolayer and MCAs (New England Biolabs, n.d.). For this assay, $KBrO_3$ was selected as a positive control for the enzymatic version of the comet assay, as described by (Møller et al., 2020). The positive controls were optimized for the MDA-MB-231 cell line, cultured at monolayer and MCAs cell culture conditions.

Monolayer and MCAs were obtained and exposed as previously described in sub-section 8.1 Single-cell gel electrophoresis. Furthermore, as a positive control, for the enzymatic version of the SCGE, cells in monolayer and MCAs conditions were exposed to $KBrO_3$ at 4.5 mM in supplemented DMEM (100 µl in monolayer cell culture and 200 µl in MCA's) for 1 h, at standard incubation conditions (Møller et al., 2020).

After exposure, monolayer and MCAs cells were collected into 1.5 ml tubes, counted, and the gels were obtained and subjected to lysis as also described above (8.1 Single-cell gel electrophoresis). After lysis, the slides were washed three times for 5 min at 4 °C with cold buffer F. This was prepared as a stock solution of 10 ×, with pH adjusted to 8, kept at -20 °C and diluted, right before use, to a concentration of 1 × with 40 mM HEPES, 0.1 M KCl, 0.5 mM EDTA, 0,2 % (w/v) BSA. The excess of buffer F was dabbed from the slides and 50 µl of either buffer F or FPG enzyme at a dilution of 1:10000 in buffer F were pipetted onto the gel surface. The concentration of enzyme required was previously optimized for this cell type. The gels were covered with a 22 x 22 mm coverslip and incubated in a moist box at 37°C for 30 minutes, protected from light. The alkaline treatment, electrophoresis, dehydration, staining, and % tDNA quantification, were carried out as described previously (8.1 Single-cell gel electrophoresis). For the evaluation of FPG-sensitive sites, the mean of the % tDNA from buffer F incubated slides was subtracted from the obtained mean of the % tDNA of the slides incubated with the FPG enzyme. Five independent assays were performed, each on different days.

9. Annexin V - PI assay

The annexin V - PI assay is used for the detection of apoptotic membrane changes allowing the distinction of early apoptosis from late apoptosis/necrosis (Crowley et al., 2016). Annexin V is a protein capable of sensitively binding, in a calcium-dependent manner, to the phosphatidylserine residues of phospholipids in the presence of calcium, which are normally found in the innermost layer of the cell membrane. During early apoptosis, this residue is translocated to the outer phospholipidic layer (with loss of plasma membrane asymmetry) of the cell membrane, and with the usage of a fluorochrome-labeled annexin V protein, it is possible to identify apoptotic cells. If a DNA labeling compound is simultaneously used, such as PI, it is possible to distinguish early apoptotic from late apoptotic and necrotic cells. In the late apoptotic and necrotic stages, cells show membrane disruption, allowing the DNA to be stained by the PI. In early apoptotic cells, despite the changes in the cell membrane asymmetry, the membrane integrity is preserved, and the DNA dye cannot enter the cell. In

this way, viable cells will appear unstained, early apoptotic cells will stain only with the labeled Annexin V, and the late apoptotic and necrotic cells will appear both stained by the labeled Annexin V and by the PI (Crowley et al., 2016; Vermes et al., 1995).

To analyze if preussin could induce cell death and whether it would be early or late apoptosis, or necrosis the Annexin V-PI was performed by flow cytometry. For monolayer cell culture, 2 x10^5 cells/well were seeded in 6 well plates at a density of 1x10^5 cells/ml and left to adhere for 24 h. The cells were then exposed to preussin for 72 h at the concentrations of 25 and 35 µM (the concentrations that exerted an effect on cell viability at these incubation conditions). After exposure, the supernatant was collected into 15 ml tubes, and the remaining adherent cells were collected by trypsinization. First, the cells in monolayer cell culture were washed two times with 1ml of PBS. Secondly, the cells were incubated for 3 min with 500 µl of trypsin-EDTA, and later the effect of the enzyme was stopped by adding 1 ml of supplemented cell culture medium, and the cells were collected into 15 ml tubes and centrifuged for 5 min at 280 g.

In 3D cell culture, three MCAs per triplicate were obtained (as described in section 3.1. MCAs obtention) and were exposed for 96 h to the selected conditions of preussin at 25 and 35 µM. Following, the supernatant and the MCAs were collected into 1.5 ml tubes and the cell disaggregation proceeded with trypsin-EDTA as described in section 3.2. MCAs disaggregation. Simultaneously, negative control, solvent control, and positive control (1 µM of Dox in 2D culture or 5 µM in MCAs) groups were added. To be used subsequently for the correction of the fluorescence data, additional MCAs and monolayer cell cultures of the negative control were maintained.

After cell collection, the monolayer and MCAs derived cell suspensions were centrifuged at 300 g, the supernatant removed, and the cells resuspended in 50 µl of Annexin V buffer. Then, 50 µl of the cell suspension were transferred into flow cytometry tubes and the cell suspensions were then incubated with 0.5 µl of FITC-conjugated Annexin V for 15 min at room temperature, protected from light. Right before analysis, 0.5 µl of PI at 0.25 mg/ml was added to each cell suspension. Cell analysis was performed using a FACSCanto II flow cytometer (BD Biosciences, New Jersey, USA) and the BD FACSDiva™ Software. Simultaneously from negative control cells (both from MCAs and monolayer cultures) flow cytometry controls were obtained (Annexin V, PI, and unstained controls), for later correction of fluorescence readings. The results were analyzed using the FlowJo™ v10 Software (BD Biosciences, New Jersey, USA). Before analysis, the data samples were corrected for fluorescence spillover emissions, a process called compensation, with the usage of single stained controls (stained only with Annexin V or PI). After compensation, the samples were

gated, first to exclude debris and, secondly, for the selection of single cells (with the exclusion of aggregated cells). At last, four-quadrant gates were defined based on the single stained controls. In this way, three cell populations were defined: alive cells (Annexin V−/PI), dead cells (Annexin V+/PI+ or Annexin V-/PI+), and apoptotic cells (Annexin V+/PI-). The assay was performed in 5 independent replicates (each on different days) with triplicates for each replicate.

10. Morphological analysis

10.1. Phase-contrast microscopy and stereomicroscopy

For every executed assay, either in a monolayer or 3D cell culture model, a daily analysis of the morphological alterations caused by the exposure to preussin was performed. Whenever the defined time point was reached and before proceeding with the assay, representative images of the structural changes in each condition were acquired (for every assay and cell culture model). For the monolayer cell culture, the cells were photographed with a CKX41 inverted phase-contrast microscope using an M5DC-CYL camera. As for 3D cell culture, the MCAs were photographed with an SZX10 stereomicroscope using the darkfield filter and a DP21 camera (Olympus, Tokyo, Japan).

10.2. Electron microscopy

To observe ultrastructural alterations that could have been caused by the exposure to preussin, cells from monolayer cell culture and MCAs were collected and processed for electron microscopy. For monolayer cell culture, 2 x 10^5 cells/well were seeded in 6 well plates at a density of 1 x 10^5 cells/ml, for 24 h at 37°C and 5% CO_2. In its turn, two MCAs per condition were obtained as described in section 3.1 MCAs obtention. After obtaining the cell cultures, the MCAs and the cells in monolayer cell culture were exposed to preussin at 5, 15, 25, and 35 µM, either for 72 h (monolayer cell culture) or 96 h (MCAs), at 37°C and 5% CO_2. Simultaneously, negative control, solvent control, and positive control (1 µM of Dox in 2D culture or 5 µM in MCAs) groups were added. After the defined time exposures, monolayer cell culture cells were harvested through trypsinization by first washing two times with 1ml of PBS and later adding 500 µl of trypsin-EDTA. After 3 min, the effect of the enzyme was stopped by adding 1 ml of supplemented cell culture medium, and the cells were collected into 1.5 microtubes and centrifuged for 5 min at 280 g. The supernatant was removed, and the cells were immediately fixed for 2 h at 4 °C, with freshly prepared 2.5%

glutaraldehyde in sodium cacodylate-HCl buffer (0.1 M, pH 7.2). In MCAs, after exposure, 150 µl of cell culture medium was removed and the same volume of fixative was added for 15 min. The MCAs were then collected into 1.5 ml tubes with a 1000 µl pipette whose tip was cut off, to enlarge its diameter and avoid MCAs destruction. The exceeding medium was removed, and the MCAs were fixed as described above for the monolayer cell culture.

After fixation, cells were washed 2 times with the same 0.1 M cacodylate buffer (10 min each) and post-fixed in 1% osmium tetroxide in the same buffer for 2 h at 4 °C. Cells were then washed 2 times with 0.1 M cacodylate buffer (10 min each) and dehydrated in 50% ethanol, 70%, ethanol, 96% ethanol, two times in absolute ethanol, and two times in propylene oxide, for 30 min in each step. Cells were then gradually embedded in epoxy resin through the usage of a gradient of concentrations of the epoxy with propylene oxide (respectively in the proportions of 1:3; 1:1 and 3:1), and a final solution of only epoxy resin, for 1h in each step, plus 10 min at 60 °C for evaporation of propylene oxide residues. At last, the monolayer cells and the MCAs were placed in electron microscopy rubber embedding molds with freshly prepared epoxy resin and incubated for 48 h at 60 °C, for resin polymerization. After polymerization, the hardened blocks were manually trimmed with a razor blade and later sectioned with an EM UC7 ultramicrotome (Leica, Wetzlar, Germany) with diamond knives (Diatome, Nidau, Switzerland). First, 1 µm semithin sections were collected onto adhesive glass microscope slides (VWR, Pennsylvania, USA) and stained with a 1:1 mixture of 1 % methylene blue and 1 % azure II. After washing with distilled water, drying at 60 °C, and mounting with the synthetic mounting medium, Bio Mount HM (Bio-Optica Milano, Italy), the slides were observed under a BX50 microscope (Olympus, Tokyo, Japan) and photographed with an EP50 Microscope Digital Camera (Olympus, Tokyo, Japan) camera. For ultrastructural analysis, 90 nm thick ultrathin sections were obtained(Reynolds, 1963). The grids were later observed under a JEOL 100CXII transmission electron microscope (JEOL, Tokyo, Japan), operated at 60 kV. Representative photographs of the ultrastructural changes were captured using an Orius SC1000 CCD digital camera (Gatan, California, USA). The assay was performed using independent duplicates.

11. Statistical analysis

Statistical analysis was performed using GraphPad Prism 9.0 software (GraphPad Software, California, USA). The results are presented as mean ± standard deviation (SD), from five independent assays. Statistical significances ($p < 0.05$) were evaluated using the One-Way ANOVA test followed by the post-hoc Holm-Šídák multiple comparisons (between the

negative control and the exposed groups); when the ANOVA displayed significant differences. The ANOVA assumptions of normality and homogeneity of variance were confirmed by the Shapiro-Wilk's and Levene's tests, respectively, using the PAST 4.09 software (Hammer et al., 2001). Whenever the homogeneity of variances was not observed, the differences were assessed by the Welch ANOVA test. When this indicated significant differences ($p < 0.05$), Dunnett's T3 multiple comparisons test was applied.

The significance of the results is indicated according to the p values with one, two, three, or four of the used symbol (*) corresponding, respectively, to a p-value inferior to 0.05, 0.01, 0.001, 0.0001.

Results

1. Assessment of cell viability – MTT assay

1.1. Monolayer cell culture

In 2D cell culture, cell viability effects of preussin in the TNBC cell line MDA-MB-231 were accessed by the MTT assay after 24, 48, and 72 h of incubation. For comparison purposes, several control groups were used: negative control with untreated cells (cells incubated only with cell culture medium), solvent control with cells exposed to 0.1% (v/v) DMSO, and positive control with cells exposed to Dox at 1 μM.

Preussin showed an accentuated effect on cell viability over time (Figure 6). Cells exposed to preussin at 50 μM showed a decrease in cell viability even at 24 h of exposure, with a decrease of cell viability to 36.4%, in relation to the control. At 35 μM, preussin could decrease cell viability in comparison to the negative control at times of exposure above 48 h. At 48 h of exposure, preussin at 35 μM showed a decrease in cell viability, below 45.5%, and at 72 h the cell viability was 29.1% (compared to the negative control group) (Figure 6b and c). At 72 h of exposure, preussin at 25 μM was the lowest concentration to decrease the cell viability significantly to 67.5 %, compared to the negative control (Figure 6c). Similarly to what was observed for preussin at 35 μM, Dox at 1 μM only exhibited decreased cell viability with incubation times above 48 h, showing cell viability of 65.9% and 33.1% at 48 h and 72 h of exposure, respectively (Figure 6b and c, respectively). There were no statistically significant differences between negative control and solvent groups at all exposure times (Figure 6).

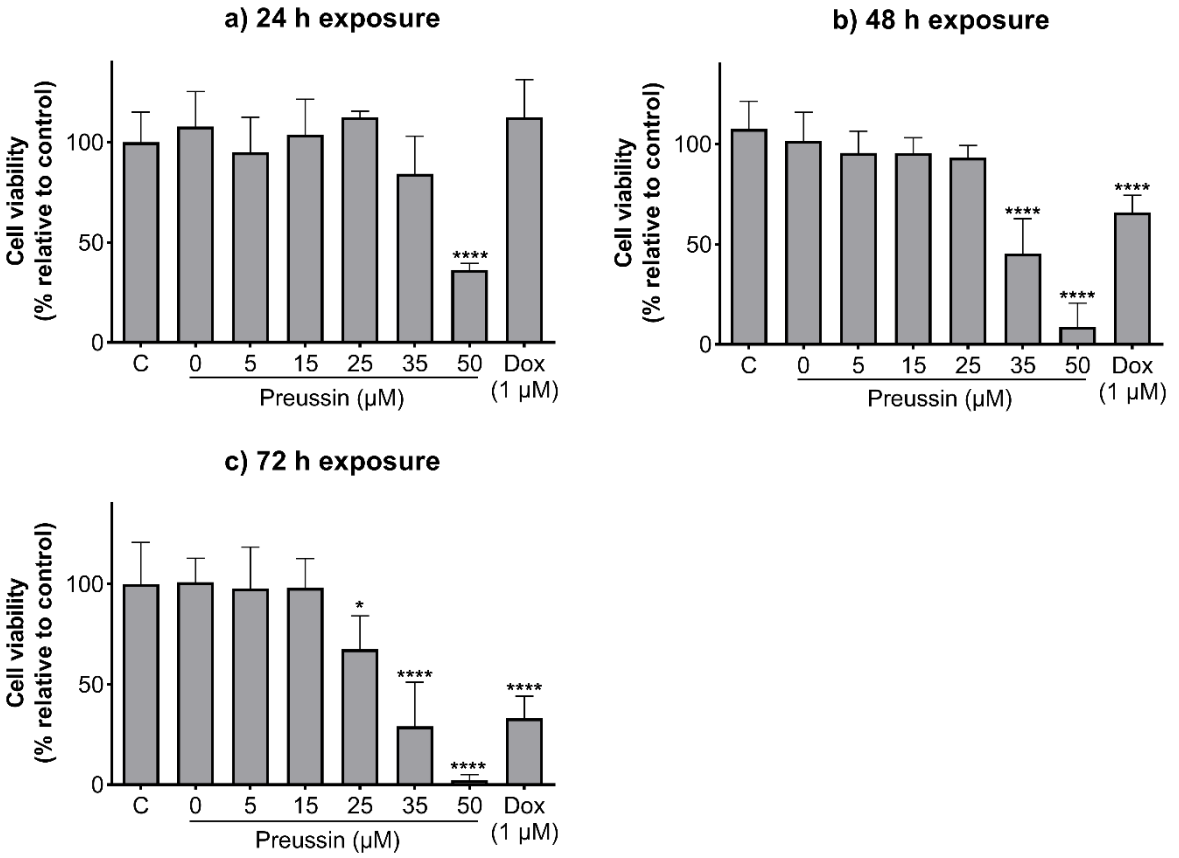

Figure 6 – Effects of preussin on cell viability of MDA-MB-231 cells in monolayer cell culture assessed by the MTT assay after 24 h (**a**), 48 h (**b**), or 72 h (**c**) of exposure. Negative control (C) (cells in cell culture medium), solvent control (0 µM of preussin and 0.1% of DMSO), and positive control (cells exposed to 1 µM of Dox) groups were included. The results are expressed as the percentage of cell viability relative to the negative control and are expressed as mean ± SD of n=5. Significant differences, represented with asterisks (* $p<0.05$; ** $p<0.01$; **** $p<0.0001$) were tested by one-way ANOVA, followed by post-hoc Holm-Sidak's multiple comparison test.

1.2. MCAs

The effects on cell viability of the selected concentrations of preussin, in MDA-MB-231 cells cultured as MCAs, were accessed by the MTT assay, after 96 h of incubation. Negative control (with cells incubated only with culture medium), solvent control (with cells exposed to 0.1% (v/v) DMSO), and positive control (with cells exposed to Dox at 5 µM), were added for comparison.

With 96 h of exposure, all the tested concentrations of preussin showed decreased cell viability when compared to the control, as shown in Figure 7. This decrease was higher at 50 µM of preussin, where the observed cell viability was 33.4%. At 25 and 35 µM of preussin and 5 µM of Dox, the decrease in cell viability was similar to the cell viability calculated

values of 72.3%, 67.7%, and 65% (Figure 7). Statistically significant differences were not observed between the negative control and the solvent control groups (Figure 7).

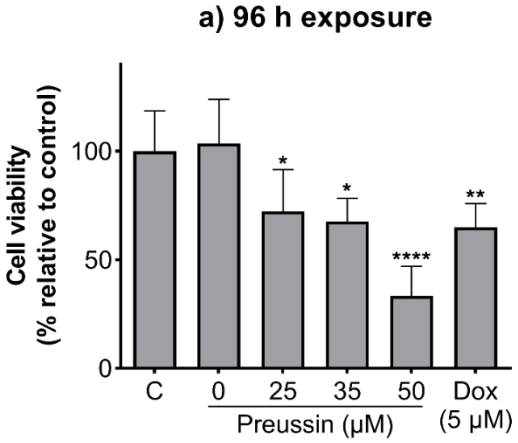

Figure 7 – Effects of preussin on cell viability in MDA-MB-231 cells, cultured as MCAs, assessed by the MTT assay after 96. Negative control (C) (cells in cell culture medium), solvent control (0 µM of preussin and 0.1% of DMSO), and positive control (cells exposed to 5 µM of Dox) groups were included. The results are expressed as the percentage of cell viability relative to the negative control and are expressed as mean ± SD of n=5. Significant differences, represented with asterisks (* $p<0.05$; ** $p<0.01$; **** $p<0.0001$) were tested by one-way ANOVA, followed by post-hoc Holm-Sidak's multiple comparison test).

2. Analysis of long-term survival – clonogenic assay

The effects of preussin on long-term survival were evaluated with the clonogenic assay, both in monolayer and MCAs. After 72 h (monolayer cell culture) or 96 h (MCAs) of exposure, 500 cells, per condition, were seeded in 6 well plates and left to grow for 21 days. After staining with crystal violet, the obtained colonies, composed of 50 or more cells, were counted using a stereomicroscope. Both in monolayer and MCAs, negative control with cells in culture medium only, solvent control with cells exposed to 0.1% (v/v) DMSO, and positive control with cells exposed to Dox at 1 µM (in monolayer cell culture) or 5 µM (MCAs), were added. Initially, we proposed to test the effects of preussin in long-term survival with concentrations of 35 and 50 µM. After the 72 h or 96 h of exposure (in 2D and 3D cell culture models, respectively), it was observed that in the 50 µM preussin exposed groups, the levels of cell death were high enough to make it impossible to re-seed 500 cells to proceed with the assay (in both cell culture models). For this reason, a set of lower concentrations (5, 15, 25, and 35) were selected to evaluate the effects of preussin on long-term survival.

In all the exposure conditions, the obtained colonies were not uniform (Figure 8). Some of the colonies were small and composed of densely packed cells. These cells appeared light-

stained, round-like to spindle-shaped cells (Figure 8a). Other colonies appeared to be bigger in diameter, irregularly shaped, and constituted by dispersed heavily stained slender cells (Figure 8b). The last type of observed colonies showed a mixture of the characteristics described for the colony types described above. These colonies were irregular-shaped and composed not only of both spindle-shaped slender and densely stained cells but also of spindle-shaped with abundant and lightly stained cytoplasm cells, as observed in Figure 8c. No specific distribution of the type of colonies was observed between the different groups of exposure or between the model of culture.

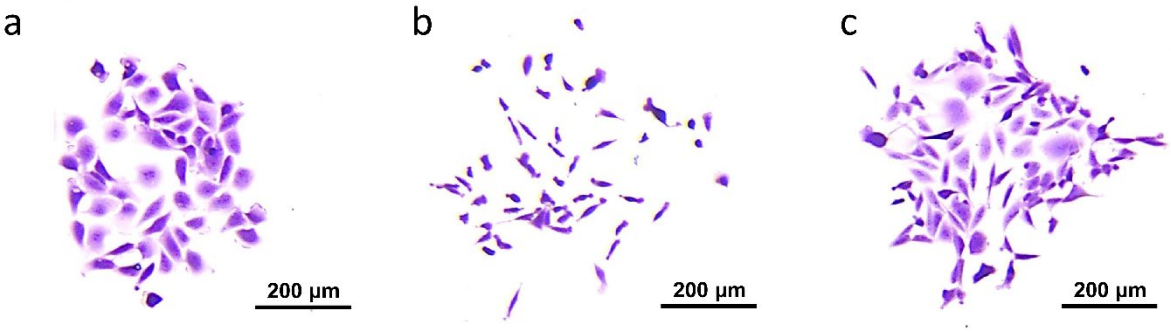

Figure 8 – Representative images of the colony types obtained for the MDA-MB-231 cell line in the clonogenic assay. Small colonies and composed of densely packed round-like to spindle-shaped cells cells (**a**), Colonies of high diameter, irregularly shaped, with slender cells (**b**), and mixed colonies with spindle-shaped slender cells and round-like to spindle-shaped cells (**c**). After exposure (for 72 h in monolayer cell culture or 96 h in MCAs), 500 viable cells were incubated for 21 days in 6-well plates, for colony formation. The obtained colonies were later stained with crystal violet. Colonies were considered only when composed of 50 cells or more.

Overall, in the cells initially cultured and exposed as a monolayer, the number of obtained colonies was consistently higher than in those initially cultured and exposed as MCAs. As represented in Figure 9, the described trend existed in all the exposure groups (excluding the positive control group). Data from the positive control was not included in the statistical analysis since no colonies were observed, in any of the performed replicates, both from 2D and 3D cell culture models, as represented in Figures 9a and 9b, respectively.

Furthermore, in both cell culture models, high variability was observed in the number of obtained colonies between the independent replicates, which was more accentuated in the preussin-treated groups. This unevenness translates into high variability in the calculated surviving fractions. No statistically significant differences were observed between the negative and solvent control groups or between the negative control and the preussin exposed groups (Figure 10).

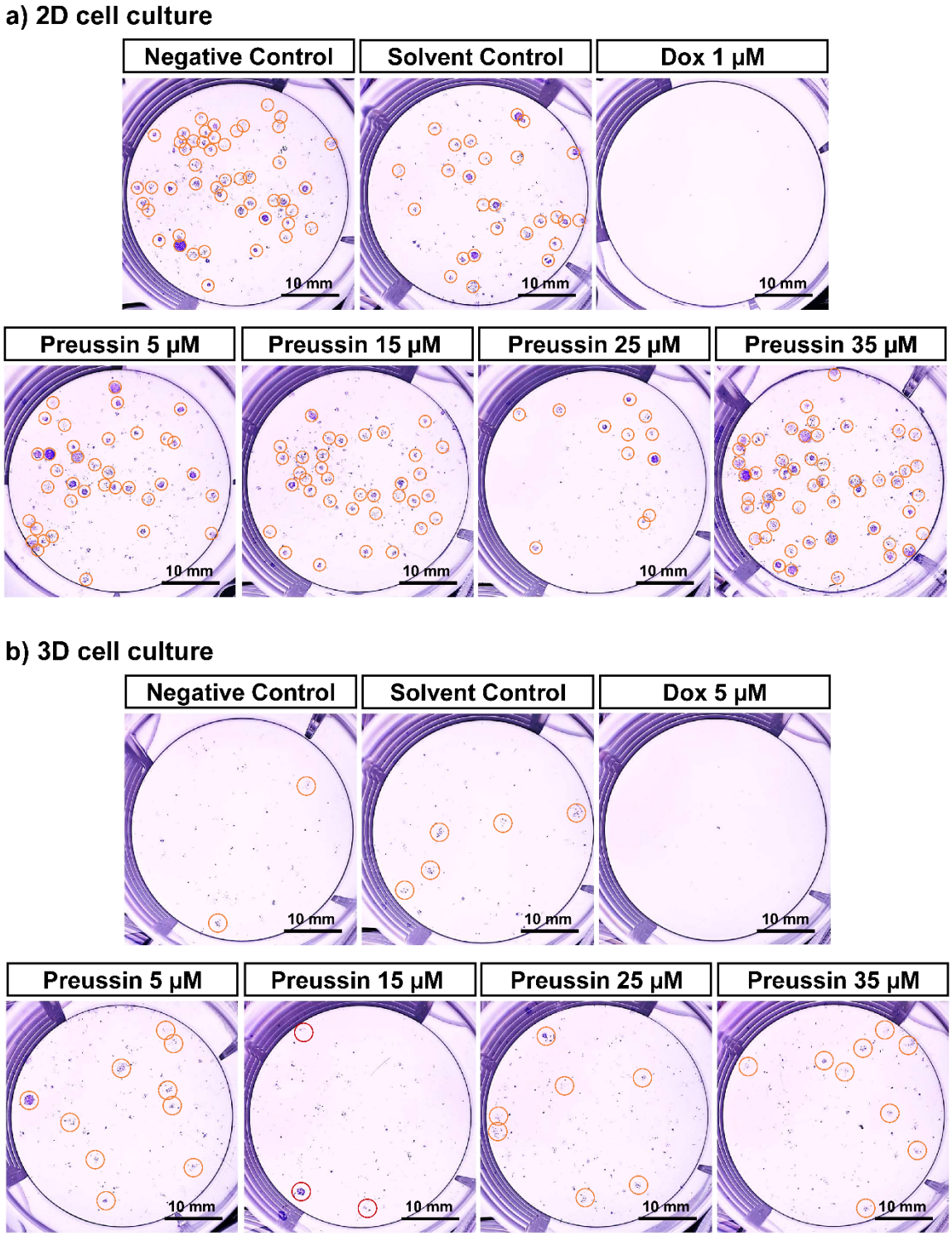

Figure 9 – Representative effects of preussin on colony formation capability on the MDA-MB-231 cell line, accessed through the clonogenic assay. Cells exposed to preussin in the 2D cell culture model (**a**) or in the 3D cell culture model (**b**). 500 viable cells were re-seeded in 6 well culture plates for 21 days. Colonies were stained with crystal violet, counted (colonies with 50 or more cells), and photographed in an inverted phase-contrast microscope. Cells exposed only to the cell culture medium and to 0.1% of (v/v) of DMSO were added as negative and solvent controls, respectively. Additionally, positive control of 1 µM of Dox in monolayer cell culture (**a**) or 5 µM of Dox in MCAs (**b**), was added. The counted colonies are encircled in orange.

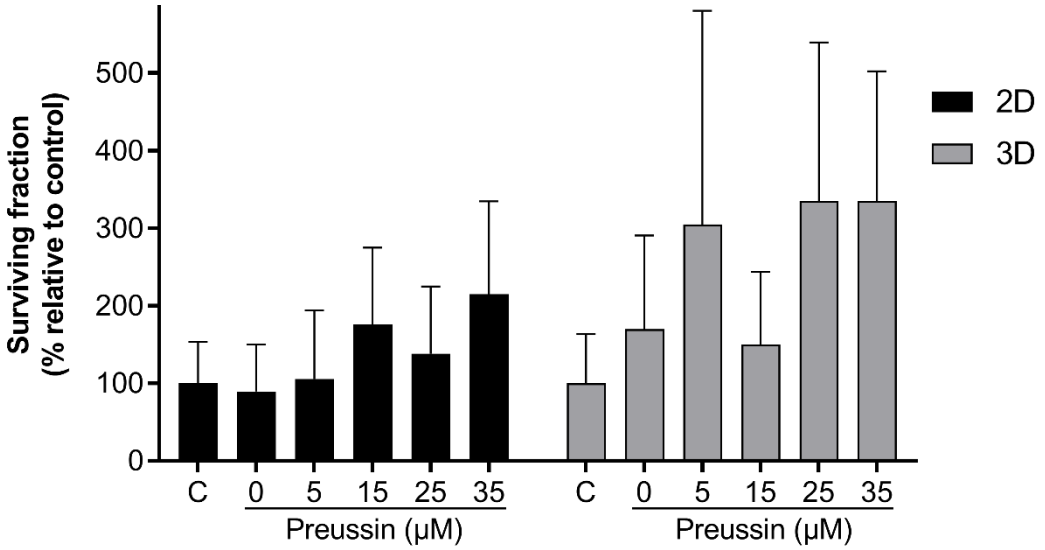

Figure 10 – Effects of preussin on long-term survival of MDA-MB-231 cells, cultured in 2D or 3D cell culture models, assessed by the clonogenic assay. After 72 h (monolayer cell culture) or 96 h (MCAs) of exposure, 500 cells were seeded in 6 well plates and incubated for 21 days. Negative control (C) (cells in cell culture medium), and solvent control (0 μM of preussin and 0.1% of DMSO) were included. The results are expressed as the percentage of surviving fraction relative to the negative control and are expressed as mean ± SD of n=5.

3. Effects on cell proliferation – 5′-bromo-2′-deoxyuridine (BrdU) assay

The BrdU assay evaluated whether the effects of preussin on cell viability in 2D and 3D cell culture models resulted from alterations in cell proliferation. The lower concentrations of preussin that exert an effect on cell viability (25 and 35 μM of preussin) were selected to evaluate its effects on cell proliferation. Cells cultured as a monolayer, and MCAs were exposed to 25 or 35 μM of preussin for 72 h (monolayer) or 96 h (MCAs). In both cell culture models, all the tested preussin concentrations induced a decrease in cell proliferation, which was more accentuated in the cells in the 2D cell culture model (Figure 11). In the cells cultured in monolayer, preussin significantly decreased cell proliferation by around 27.1 % and 7.6 % (compared to the negative control) for the concentrations of 25 and 35 μM, respectively (Figure 11a). As for the cells cultured in the 3D cell culture model, preussin showed a slightly lower effect in decreasing cell proliferation. Compared to the negative control group, the MCAs exposed to 25 μM of preussin showed a decrease in cell proliferation to 47.6 %, while 35 μM of preussin decreased cell proliferation to 25.7 % (Figure 11b). No statistically significant differences were observed in cell proliferation between the solvent and negative control groups. As for the positive control, in 2D and 3D cell culture models, Dox (at 1 μM in monolayer and 5 μM in MCAs) induced similar effects with a decrease in cell proliferation below 30 % when compared to the negative control groups.

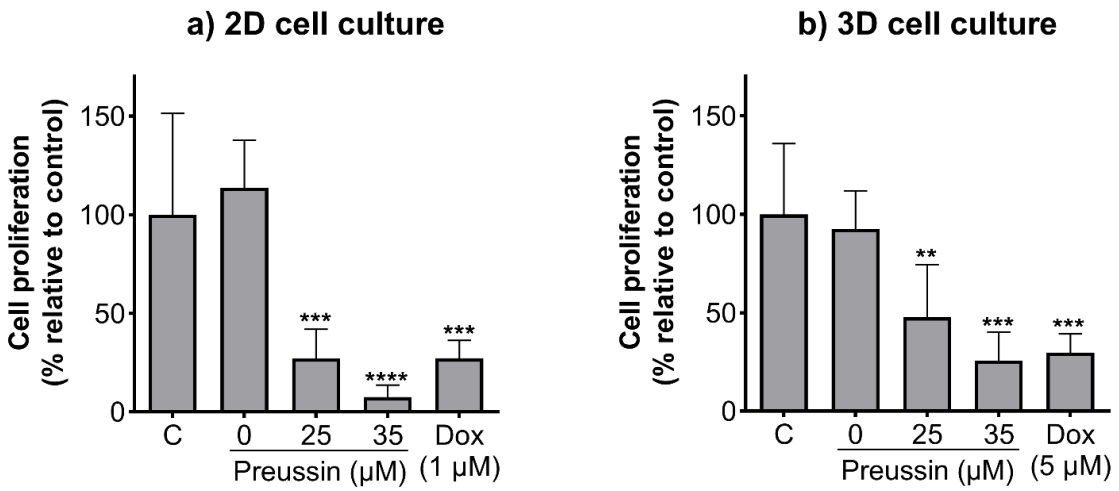

Figure 11 – Effects of preussin on cell proliferation of MDA-MB-231 cells, cultured as a monolayer and exposed for 72 h (**a**) or cultured as MCAs and exposed for 96 h (**b**), assessed by the BrdU assay. Negative control (C) (cells in cell culture medium), solvent control (0 μM of preussin and 0.1% of DMSO), and positive control (cells exposed to 1 μM (2D cell culture) or 5 μM (3D cell culture models) groups were included. The results are presented as the percentage of cell proliferation relative to the negative control and are expressed as mean ± SD of n=5. Significant differences, represented with asterisks (* $p<0.05$; ** $p<0.01$; *** $p<0.001$; **** $p<0.0001$) were evaluated by one-way ANOVA, followed by post-hoc Holm-Sidak's multiple comparison test.

4. Analysis of cell migration – *In vitro* scratch assay

The *in vitro* scratch assay evaluated the effects of preussin on MDA-MB-231 cell migration over time (at the time points of 24 h, 48 h, and 72 h of exposure). As a negative control, cells were exposed to the serum-reduced culture medium (DMEM supplemented with 1% FBS and 1% pen/strep), as solvent control cells were exposed to 0.1% DMSO (v/v) in serum-reduced culture medium, and as intern control cells were exposed to DMEM supplemented with 10% FBS.

The cells were initially exposed to preussin at a concentration of 35 or 50 μM. In the group exposed to 50 μM of preussin, all the cells presented shrunken and detached from the bottom after 24 h of exposure. As for cells exposed to 35 μM of preussin, after 24 h of incubation, some cells appeared buoyant (at a considerably higher number than what was observed for the control groups), and, after 48 h, all the cells were completely detached from the bottom of the plate, making unfeasible the measuring of the scratches (Figure 12).

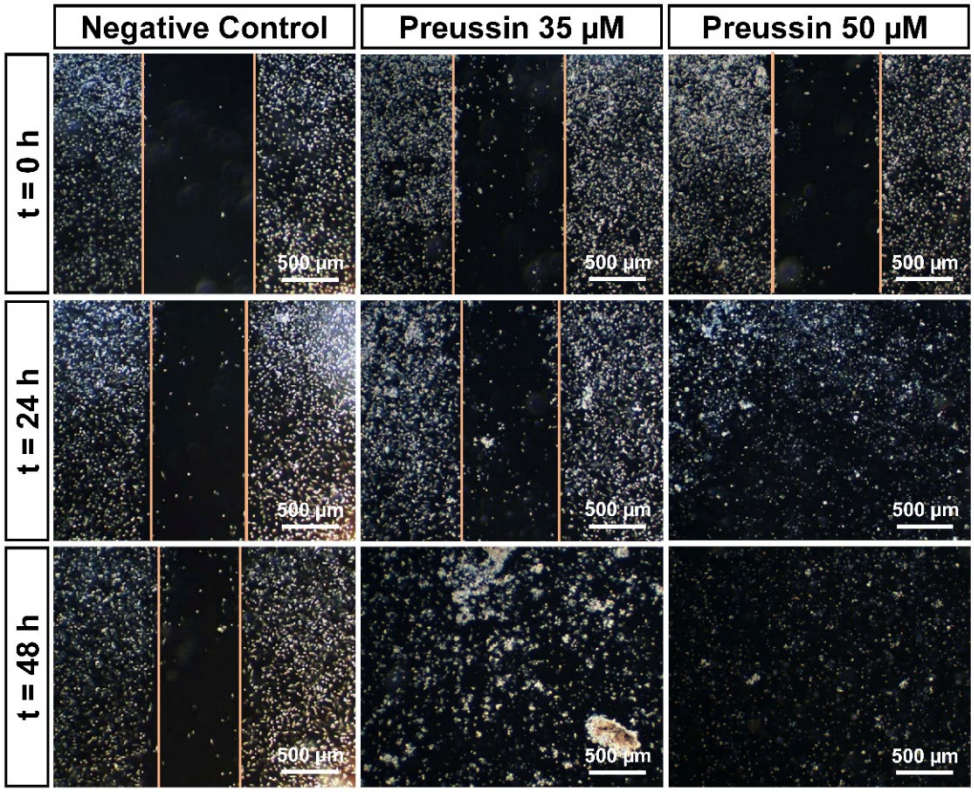

Figure 12 – Representative effects of preussin at 35 or 50 µM on cell migration, accessed through the *in vitro* scratch assay. Cells were seeded in a monolayer with high density, serum-starved for 6 h, scratched with a 100 µl micropipette tip, and exposed to the compounds in culture medium supplemented with 1% FBS. The scratches were photographed in an inverted phase-contrast microscope at 0 h, 24 h, and 48 h of exposure. The cells' front of migration is marked with orange lines. As solvent control, cells were exposed to culture medium with 1% FBS and 0.1% of (v/v) of DMSO.

The concentrations of 35 µM and 50 µM of preussin induced widespread cell death, making it impossible to measure the effects of this compound on cell migration. Therefore, lower concentrations of preussin (5 µM, 15 µM, and 25 µM) were selected to proceed with the assay.

All the tested preussin concentrations were visibly capable of decreasing cell migration, as demonstrated in Figure 13. After 24 h of exposure, cells exposed to preussin at 25 µM markedly decreased cell migration compared to solvent control. As for preussin at the concentrations of 5 µM and 15 µM, with higher exposure times, an accentuation of the preussin effect on cell migration was observed. At 25 µM of preussin, after 48 h of exposure, high levels of cell death were observed, with cells detached from the bottom of the plate. These aspects were also observed for cells exposed to preussin at 15 µM for 72 h (Figure 13). For this reason, no measures of the scratches were made for cells exposed for 48 h or 72 h to preussin at 25 µM or exposed for 72 h to preussin at 15 µM (Figure 14).

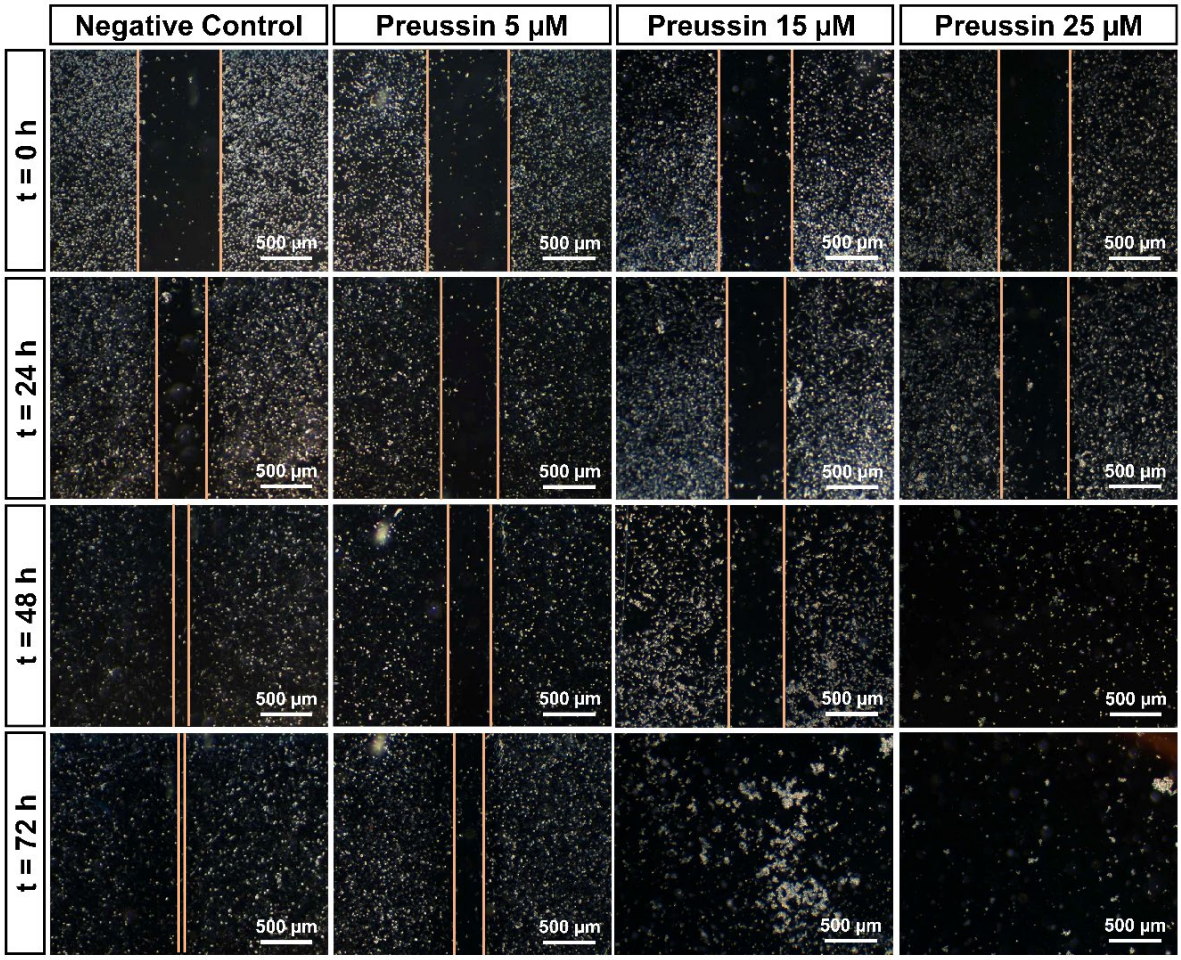

Figure 13 – Representative effects of preussin at 5, 15, and 25 µM on cell migration accessed through the *in vitro* scratch assay. Cells were seeded in a monolayer at a high density, serum-starved for 6 h, scratched, and exposed to the compounds in culture medium supplemented with 1% FBS. The scratches were photographed in an inverted phase-contrast microscope at 0 h, 24 h, 48 h, and 72 h of exposure. The cells' front of migration is marked with orange lines. As solvent control, cells were exposed to culture medium with 1% FBS and 0.1% of (v/v) of DMSO.

The effects on cell migration were analyzed by calculating the variation of the scratches' areas (in comparison to the area measured at 0 h). When compared to the negative control, all the tested concentrations of preussin could decrease cell migration at all the tested time points (Figure 14). After 24 h, the exposure to 5 µM of preussin decreased cell migration by 13.9 %, the exposure to 15 µM of preussin decreased cell migration by 21.68 %, and the exposure to 25 µM of preussin decreased cell migration by 26.89 % when comparing to the negative control group (Figure 14a). After 48 h of exposure, there was an accentuation of the effects of preussin on cell migration. While the measured migration ratio in the negative control was 67.4%, in the cells exposed to preussin at 5 µM and 15 µM, the measured migration decreased to 37.6% and 34.6%, respectively (Figure 14b). After 72 h of exposure, the negative, solvent, and intern controls showed almost complete closure of the scratches,

above 80 %. As for the cells exposed to 5 µM of preussin, a decrease of more than 30% in cell migration was observed compared to the negative control group, with a measured wound closure of 53.11% (Figure 14c). No statistically significant differences were observed between the control groups at any of the evaluated time points (Figure 14).

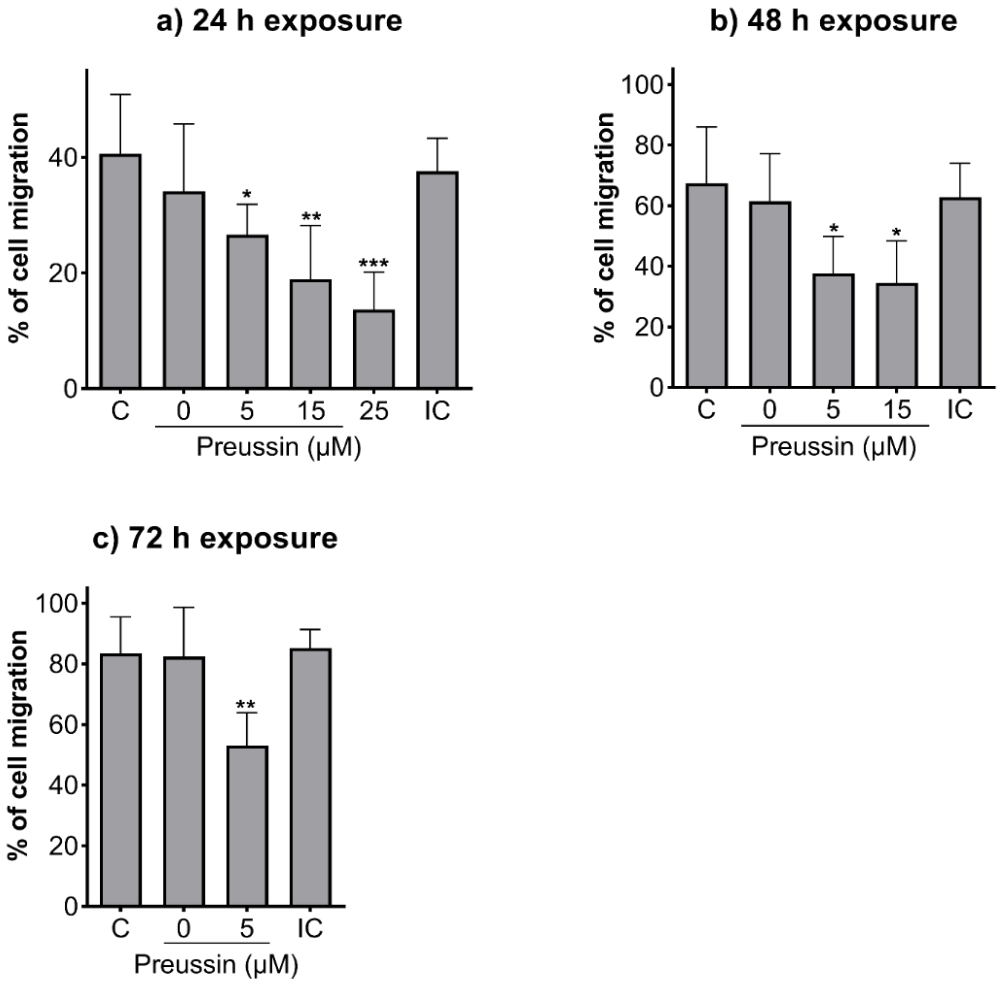

Figure 14 – Effects of preussin on cell migration of MDA-MB-231 cells cultured as a monolayer, after 24 h (**a**), 48 h (**b**), or 96 h (**c**) of exposure, accessed through the *in vitro* scratch assay. Negative control (C) (cells in DMEM supplemented with 1 % FBS), solvent control (0 µM of preussin and 0.1% of DMSO), and intern control (IC) (cells exposed to DMEM supplemented with 10 % FBS). The results are expressed as the percentage of cell migration and are expressed as mean ± SD of n=5 (three replicates per experiment). Significant differences, represented with asterisks (* $p<0.05$; ** $p<0.01$; *** $p<0.001$) were evaluated by one-way ANOVA, followed by post-hoc Holm-Sidak's multiple comparison test.

5. Detection of DNA damages – Comet assay

The standard and the enzymatic (with FPG enzyme) versions of alkaline SCGE evaluated if preussin has genotoxic effects and verified the type of DNA damage induced. Before proceeding with the assay, the selected concentrations of preussin (25 and 35 µM) were

evaluated for the effects on cell viability at 24 h of exposure through the MTT assay and confirmed that the results of the SCGE would not be impaired by high levels of cytotoxicity induced by the preussin exposure. The results obtained for the 2D cell culture model were already described (Section 1 Assessment of cell viability – MTT assay, subsection 1.1 Monolayer cell culture). In the MCAs, as was observed for the 2D cell culture, with only 24 h of exposure, neither preussin nor Dox was capable of decreasing cell viability when compared to the control (Figure 15).

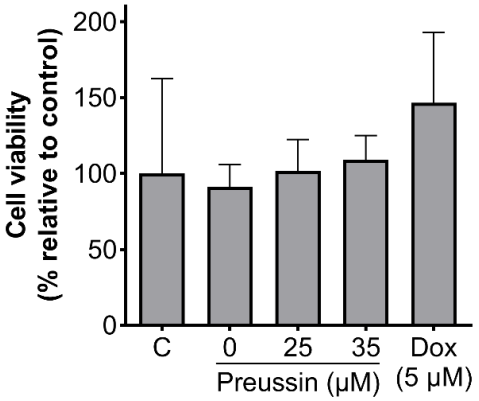

Figure 15 – Effects of preussin on cell viability in MDA-MB-231 cells, cultured as MCAs, assessed by the MTT assay after 24 h. Negative control (C) (cells in cell culture medium), solvent control (0 µM of preussin and 0.1% of DMSO), and positive control (cells exposed to 5 µM of Dox) groups were included. The results are expressed as the percentage of cell viability, relative to the negative control, and are expressed as mean ± SD of n=5.

Since no cytotoxicity was observed, the comet assay was implemented in cell monolayers and MCAs exposed to preussin at 25 or 35 µM for 2 and 24 h. No differences were observed in cell viability, between the negative control group and the exposure groups, at any time points, for the cells cultured either in 2D or 3D cell culture models (Figure 16). The cell viability measured through the trypan blue exclusion assay varied between 69 % and 83 %, with no significant differences between the cell culture model and the tested exposure time (Figure 16).

For each exposure condition, 3 slides (1 for the standard and 2 for the enzymatic versions of comet assay) with 2 gels each (with 5×10^3 cells per gel) were obtained. During analysis, in the cells with low levels of DNA damage, the DNA occurs as a nucleoid with no or a small tail (Figure 17a). As for cells with high levels of DNA damage, the DNA resembles the structure of a comet with a head and a tail with damaged DNA (Figure 17b). The higher the levels of DNA damage, the smaller the head of the comet and the higher the percentage of DNA observed in the comet's tail.

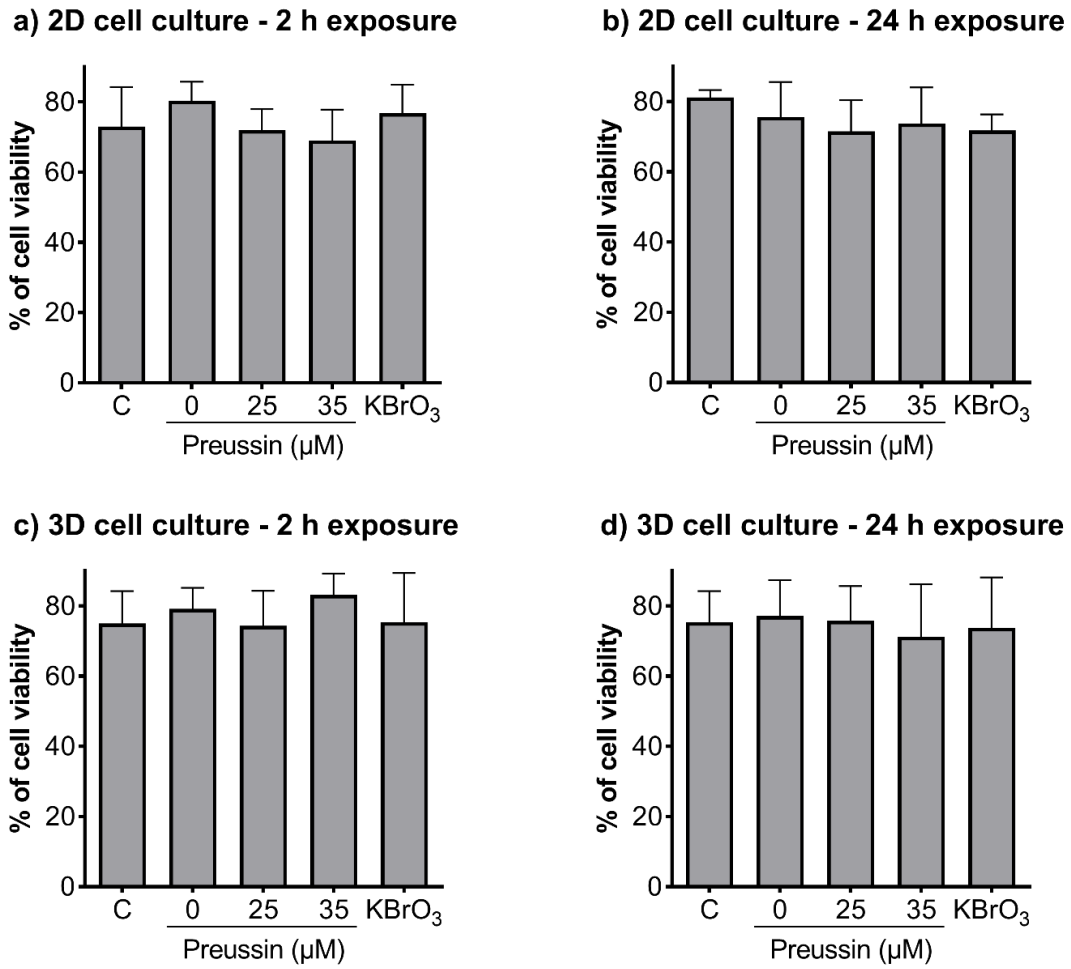

Figure 16 – Effects of preussin at 25 and 35 µM on cell viability of MDA-MB-231 cells cultured in 2D (**a** and **b**) or 3D (**c** and **d**) cell culture model after 2 h (**a** and **c**) or 24 h (**b** and **d**) of exposure. Cell viability was accessed through the trypan blue exclusion assay using an automated cell counter CountessTM. Negative control (C) with cells in culture medium, solvent control (0 µM of preussin and 0.1% of DMSO) of cells exposed to 0.1% (v/v) of DMSO, and positive control for the enzymatic version of comet assay with cells exposed to 4.5 mM of $KBrO_3$, groups were included. The results are expressed as mean ± SD of the percentage of cell viability from n=5.

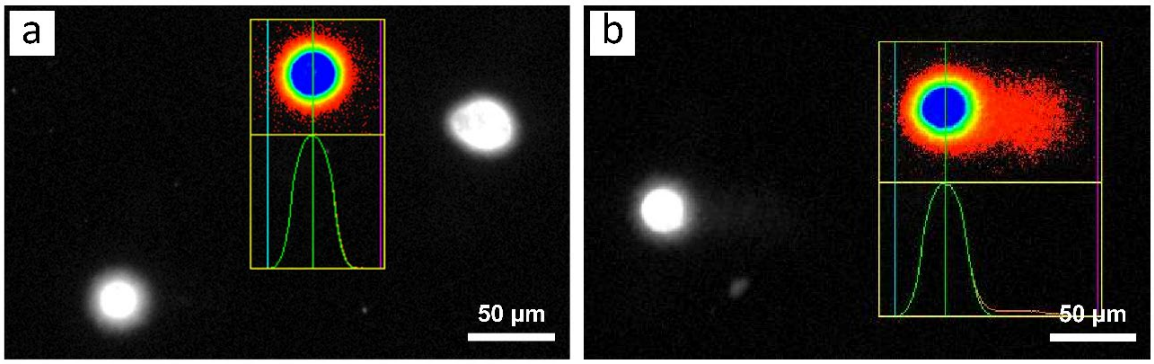

Figure 17 – Representative images of the analysis of comets from MDA-MB-231 cells, using the Comet Assay IV™ software. The blue line indicates the beginning of the head, the green line represents the middle of the head, and the pink line shows the end of the comet's tail. Comets with low levels of DNA damage, with the DNA distributed in a rounded shape, with no or a small tail, a nucleoid (**a**). Comets with higher levels of DNA damage, with a well-defined head and a tail constituted of damaged DNA (**b**).

In comparison to the negative and solvent control groups, at the tested concentrations, preussin did not induce DNA damage, either strand breaks (Figures 18 and 19) or oxidative damages (FPG sensitive sites) (Figures 20 and 21) on the MDA-MB-231 cell line. The result was alike in cells cultured either in 2D or 3D. Figures 18 and 20 illustrate results from the standard and enzymatic versions of comet assay (respectively) of cells cultured in a mono-layer or as MCAs and exposed for 24 h to preussin. In the standard version of the comet assay, low levels of strand breaks were observed for the control and preussin exposed groups, with the DNA organized as a nucleoid with no or a small tail. As for the enzymatic version of the DNA from the control and preussin exposed groups, the DNA showed to present FPG sensitive sites, with the DNA organized in the shape of a comet, with damaged DNA in the tail, but with no visual differences between these groups.

Although no differences were observed in the levels of DNA damage between the negative control and the preussin exposed groups, in MDA-MB-231 cells cultured both in 2D and 3D culture models and exposed either for 2 or 24 h, higher levels of oxidative DNA damage (FPG sensitive sites) were observed than strand breaks (Figures 19 and 21). The mean levels of oxidative damage varied between 9.7 and 21.5 %, and the levels of strand breaks varied between 2.2 % and 6.9 % in the negative and solvent controls and in the preussin exposed groups. Only the positive controls from both the standard and enzymatic versions of the comet assay (respectively 50 µM of H_2O_2 and 4.5 mM of $KBrO_3$) displayed statistically significant differences from the control, with an increase of more than 50 % in the DNA damage when compared to the negative control group (Figures 19 and 21), respectively.

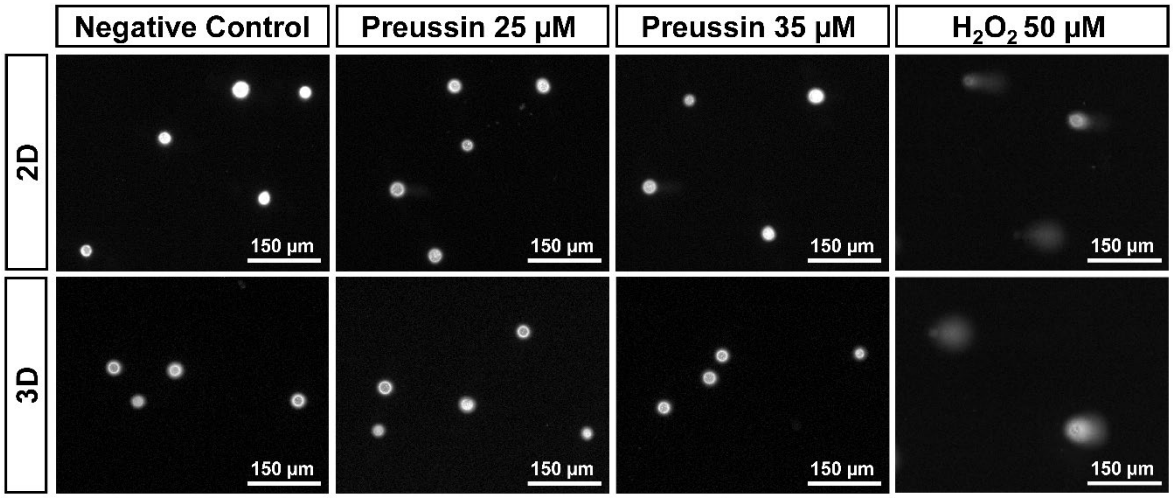

Figure 18 – Representative images of the standard version of comet assay in MDA-MB-231 cells treated with preussin at 25 µM or 35 µM, after 24 h of exposure, either cultured in a 2D or 3D cell culture model. As solvent control, cells were exposed to 0.1% of (v/v) of DMSO and for the positive control, nucleoids from a negative control group were exposed to 50 µM of H_2O_2. Samples were analyzed with the Comet Assay IV™.

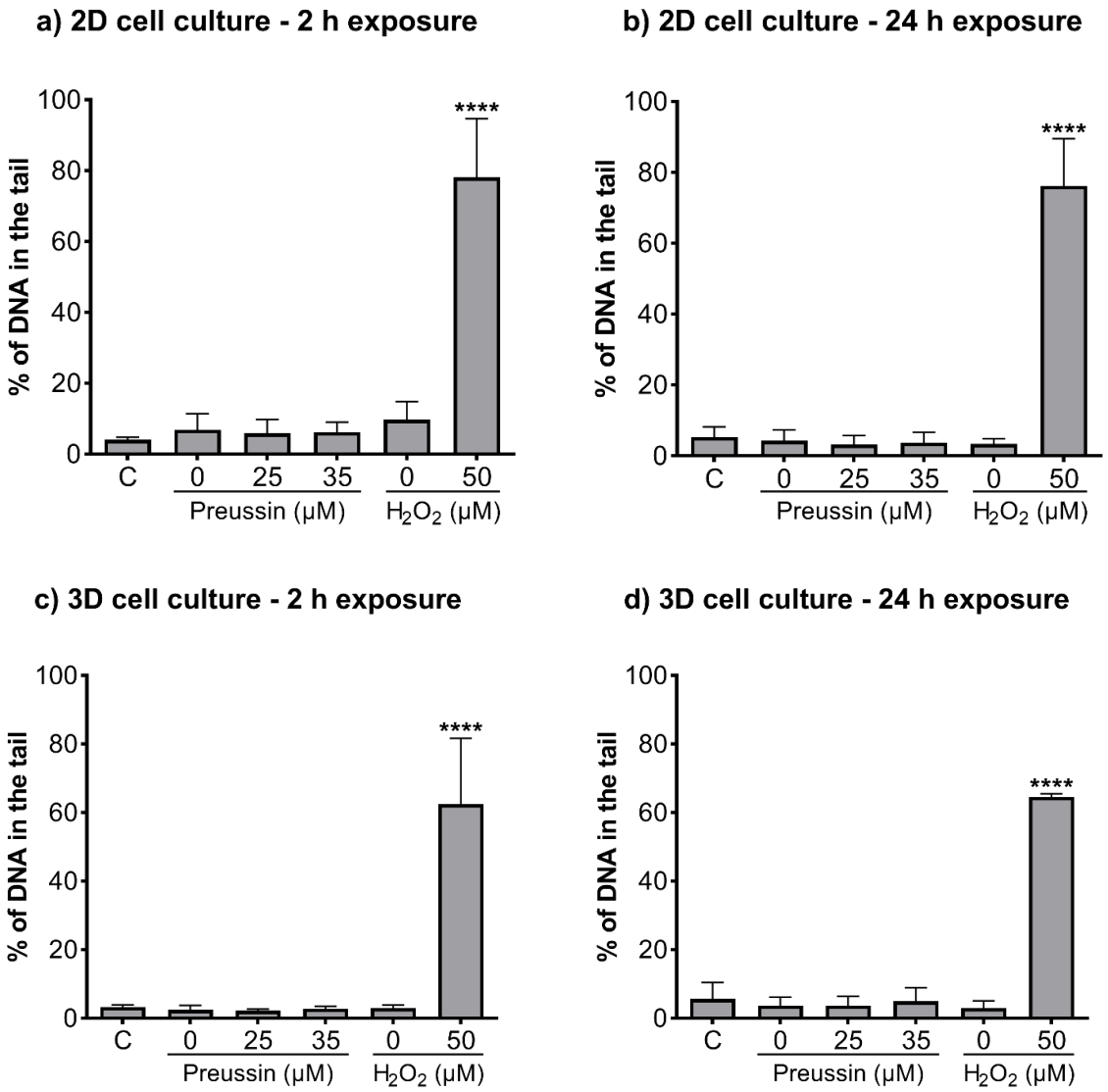

Figure 19 – Genotoxic effects (induction of strand breaks) of preussin at 25 and 35 μM on MDA-MB-231 cells cultured in a 2D cell culture model, after 2 h (**a**) or 24 h (**b**) of exposure or cultured in a 3D cell culture model and exposed for 2 h (**c**) or 24 h (**d**), measured through the standard version of the comet assay. Negative control (C) with cells exposed only to the cell culture medium, solvent control (0 μM of preussin) of cells exposed to 0.1% (v/v) of DMSO, and positive control of nucleoids exposed to 50 μM of H_2O_2 in PBS, groups were selected. The results were measured as the percentage of DNA in the comet's tail. The results are expressed as mean ± SD of n=5 (from 50 comets per gel and 2 gels per condition). Significant differences from the negative control group, represented with asterisks **** $p<0.0001$) were evaluated by one-way ANOVA, followed by post-hoc Holm-Sidak's multiple comparison test.

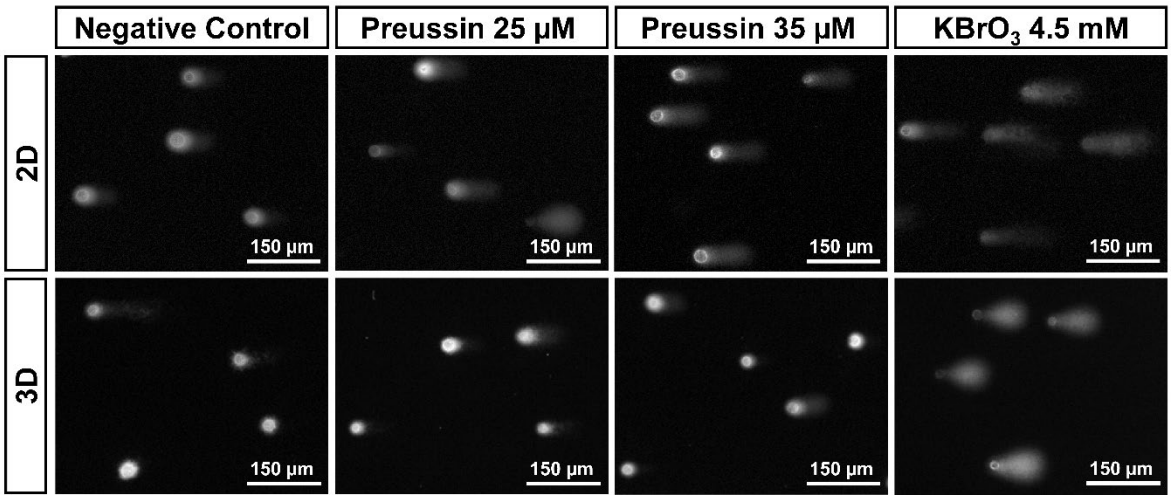

Figure 20 – Representative images of the enzymatic version of the SCGE assay, using the FPG enzyme, in MDA-MB-231 cells treated with preussin at 25 µM or 35 µM, after 24 h of exposure, cultured in a 2D or 3D cell culture model. As SC, cells were exposed to 0.1% (v/v) of DMSO, and for the positive control, nucleoids from a negative control group were exposed to 4.5 mM of $KBrO_3$. Samples were analyzed with the Comet Assay IV™.

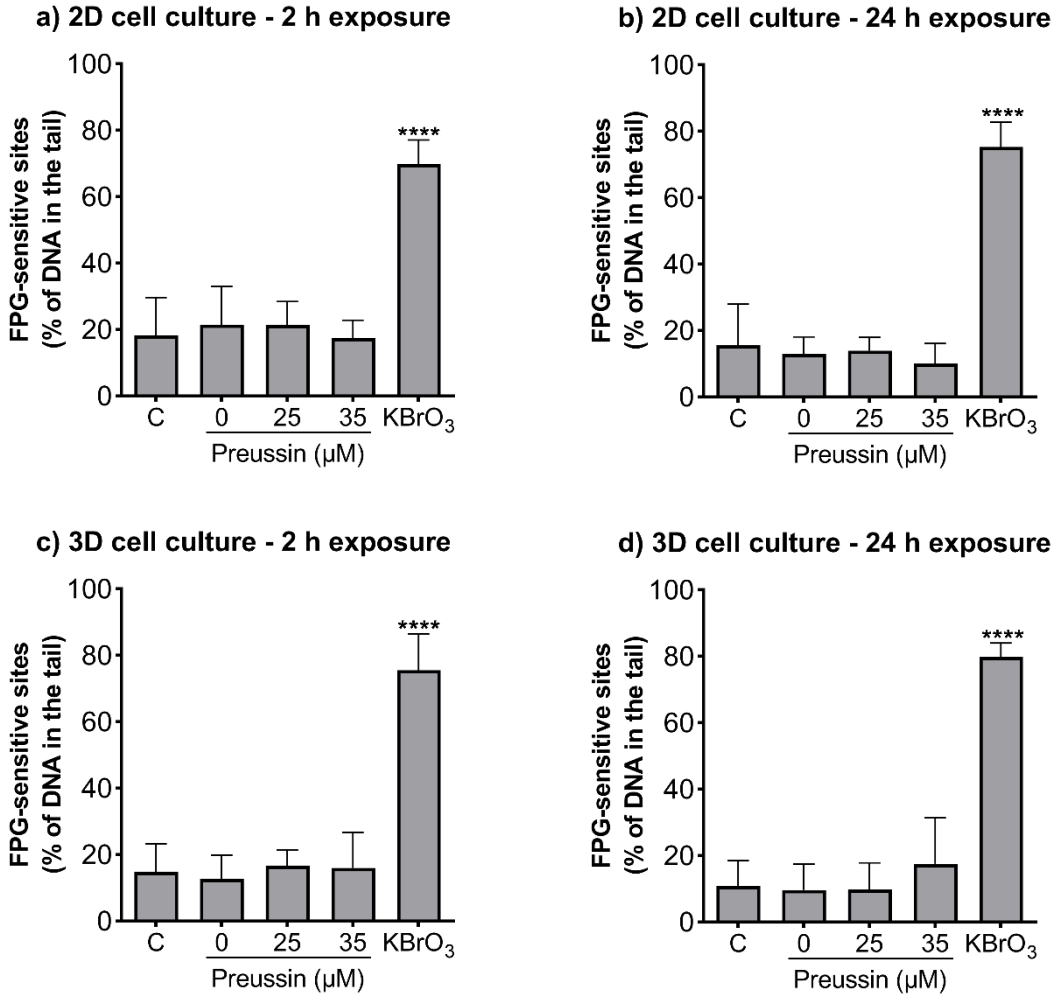

Figure 21 – Genotoxic effects (FPG sensitive sites) of preussin at 25 and 35 µM on MDA-MB-231 cells cultured in a 2D cell culture model after 2 h (**a**) or 24 h (**b**) of exposure or cultured in a 3D cell culture model and exposed for 2 h (**c**) or 24 h (**d**). Negative control (C) (cells exposed only to cell culture medium), solvent control (0 µM of

preussin) (cells exposed to 0.1% (v/v) DMSO), and positive control (cells exposed for 1 h to 4.5 mM of $KBrO_3$), groups were selected. The results were measured as the percentage of DNA in the tail of the comet and calculated by subtracting the percentage of DNA damage from the non-FPG enzyme-treated samples from the FPG enzyme-treated samples. The results are expressed as mean ± SD of n=5 (from 50 comets per gel and 2 gels per condition). Significant differences, represented with asterisks **** p<0.0001) were evaluated by one-way ANOVA, followed by post-hoc Holm-Sidak's multiple comparison test.

6. Induction of apoptosis - Annexin V - PI assay

The annexin V-PI assay was used to evaluate the effects of preussin in the induction of apoptosis in MDA-MB-231 cells. This assay detects membrane changes that occur during the apoptotic process (translocation of the phosphatidylserine residues (to which annexin-V protein binds) of phospholipids from the inner to the outermost layer of the cell membrane) and allows its distinction with necrosis and late apoptosis (where membrane disruption allows the DNA to be stained with PI) (Crowley et al., 2016).

Cells were cultured in monolayer or as MCAs and exposed for 72 h and 96 h, respectively, to preussin at 25 and 35 µM. A negative control group with untreated cells (cells incubated only with cell culture medium), solvent control with cells exposed to 0.1% (v/v) DMSO, and positive control with cells exposed to Dox (at 1 µM in 2D cell culture, or 5 µM in the 3D cell culture), groups were added. The percentage of alive, necrotic/late apoptotic, and early apoptotic cells was obtained with AnnexinV-FITC/PI double staining followed by flow cytometry and analyzed using the FlowJoTM software. Data from each condition was gated, first to exclude cell debris, second to exclude aggregated cells, and, in the end, in quadrants to distinguish the positive or negative cells for annexin V and PI based on PI/Annexin V staining (Figure 22). Viable cells presented Annexin V−/PI− staining, necrotic and late apoptotic cells showed Annexin V− or +/PI+, and the early apoptotic appeared with Annexin V^+/PI^- staining pattern

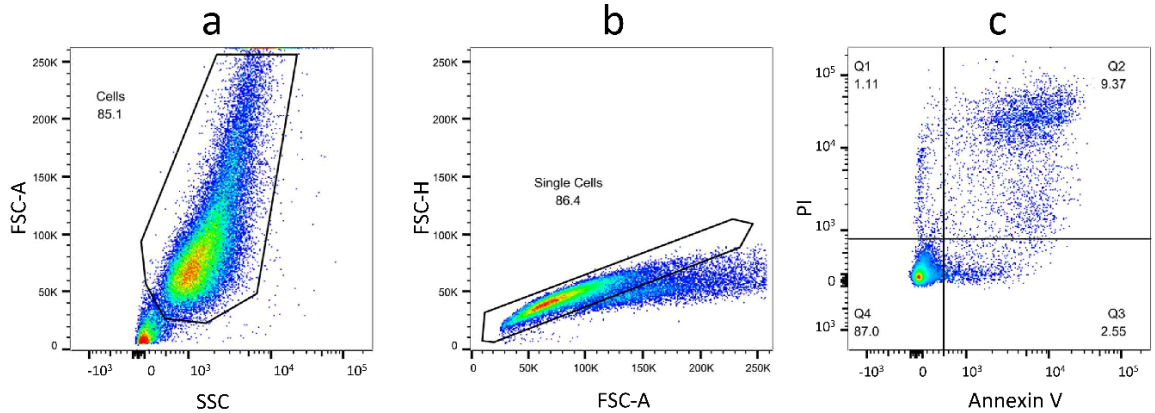

Figure 22 – Representative images of flow cytometry gating strategy used in the Annexin V-FITC/PI double staining of MDA-MB-231 cells, cultured in 3D and 2D cell culture models, to evaluate the induction of early

apoptosis and late apoptosis/necrosis. Gating for the isolation of MDA-MB-231 cells and exclusion of cellular debris (**a**), and for selecting single cells and excluding aggregated cells (**b**). The gated cells were distinguished based on the PI/Annexin V staining: Q1 + Q2 (Annexin$^{+ \text{ or } -}$/ PI^{+}) represented the cells in necrosis/late apoptosis; Q3 (Annexin^{+}/ PI^{-}) represented the cells in early apoptosis; Q4 (Annexin^{-}/ PI) represented the living cells (**c**). SCC: side-scattered light; FSC: forward-scattered light; H: height; A: area; PI: propidium iodide.

In the 2D cell culture model, only the preussin at 35 µM increased the percentage of cells in the state of late apoptosis/necrosis compared to the negative control group, with an increase of 19 % (Figure 23a). As for the 3D cell culture model, both preussin at 25 and 35 µM increased the rate of cells in late apoptosis/necrosis compared to the negative control group, with an increase of 16.9 % and 29.1 %, respectively (Figure 23b).

When evaluating early apoptosis induction, differences between the tested concentrations of preussin (25 and 35 µM) to the negative control were only observed in the 2D cell culture model cells (Figure 23). Compared to the negative control group, in the 2D cell culture, an increase of 1.9 % and 4.3 % was observed in the 25 µM and 35 µM preussin exposed groups (respectively) (Figure 23a). Although statistically significant, this increment in the percentage of early apoptotic cells was much lower than what was observed for the percentage of cells in late apoptosis/necrosis.

No statistically significant differences existed between the negative and solvent control groups in the cells from 2D and 3D cell culture models in the different cell states (alive, late apoptotic/necrotic, or early apoptotic). As for the positive control group, Dox increased the percentage of cells in late apoptosis/necrosis, both in cells cultured in 2D and 3D cell culture models, and slightly increased the percentage of cells in early apoptosis in the cells cultured as a monolayer (when compared to the respective negative control groups) (Figure 23).

When comparing the 2D and 3D cell culture models, the percentage of cells in late apoptosis/necrosis was higher for all groups (negative, solvent, and positive controls and the preussin exposed groups) in the cells cultured as MCAs than in 2D cell culture model (Figure 23).

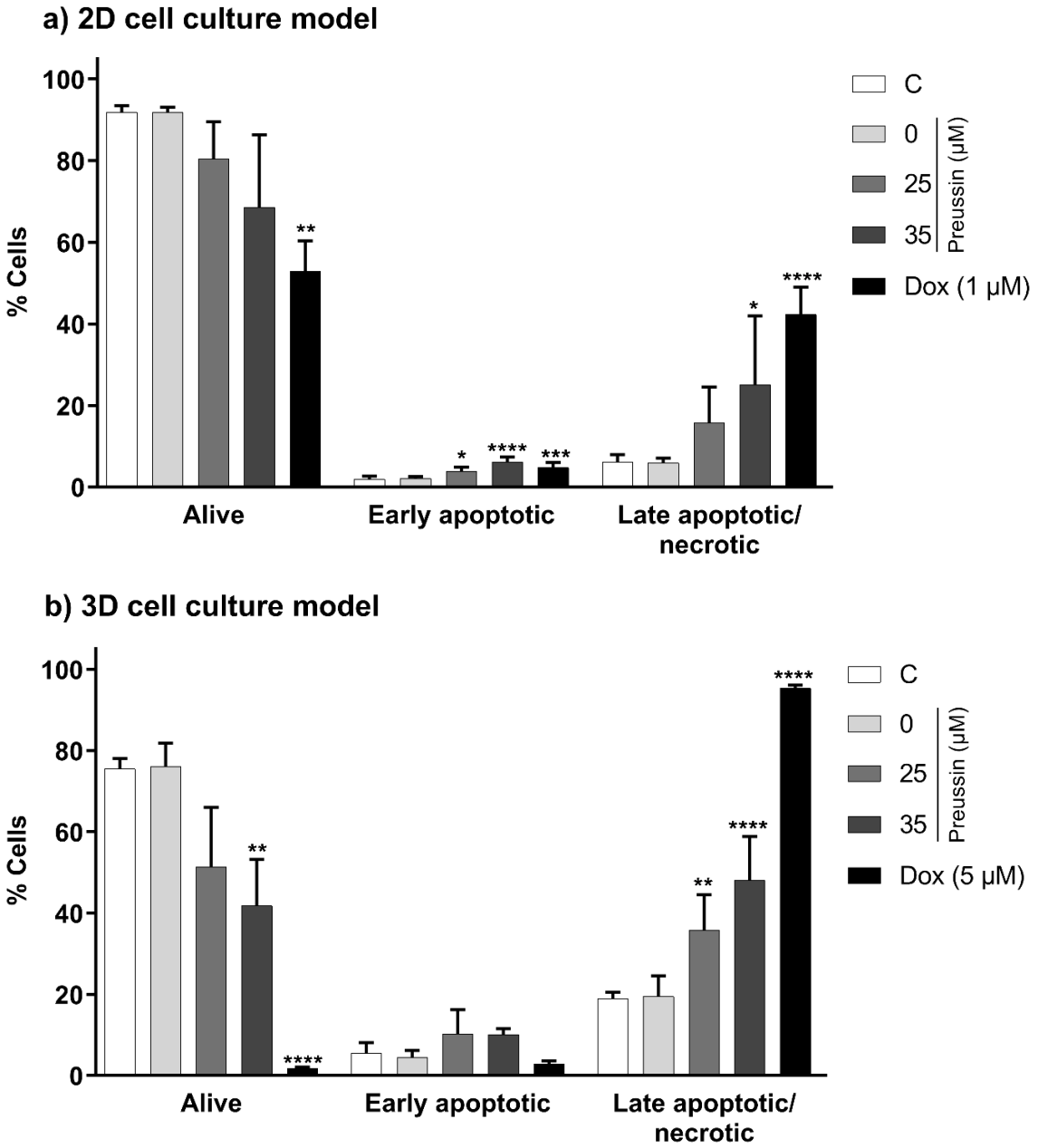

Figure 23 – Effects of preussin at 25 and 35 μM, in the induction of cell death (late apoptosis/necrosis), and early apoptosis, on MDA-MB-231 cells cultured in 2D (**a**) or 3D (**b**) cell culture models, respectively exposed for 72 h or 96 h. Early apoptosis, and late apoptosis/necrosis induction, were accessed by Annexin V-FITC/PI double staining followed by flow cytometry and analysis with the FlowJo™ software. Negative control (C) with cells exposed only to cell culture medium), solvent control (Preussin at 0 μM) of cells exposed to 0.1% (v/v) DMSO, and positive control where cells were exposed to Dox (at 1 μM in 2D cell culture and 5 μM in 3D cell culture) groups were added. The results were measured as the percentage of cells in each stage, either alive, in early apoptosis, or in late apoptosis/necrosis. The results are expressed as mean ± SD of n=5. Differences in comparison with the negative control group, in each cell state, were evaluated by one-way ANOVA, followed by post-hoc Holm-Sidak's multiple comparison test (in the early apoptotic and late apoptotic/necrotic cells groups) or Brown-Forsythe and Welch ANOVA tests (in the alive cells groups). Statistically significant differences are represented with asterisks (* $p<0.05$; ** $p<0.01$; **** $p<0.0001$).

7. Effects on cell morphology

7.1. Phase-contrast microscopy and stereomicroscopy

7.1.1. Monolayer cell culture

For each assay, a daily analysis of the morphological alterations induced by the exposure to preussin was performed (24 h, 48 h, and 72 h of exposure) by observation with an inverted phase-contrast microscope. At each analysis time, representative images of the morphologic alterations observed in every exposure group were acquired (Figure 24).

The positive control (Dox at 1μM) experienced a decrease in cell density after 48 h of exposure compared to the negative and solvent control groups. Furthermore, after 72 h of exposure, some cells became more spherical, while there was an increase in cell debris caused by cell detachment associated with cell damage (Figure 24). As for preussin exposed cells, there was a dose-dependent response, and the effects were accentuated with the time of exposure. After 24 h of incubation, the exposure to preussin at 25 μM or above, induced the appearance of cytoplasmatic granules. Cell rounding up, decreased substrate adherent cells, and the emergence of cell debris were also identified after exposure to preussin at 50 μM. After 48 h of exposure to the latter chemical compound, cell morphology alterations appeared at lower concentrations when compared to solvent and negative controls. Cytoplasmatic granules were observed with exposure to preussin at a concentration of 15 μM or higher. A decrease in cell density, cell rounding up, and cytoplasm vacuolization was noted with exposure to 25 μM, or higher concentrations of preussin. When cells were incubated with it preussin at 35-50 μM, most cells appeared round-shaped with cell debris in the background and just a few cells remained adherent to the substrate.

After 72 h of exposure, preussin exerted similar effects to those described above, with a decrease in the number of cells adhering to the substrate, more cells rounding up, and abundant cytoplasmatic granules starting at a concentration of 15 μM. Above 25 μM of preussin, there was an increasing cell rounding up and cell debris, with just a few cells being adherent to the substrate.

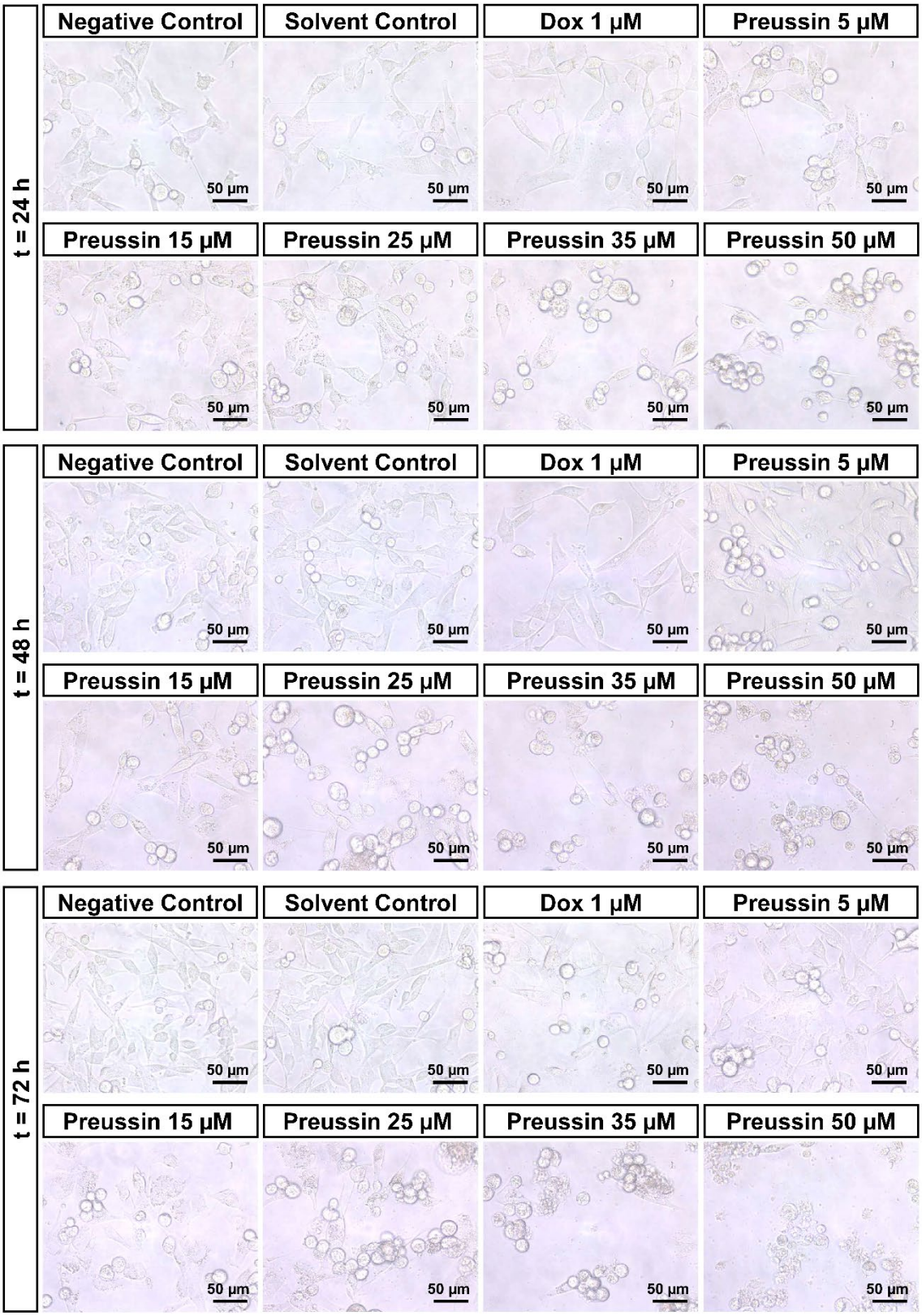

Figure 24 – Representative effects of preussin on cell morphology, in cells cultured in a monolayer cell culture model, and photographed in an inverted phase-contrast microscope. Cells were exposed to preussin at 5, 15, 25, 35, or 50 µM, during 24, 48 h, and 72 h. Cells exposed only to cell culture medium, to 0.1% of DMSO or 1 µM of Dox, were included as negative, solvent, and positive control groups, respectively.

7.1.2. MCAs

As described for the monolayer cell culture, the MCAs were observed daily. After 3 days of formation, similar-sized and oval-shaped (with a slightly flattened bottom) MCAs were obtained (Figure 25). Following the period of formation, the MCAs were incubated for 96 h either to preussin, 5 μM of Dox (positive control), 0.1% DMSO (solvent control), or DMEM (negative control), and daily analysis of morphologic alterations was performed at the end. The MCAs were photographed with the darkfield filter of the stereomicroscope (Figure 26).

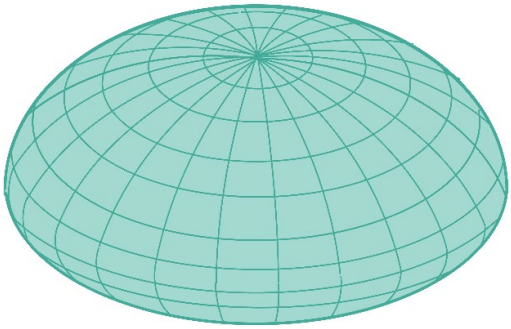

Figure 25 – Schematic representation of the shape of the MDA-MB-231 cell line obtained MCAs.

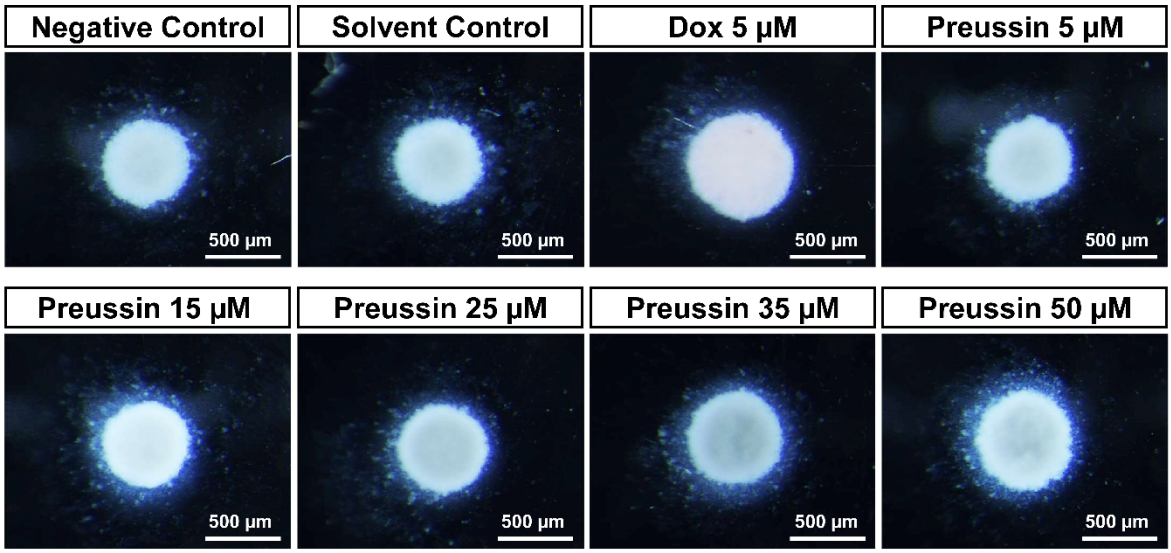

Figure 26 – Representative effects of preussin on MCAs morphology and photographed in the dark field of a stereomicroscope. MCAs were exposed to preussin at 5, 15, 25, 35, or 50 μM, for 96 h. Cells exposed only to cell culture medium, to 0.1% of DMSO or 5 μM of Dox, were included as negative, solvent, and positive control groups, respectively.

At the end of the exposure period, the MCAs from the negative and solvent control groups and the MCAs exposed to 5, 15, 25, and 35 μM of preussin appeared similar in shape to the MCAs after the formation period but slightly smaller and denser. No apparent visual

differences were observed between these groups. In contrast, the MCAs exposed to 50 μM of preussin or 5 μM of Dox showed higher diameter, less density, and were more flattened compared to the negative and solvent control groups.

During MCAs manipulation, some differences between controls and exposure groups were also noted, namely MCAs cell cohesion. These differences were apparent from observing the MCAs' integrity during its manipulation, where some groups disaggregate more easily, even with gentle manipulation. The positive control and the 50 μM preussin exposed MCAs showed less cell cohesion, with poor shape and integrity maintenance. Similarly, the MCAs exposed to 35 μM of preussin had slightly poorer shape and integrity during their manipulation than the negative and solvent control groups.

7.2. Transmission electron microscopy

Cells cultivated in monolayer and MCAs were subjected to preussin (for 72 hours and 96 hours, respectively) at concentrations of 5, 15, 25, or 35 M to assess ultrastructural effects. As a negative control cells in monolayer and MCAs were incubated only with DMEM, as solvent control incubated with 0.1% (v/v) DMSO, and as a positive control exposed to Dox at 1 or 5 μM. After exposure, cells in monolayer and MCAs were observed with an electron microscope.

7.2.1. Monolayer cell culture

In the cells cultured in monolayer, no morphological differences were observed between cells from the negative and solvent control groups (Figure 27). In these two groups, cells presented irregular-shaped nuclei with prominent nucleoli (Figure 27c,d). Moreover, in the cytoplasm, there were abundant rough endoplasmic reticulum and mitochondria (Figure 27a-c), some lipid droplets, dilated cisternae, prominent vesicles, and multivesicular bodies (Figure 27b, d). The cell surface evidenced membrane blebbing (Figure 27a,c,d) and finger-like structures (Figure 27b).

In the preussin-treated cells, the ultrastructural alterations were dose-dependent. With 5 μM of preussin (Figure 28a), there were no significant visual differences in comparison with the control groups. Above 15 μM of preussin, a higher number of pleomorphic multi-vesicular bodies of different sizes were observed, some of which with heavily electron-dense bodies inside (Figure 28b,d-f). Similarly, more enlarged cytoplasmic vesicles were observed (Fig-

ure 28d,e). The number and pleomorphism of larger cytoplasmatic vesicles and multi-vesicular bodies (mainly the multivesicular bodies containing electron-dense material) highly increased with the concentration of preussin. Furthermore, above 15 μM of preussin, mitochondria exhibited considerable damage, with their cristae becoming more structurally disordered (Figure 28c) and faded (Figure 28f).

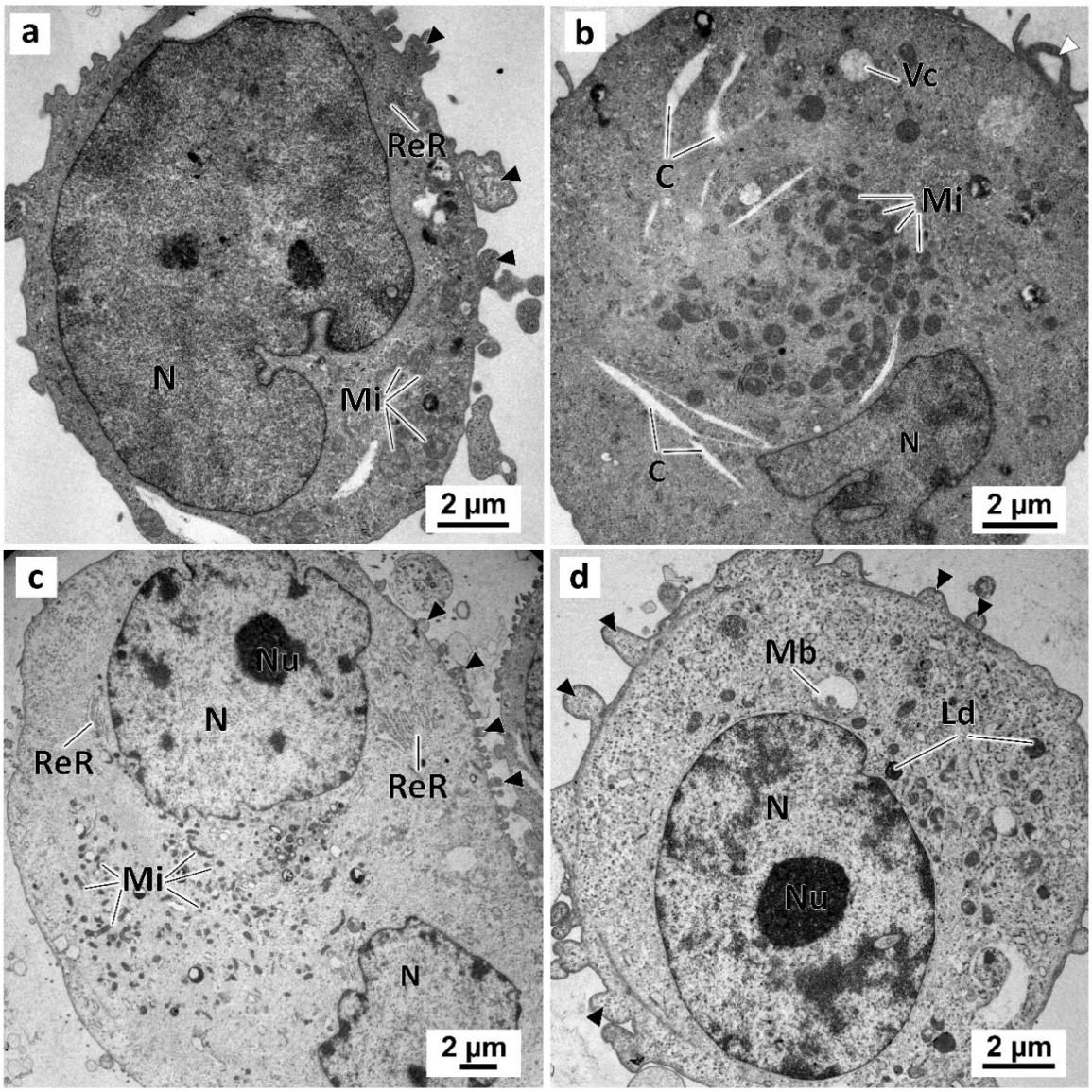

Figure 27 – Representative images of TEM analysis of MDA-MB-231 cells cultured as a monolayer. Cells were exposed for 72 h only to DMEM, in the negative control (**a** and **b**), or to 0.1 % (v/v) DMSO, in the solvent control (**c** and **d**). Black arrowheads: membranes blebs; White arrowheads: slender finger-like structures; C: dilated cisternae; Ld: lipid droplets; Mb: multivesicular bodies; Mi: mitochondria; N: nucleus; Nu: nucleolus; ReR: rough endoplasmic reticulum; Vc: vesicles.

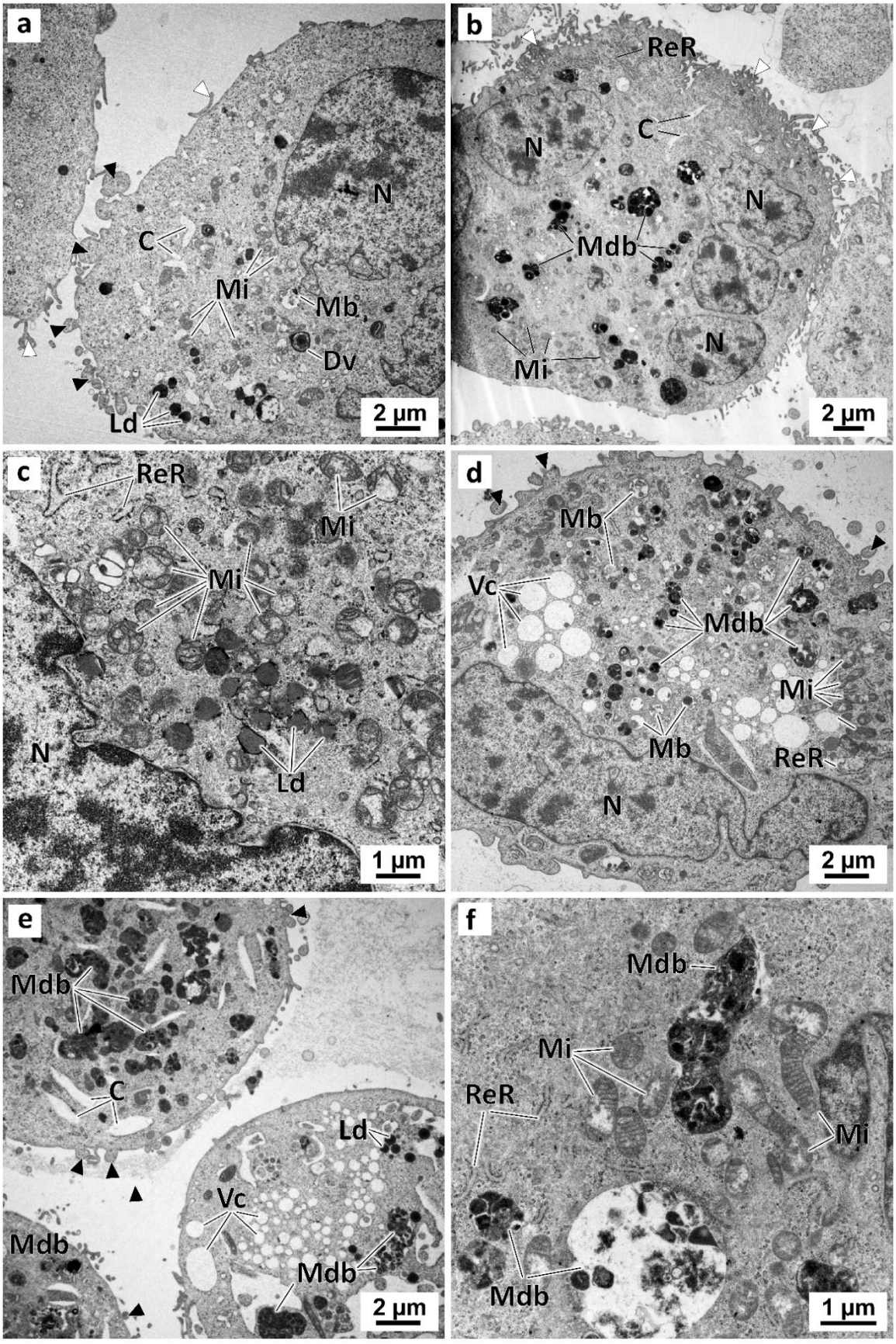

Figure 28 – Representative images of TEM analysis of preussin exposed MDA-MB-231 cells cultured as a monolayer. Cells were exposed for 72 h to several preussin concentrations: 5 µM (**a**), 15 µM (**b** and **c**), 25 µM (**d**), and 35 µM (**e** and **f**). Black arrowheads: membranes blebs; White arrowheads: slender finger-like structures;

C: dilated cisternae; Dv: degenerative vesicles; Ld: lipid droplets; Mb: multivesicular bodies; Mdb: multivesicular electron-dense bodies; Mi: mitochondria; N: nucleus; ReR: rough endoplasmic reticulum; Vc: vesicles.

7.2.2. MCAs

The MDA-MB-231 MCAs cells displayed similarities and differences from the patterns found in the monolayer cultured and exposed cells. Similarly to the 2D cell cultures, no relevant morphological differences were observed between the MCAs from the negative and solvent control groups (Figure 29). Irrespective of that, the analysis of semi-thin sections revealed that some of the MDA-MB-231 MCAs had a necrotic-apoptotic core filled up with dead cells, cell debris, and dense intercellular material (Figure 29a,b). Under electron microscopy, the MCAs from the control groups had irregular-shaped nuclei and well-developed organelles (mainly mitochondria) (Figure 29d-g).

In contrast to the observations in the 2D cell culture model, the cells from MCAs displayed a significantly higher quantity of lipid droplets in the cytoplasm (Figure 29c, e and f) and some pleomorphic multi-vesicular electron-dense bodies (Figure 29e,f). MCAs from the control groups also showed high cell-to-cell adhesion, with cells connecting in several regions alongside the cellular membranes. It was also possible to observe the formation of lumen-like structures, between cells, with membrane blebbing and short finger-like structures on the cell surface (Figure 29d,g). Furthermore, these lumen-like structures were sometimes filled with electron-dense material, either amorphous or slightly granular (Figure 29d and e). In some of these luminal structures, it was possible to observe necrotic cells, evidencing shrinkage, nuclear pyknosis, and some degree of cytoplasmatic vacuolization, and apoptotic shrinking cells, with chromatin condensation and preservation of cell integrity and membranes (Figure 29g).

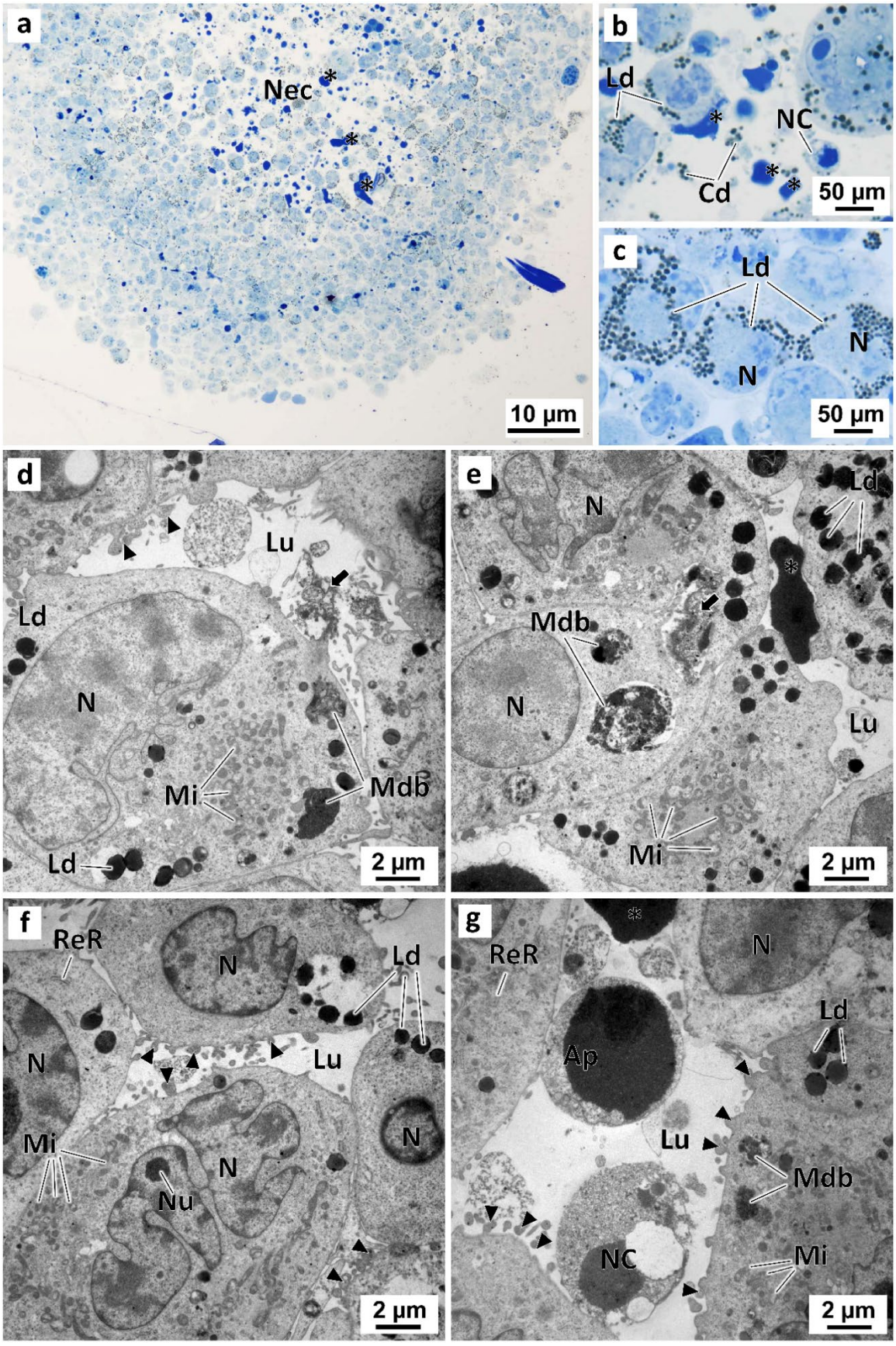

Figure 29 – Representative images of semithin sections (**a**, **b**, and **c**) and TEM (**d**, **e**, **f**, and **g**) analysis of MDA-MB-231 MCAs. The MCAs were exposed for 96 h only to DMEM in the negative control (**a** - **e**), or to 0.1 % (v/v) DMSO, in the solvent control group (**f** and **g**). Asterisk: electron-dense amorph material; black arrows: electron-

dense slightly granular material; black arrowheads: membranes blebs; white arrowheads: finger-like structures; Ld: lipid droplets; Lu: lumen-like structures; Mdb: multivesicular dense bodies; Mi: mitochondria; N: nucleus; Nec: necro-apoptotic core NC: necrotic cells; Nu: nucleolus; ReR: rough endoplasmic reticulum; Vc: vesicles.

In the preussin-exposed MCAs, ultrastructural morphological alterations occurred in a dose-dependent manner. With the increase in preussin concentration, the number of cells having pleomorphic multivesicular structures with electron-dense bodies inside increased. The higher the preussin concentration, the greater the pleomorphism of these multivesicular dense bodies and degenerative vesicles (Figure 30). Also, with increasing preussin levels, the amorph or slightly granular electron-dense material grew in the lumen-like structures. Accordingly, it was also observed higher cell debris, a higher number of necrotic cells (with cell loss of organelles and membrane rupture), and apoptotic cells (with cell shrinkage, pyknosis, and DNA condensation) were also observed, in those lumen-like structures. At least, higher levels of preussin lead to less cell aggregation (Figure 30). Accordingly, it was also observed higher cell debris, a higher number of necrotic cells with loss of organelles, and membrane rupture. Apoptotic cells were also observed, in the lumen-like structures, with cell shrinkage, pyknosis, and DNA condensation. Also, with the increase in preussin concentration, less cell aggregation was observed (Figure 30).

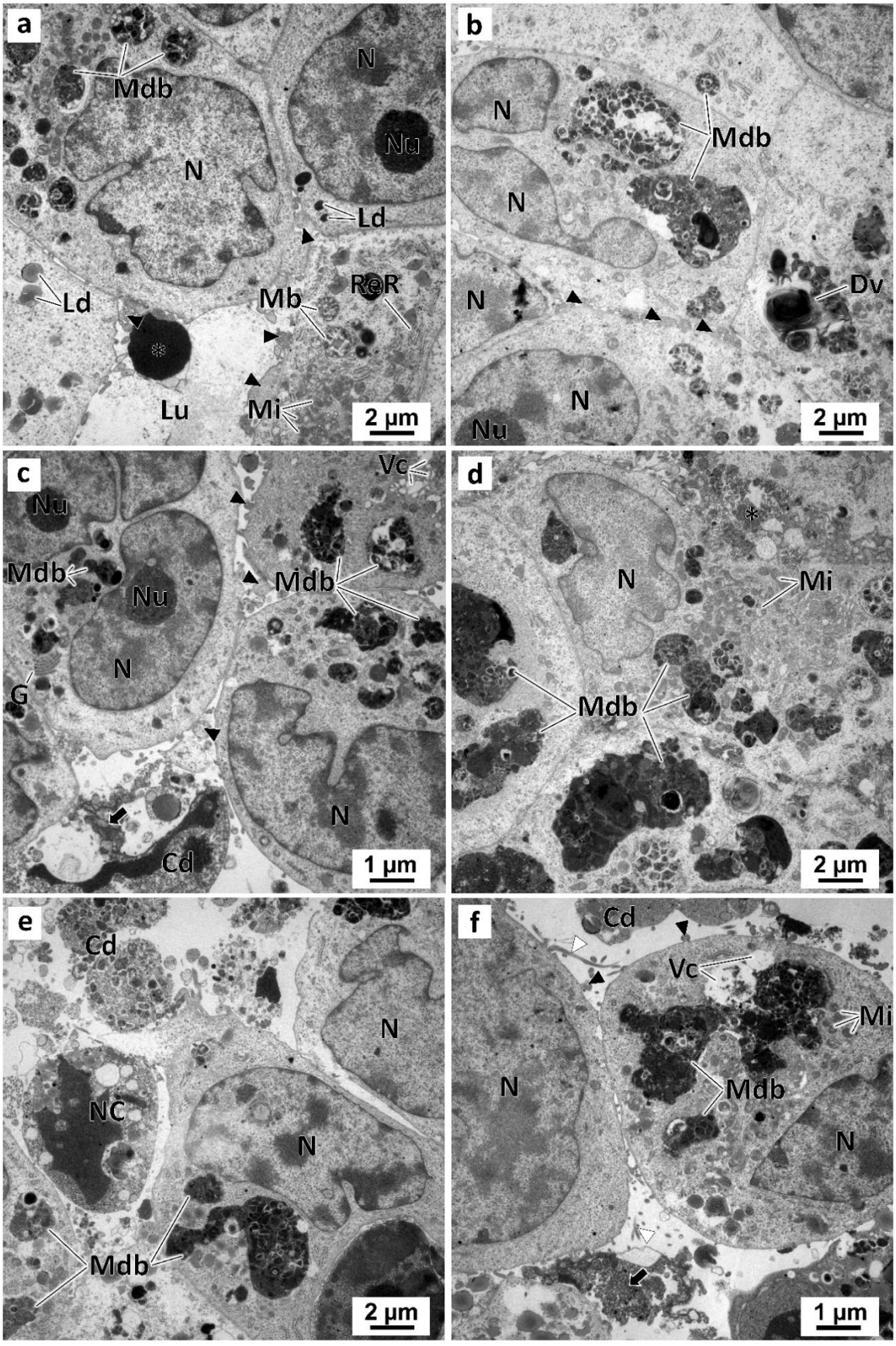

Figure 30 – Representative images of TEM analysis of preussin-exposed MDA-MB-231 MCAs. The MCAs were exposed for 96 h to preussin at a concentration of: 5 µM (**a**), 15 µM (**b**), 25 µM (**c** and **d**), and 35 µM (**e** and **f**).

Asterisk: electron-dense amorph material; black arrows: electron-dense, slightly granular material; black arrowheads: membranes blebs; white arrowheads: microvilli-like structures; Dv: degenerative vesicles; G: Golgi complex; Ld: lipid droplets; Lu: lumen-like structures; Mb: multivesicular bodies; Mdb: multivesicular dense bodies; Mi: mitochondria; N: nucleus; Nc: necrotic cells; Nu: nucleolus; Vc: vesicles.

Discussion

TNBC is an aggressive subtype of breast cancer characterized by an invasive nature, rapid disease progression, low survival, and high recurrence rates. Furthermore, it has few therapeutic options (Badve et al., 2011; Bauer et al., 2007; Dent et al., 2007; Harris et al., 2006). This study elucidated the *in vitro* anticancer activities of the underly studied marine fungi-derived compound, preussin, in a TNBC cell line, MDA-MB-231, both in 2D culture and in a more representative model of the tumor behavior *in vivo*, the 3D cell culture model. We confirmed preussin's antiproliferative and cytotoxic effects in a TNBC *in vitro* culture model and described, for the first time, its ability to induce late apoptosis/necrosis, as well as its incapacity to cause genotoxic effects. We further characterized the preussin-induced ultrastructural changes, a frequently neglected type of analysis. To our knowledge, we also first described its anti-migratory effects. At last, we further compared the differences between the used 2D and 3D cell culture models for testing preussin and Dox (reference control).

Previously, in our group, the effects of preussin were tested in a set of BC cell lines, including SKBR3, MCF-7, and MDA-MB-231 (each one representing a different clinicopathological surrogate subtype of BC), and a non-tumoral breast cell line, MCF-12-A, where it was observed a cytotoxic effect of preussin at 50 μM, for all tested cell lines cultured in a 2D cell culture model (Malhão et al., 2019). However, the MDA-MB-231 cell line showed a higher resistance when compared to the other BC cell lines. MDA-MB-231 is a mesenchymal-stem-like BC adenocarcinoma cell line characterized by the lack of expression of ER, PGR, and HER2 markers, which classifies it as a TNBC cell line (Dai et al., 2017; Neve et al., 2006). The MDA-MB-231 cell line can be further characterized according to its intrinsic subtype into basal-like BC (Dai et al., 2017; Neve et al., 2006) or, as described by some authors, as a claudin-low intrinsic subtype of BC (Prat et al., 2010). Following the line of thought of Fougner et al. (2020), these classifications of MDA-MB-231 as a basal-like or claudin-low intrinsic subtype might not be mutually exclusive but complementary, with claudin-low representing a more aggressive phenotype of the basal-like BC subtype. Despite its intrinsic BC classification, MDA-MB-231 represents an invasive and aggressive subtype of BC, for which there are limited therapeutic options, especially compared to other BC subtypes. Therefore, MDA-MB-231 cells were selected as a proxy to evaluate and expand the properties of preussin and determine the lowest concentration to induce cytotoxic effects, as a continuation of the work of Malhão et al. (2019).

First, we proposed to select the lowest concentration of preussin to induce alterations in cell viability. In the present study, over time, the MDA-MB-231 cells cultured in a 2D cell culture model observed a gradual decrease in cell viability after exposure to preussin. At 24 h,

preussin showed effects only at 50 μM. Accordingly, when evaluating cell viability by trypan blue assay (that assesses effects on membrane integrity), preussin showed no effects at 25 and 35 μM with exposure times of 2 and 24 h, with no differences between 2D and 3D cell culture models. Increasing the exposure time, we observed an accentuation of the preussin capability to decrease cell viability for all the concentrations tested. For instance, at the highest exposure time, 25 μM of preussin reduced cell viability (to 67.5 % in 2D cell culture and 72.3% in the 3D cell culture model) compared to the respective negative control group in 2D and 3D cell culture models. These results were similar to what we found for other assays (including BrdU assay, annexin V-PI, and colony assay), mainly when observing the cell morphology alterations. When performing the clonogenic assay, the used concentrations of preussin had to be lowered since at 50 μM there were not enough cells to replate after exposure. With 35 μM and 25 μM of preussin, there were scarce viable cells, but enough to perform the assay.

Regarding the decrease in cell viability induced by preussin, it was previously described that preussin reduces MDA-MB-231 cell viability only at a concentration of 50 μM in 2D and 100 μM in 3D cell culture models (when using the MTT assay), higher than what we observed (Malhão et al., 2019). Although preussin was isolated from the same species and extracted using the same method (as described by Buttachon et al. (2018)), the one that was used in this dissertation was obtained from different batches of extraction, which may represent a source of variability. Furthermore, it has already been described that a drawback of natural products is their instability and high rate of degradation during storage (Atanasov et al., 2021; Beck et al., 2017; Large et al., 2021; Mitchell et al., 2021). The cell passage number may also introduce variability in drug sensitivity. These factors may have contributed to the differences between the present results and those reported by Malhão and collaborators (Malhão et al., 2019).

Other authors have previously described the cytotoxic effects of preussin on cells cultured in monolayers. In the present study, the lowest concentration required to induce a decrease in cell viability (over 50% decrease) was 35 μM preussin. Achenbach et al. (2000) showed that the preussin obtained through synthesis decreased cell viability below 50% in various cell lines (with 48 h of exposure) at lower concentrations, between 1.2 and 4.5 μM, in a wide subset of cell lines (HL-60, HeLa, A549, MCF-7, PC-3, DU-145, LNCaP, and MeWo). Buttachon et al. (2018) showed preussin capability to decrease cell viability to 50% at higher concentrations than the ones described by Achenbach et al. (2000), with IC_{50} effects at 47.9 and 53.6 μM, in the cell lines A549, and MCF-7, respectively. Preussin effects were also tested in other cell lines (HT29, HCT116, A375, HepG, A549, T98G, and U251) with the IC_{50} concentrations ranging from 12.3 μM to 74.1 μM (Buttachon et al., 2018). Accordingly,

Malhão et al. (2019) concluded that preussin reduced cell viability in MCF-7, SKBR3, MDA-MB-231, and MCF-12-A cell lines only at 50 μM after 72 h of exposure. Kasahara et al. (1997) also reported preussin to induce cytotoxic effects in the rat fibroblast cell line 3Y1 at higher concentrations (31.7 μg/ml, 99.8 μM) than those that other authors or we described.

The use of *in vitro* 3D cell culture models to study preussin effects in cell culture has only been evaluated once by Malhão et al. (2019). In the latter study, the MCAs from different breast cell lines, including MDA-MB-231, showed higher resistance to preussin-induced reduction of cell viability. Nonetheless, this tendency was not directly observed in our study since the lowest concentration of preussin that triggered cytotoxic effects in a monolayer induced cytotoxicity in a 3D cell culture model. It is important to note, however, that even though the tested concentrations of preussin were the same in these two culture models, the time of exposure to preussin was different (72 h in the 2D cell culture model and 96 h in the 3D cell culture model). Therefore, our findings indirectly suggest that MDA-MB-231 MCAs are more resistant to preussin than the 2D culture models.

Concerning the Dox exposure (positive control) on MDA-MB-231 cells, the 2D cell cultures also displayed higher sensitivity to the drug than the cells cultured in 3D cell culture. In the 2D cell cultured MDA-MB-231 cells, we observed a high decrease in cell viability (to 33.1%) after exposure to Dox at 1 μM. When cultured in a 3D cell culture model, MDA-MB-231 cells showed higher resistance to Dox at 5 μM (decreasing cell viability to 65 %).

According to the literature, different cell lines in 3D can display either higher resistance or higher sensitivity to drugs when compared to cells cultured in 2D. Nonetheless, the first is far more common (Z. Huang et al., 2020; Imamura et al., 2015; Muguruma et al., 2020), as we and other authors observed for the MDA-MB-231 cells in the 3D model, where 3D cultured cells presented higher resistance to Dox than 2D cultured cells (Lovitt et al., 2018; Nigjeh et al., 2018). In its turn, it has previously been shown, by Imamura et al. (2015), that MDA-MB-231 spheroids had a similar resistance towards Dox exposure when compared to the cells cultured in a monolayer, in contrast to what we observed. These authors also observed a variable resistance (either a higher or similar resistance) to drugs when comparing cells in monolayer and 3D cultures for other cancer cell lines. Cells that formed looser spheroids tended to display equivalent resistance to drugs compared to those in monolayer. Moreover, cell lines forming more cohesive spheroids tended to show higher resistance to Dox and paclitaxel than cells cultured in 2D cell culture models.

The 3D architecture of MCAs may explain the higher resistance to drugs in comparison to 2D cell culture, possibly due to the differences in drug penetration, described between the 2D and 3D cell cultures (Mehta et al., 2012). Similarly, the MDA-MB-231 MCAs architecture

as well as the cell cohesiveness may reduce preussin and Dox penetration, resulting in a lower bioavailability of the compounds to all cells.

Ivascu & Kubbies (2007) also found that spheroids with lower disaggregation were more resistant to various anticancer drugs (cisplatin, docetaxel, and anthracycline epirubicin). It is important to note, however, that different authors described the obtention of MDA-MB-231 cell line 3D structures with varying levels of cohesiveness (Dubois et al., 2017; Froehlich et al., 2016; Imamura et al., 2015; Ivascu & Kubbies, 2007; Malhão et al., 2022; Muguruma et al., 2020; Scolamiero et al., 2018; Vinci et al., 2012). The 3D cell cultures we obtained with the MDA-MB-231 cell line using the ULA plates may be considered to have an ellipsoid form and intermediate cohesion. Malhão et al. (2022), using the same cell line and method for the obtention of 3D culture, described the MCAs of MDA-MB-231 with an ellipsoid form while being cohesive 3D structures. The existence of cell adhesions when observing the ultrastructure of these MCAs, similar to what Malhão et al. (2022) described, may further confirm the cohesiveness of the MDA-MB-231 MCAs. Several factors may influence the differences observed in the literature regarding the obtained MDA-MB-231 cell line 3D structure, both in terms of shape and cohesiveness, including the method of obtention, cell culture medium and respective supplementation, cell seeding density, and cell passage number.

Furthermore, in the 3D cell cultures, the cell-cell and cell-EMC interactions and the cell cycle distribution may also affect drug response when comparing different cell culture models (Ivascu & Kubbies, 2007; Mehta et al., 2012). Because of their tridimensionality, MCAs, similar to what is described for spheroids (Ivascu & Kubbies, 2007; Lovitt et al., 2018), may display higher cell-cell interactions and cell-ECM interactions, which may also confer higher resistance to drugs. Those interactions may modulate protein expression, including up-regulation of pro-survival proteins, leading to drug resistance (Ivascu & Kubbies, 2007; Lovitt et al., 2018). For example, MDA-MB-231 cells are described to spontaneously form 3D structures, induced by the interaction of collagen I with β1 integrin, which is considerably more expressed in the 3D cell culture model than in 2D cell culture (Ivascu & Kubbies, 2007). Integrins have been described as transmembrane linkers with essential functions in mediating cell-cell and cell-ECM interactions and intracellular signaling pathways (Alberts et al., 2022). The collagen/β1 integrin signaling has been implicated in chemoresistance to various drugs (including Dox) in leukemia and BC cell lines (including the MDA-MB-231 cell lines). The higher expression of collagen I with the β1 integrin in the MDA-MB-231 spheroids may explain the higher resistance to Dox (El Azreq et al., 2012), as we also observed. The differences in the expression and spatial organization of surface receptors between the cells cultured in 2D and 3D culture models may therefore affect the binding efficacy of the drugs

to the cells since drugs often target determined receptors on the surface of cells (Langhans, 2018; Lv et al., 2017).

We may also raise the question of whether cell responses to preussin influences the cell-cell and cell-ECM interaction molecules. A visual increase in MCAs diameter was observed in MDA-MB-231 MCAs exposed to preussin (at cytotoxicity-inducing concentrations) and Dox. Also, when MCAs exposed to preussin were manipulated, they tended to disaggregate more easily than non-exposed MCAs or MCAs subjected to low concentrations of preussin. Both observations indicate a decrease in cell cohesion. Nonetheless, the increase in MCAs diameter and loss of MCAs cohesiveness were considerably less marked in the preussin group than in the Dox-exposed MCAs. However, it is important to note that in the preussin-exposed MCAs, a decrease in cell cohesion was observed at higher concentrations of the compound, in accordance with the lower cell viability detected at higher concentrations of preussin. Therefore, the decrease in cell cohesiveness may be correlated to the increase in cell death induction and not necessarily caused by a reduction in cell adhesion.

Other factors have been proposed for the higher resistance of 3D cell cultures compared to that of 2D cell cultures. Lovitt et al. (2018) correlated the lower cytotoxicity of Dox in 3D cell culture models with the lower proliferation rate observed in this cell culture model compared to the 2D cell culture. This lower proliferation rate may result in a lower sensitivity to drug cytotoxicity compared to cells with higher doubling times (Lovitt et al., 2018).

Hypoxia and pH may also arise as resistance mechanisms. In spheroids, as it is described for solid tumors, a gradient of oxygen is observed throughout the layers of cells. The cells in the outer layers have higher bioavailability of oxygen, whereas the inner cells have lower availability, not only dependent on the oxygen diffusion throughout the spheroid/tumor but also on its consumption by the outer cells (Zanoni et al., 2016). This differential accessibility induces hypoxia in the inner cells, which in turn may induce the expression of molecules responsible for external drug export, the activation of antiapoptotic factors, the expression of growth factors, and the inhibition of oxidative stress due to the inexistence of oxygen (Nunes et al., 2019). Furthermore, oxygen-deprived cells produce lactate, which decreases the pH of the inner portion of the spheroid (Nunes et al., 2019). Low pH values may affect drug action by impairing the uptake of some drugs, as is described to occur with Dox (Nunes et al., 2019).

Regarding the variable results described in the bibliography for the preussin-induced decrease in cell viability, it is important to mention that all methods used were different, which may translate into variability in the obtained conclusions. In the present study, as observed by other authors (Buttachon et al., 2018; Malhão et al., 2019), the MTT assay was used to

evaluate the effects of preussin on cell viability. Achenbach et al. (2000) calculated the cell viability by measuring the crystal violet dye retained by the cells after 48 h of exposure to preussin, followed by incubation in a drug-free medium for another 48 h. Malhão et al. (2019) previously showed that the evaluation of cytotoxicity of preussin in a 3D cell culture model, assessed through multiple assays (including MTT, LDH, and resazurin reduction assays), retrieved different results since they evaluated several targets of cell viability (either cell metabolism or cell membrane integrity). Overall, careful analysis and comparison of the results should be taken when comparing the viability obtained through different proxies and the conclusions drawn from these assays.

It is also important to note that in the scratch assay (performed to study the effects of preussin in cell migration), the results were not similar to what we observed with the MTT assay. In fact, in the scratch assay, cells were more sensitive to the effects of preussin. Lower concentrations of preussin could induce aspects of cell death, including a detachment of cells from the plate surface. However, the scratch assay, some alterations in the culture conditions were implemented compared to other assays, such as serum deprivation and reduced concentration of FBS during cell exposure. With serum starvation and serum reduction, we intended to decrease cell proliferation, which may appear as a confounding factor in this assay, whose objective is to measure cell migration.

The serum contains growth and adhesion factors to promote cell proliferation and attachment. Mammalian cells require growth factors to enter and progress through the cell cycle (Freshney, 2010). Additionally, serum starvation is described to synchronize and inhibit cell proliferation, in some cancer cell lines, by arresting these cells at the G0/G1 phase of the cell cycle (Odom et al., 2009; Rajh et al., 2016; Shin et al., 2008; White et al., 2020). Furthermore, by reducing the concentration of FBS for culture maintenance, we intended to decrease cell growth and, consequently, proliferation (Gstraunthaler et al., 2013; Jayme et al., 1997; White et al., 2020). Nonetheless, no differences existed between the cells cultured in serum-reduced or serum-complete conditions, where a similar pattern of migration and/or growth was observed. These may either indicate an ineffective inhibition of cell proliferation with the serum-reduced medium or the induction of a more invasive phenotype in the MDA-MB-231cells when exposed to the serum-reduced conditions conjugated with simultaneous cell proliferation in the normal serum conditions cultured cells. It was previously described that in some cancer cell lines, using serum reduced medium can decrease cell proliferation (White et al., 2020). Furthermore, Ye et al. (2013) reported that MDA-MB-231 cells display a more aggressive phenotype, with higher invasiveness, in a phospholipase D2-dependent manner when serum-deprived. Nonetheless, we believe that more research should be con-

ducted to compare different culture conditions (such as serum reduction versus normal serum conditions) and their effects on cell proliferation and invasiveness, elucidating the mechanisms causing scratch closure.

In this assay, we observed that with serum deprivation and depletion, MDA-MB-231 cells became more sensitive to the effects of preussin. For instance, we observed aspects of cell death (cell detachment and alteration of cell morphology) in cells exposed to concentrations of preussin that had not previously decreased the cell viability (in normal serum culture conditions). In some cancer cell lines, serum depletion is described to increase cell cancer resistance to oxidative stress (White et al., 2020). These authors also suggested that serum deprivation may be related to *in vitro* multidrug and chemoresistance by inducing a reversible proliferation arrest of cancer cells (White et al., 2020). Other authors described a higher sensitivity (with lower doses of compounds causing a decrease in cell viability) of cancer cell lines to compounds when cells were cultured under serum-reduced culture conditions (Sainz-Cort et al., 2020; Zhao et al., 2017).

We may also raise the question of whether preussin affects cell adhesion. This action would explain that at low serum dosages, preussin showed higher effects in inducing aspects of cell death, including cell detachment. Lower serum concentrations translate into a lower bioavailability of adhesion factors (Freshney, 2010) which could lead to a higher effect of compounds affecting cell adhesion. In this case, preussin could be sensitizing cells to anoikis, a non-apoptotic programmed cell death type induced in adherent cells that lose the cell-ECM interaction (Kornienko et al., 2013). Even though we observed an increase in the percentage of cells in apoptotic processes after exposure to preussin, we did not notice an increase in ultrastructural aspects suggestive of apoptosis induction (such as cell shrinkage, membrane blebbing, DNA condensation and fragmentation; nuclear membrane rupture, loss of organelles placement (Yan et al., 2020)).

With the decrease in cell viability, we further investigated some cellular processes that could explain the decrease in cell viability and could be attributed to preussin, including cell death induction, either by necrosis or apoptosis (early or late), cell proliferation, and genotoxicity induction.

To explore the type of cell death mechanisms involved in reducing cell viability, we further performed the annexin V-PI assay, which distinguishes alive cells from cells in processes of apoptosis (either early or late apoptosis) and necrosis. The assay showed that preussin decreased cell viability partially due to cell death induction. The compound induced a slight increase in the percentage of cells in early apoptosis, mainly in the 2D cell cultured MDA-MB-231 cells, and a higher increase in the percentage of cells in late apoptosis/necrosis

state. Interestingly, this increase in late apoptosis/necrosis induction appeared to be greater in the 3D than in the 2D cell cultured cells. Indeed, the lowest tested concentration of preussin only induced an increase in late apoptosis/necrosis on the MDA-MB-231 MCAs.

Achenbach et al. (2000) previously noticed that higher concentrations of preussin increased chromatin condensation, indicating cell apoptosis induction in the HL-60 cell line. Similarly to what we observed for the TNBC cell line MDA-MB-231, preussin has previously been shown to induce necrosis and apoptosis (without a distinction between early and late apoptosis) in the HL-60 cell line, postulated to occur in a p53 and BCL-2 independent manner (Achenbach et al., 2000). Achenbach et al. (2000) further described the occurrence of apoptosis through caspase 8 and cytochrome c-caspase 9 apoptotic pathways. Accordingly, Malhão et al. (2019) described the induction of caspase-dependent apoptosis by demonstrating the expression of caspase 3 in different BC cell lines, including the MDA-MB-231 cell line, after exposure to preussin.

Apoptosis may be a secondary response to DNA damage (Kieffer & Lowndes, 2022). In this line of thought, we postulated whether preussin induced genotoxic effects on the TNBC cell line MDA-MB-231, as described in *Saccharomyces cerevisiae* yeast (Overhand & Hecht, 1994). Since apoptosis occurs as a secondary response to DNA damage (Kieffer & Lowndes, 2022) and because at late phases of necrosis DNA damage may also occur (Yasuhara et al., 2003), we tested the effects of preussin at early time points (2 and 24 h) after exposure. Nonetheless, we observed that preussin did not induce DNA damage, either strand breaks or DNA oxidative damage (oxidized purines, like 8-oxo-7,8-dihydroguanine or formamidopyrimidines, and adducts of ring-opened N7 guanine (Azqueta & Collins, 2013)), at any of the time points in any of the cell culture models, assessed through the standard version and FPG enzymatic version of SCGE.

In agreement with the observation of preussin induction of cell late apoptosis/necrosis, it was possible to confirm signals of apoptosis and necrosis in the MDA-MB-231 cells when analyzing the alterations in the cell ultrastructure. In fact, with increasing concentrations of preussin, higher cell debris (indicating a process of cell destruction) and cells with aspects of apoptosis or necrosis were observed. With increasing concentrations of preussin, it was also possible to visualize the presence of multivesicular bodies containing electron-dense material. These structures were also present at higher quantities in the MDA-MB-231 MCAs than in the monolayer cultured cells. We postulated that these membrane-bounded vesicles might be a result of cell autophagy. The process of autophagy consists of the formation of double-membrane vesicles that engulf cytoplasm and organelles, which are degraded after

fusion with lysosomes (Han et al., 2018; Mariño et al., 2014; Niklaus et al., 2021). Nonetheless, due to the high electron density of the multivesicular structures, the observation of the double bounding membrane was not possible.

Autophagy arises as a protective mechanism of the cell to maintain homeostasis and overcome stress stimuli, such as the lack of nutrients or damages caused by exposure to chemical agents (Cocco et al., 2020; Mariño et al., 2014; Niklaus et al., 2021). Autophagy represents a vital process both in normal and tumoral tissues (Cocco et al., 2020). In cancer, autophagy may arise as a protective or resistance mechanism to the cytotoxicity induced by anticancer drugs (Niklaus et al., 2021). Autophagy is correlated with regulated cell death, through various pathways in a two-way relation, with autophagy regulating cell death and cell death regulating autophagy (Napoletano et al., 2019).

In the MDA-MB-231 cells, we observed an increase in the number and dimensions of the pleomorphic vesicles, postulated to be autophagic vesicles. Whether those vesicles are in fact autophagic vesicles acting as a protective or a death-inducing mechanism, and if they lead to cell death, is still unknown. To confirm the origin of those vesicles, autophagy markers (such as autophagic protein LC3 detection) and autophagy flux assays (LC3 or p62 degradation, lysosome delivery of LC3 labeled with fluorescent proteins, or others) can be used (Mizushima & Murphy, 2020; Napoletano et al., 2019). Each way, it would be relevant to administer preussin in conjugation with autophagy inducers or inhibitors to test both hypotheses and know whether preussin activity could be potentiated. It is described that the culture model alters the expression of autophagy-related genes and transcription factors that regulate autophagy, with 3D cell culture better correlating with the tumor than the cells cultured in a monolayer (Follo et al., 2019). In our results, we observed that, when cultured in 3D cell culture models, cells presented a higher number of multivesicular dense bodies, which have also been described previously by other authors to occur in this cell line (Ivers et al., 2014; Malhão et al., 2021). Furthermore, the MDA-MB-231 cells exposed to preussin had a higher number, pleomorphism, and size of the multivesicular bodies. This may indicate that the autophagy process induced by exposure to preussin in the MDA-MB-231 cells might be better represented in the 3D cell cultured cells.

When analyzing apoptosis, necrosis, and cell survival induced by preussin, we noted that the decrease in cell viability was higher than the increase in apoptosis (mainly late apoptosis) and necrosis. The annexin V-PI assay measures changes in the cell membrane, including the loss in its polarity or integrity, distinguishing apoptotic and necrotic cells from alive cells (Crowley et al., 2016; Vermes et al., 1995). In contrast, the MTT assay measures mitochondrial metabolic activity (Meerloo et al., 2011; Präbst et al., 2017). These results

may indicate that the preussin mechanisms of action in the MDA-MB-231 cells may also occur through other processes besides cell death induction (confirmed by the annexin V-PI assay) and may include impairment of cell metabolism and proliferation.

Notably, Dox-induced high levels of necrosis and late apoptosis, mainly in the MDA-MB-231 MCAs, even though at these concentrations, the measured cell viability, through the MTT assay, did not decrease below 50%. It is important to mention that previous studies have shown MTT to be inconsistent and nonspecific (Jakštys et al., 2015; Stepanenko & Dmitrenko, 2015; van Tonder et al., 2015; P. Wang et al., 2010).

With the decrease in cell viability induced by preussin in both 2D and 3D cell cultures, we further investigated whether that fact would also translate into a reduction in long-term survival, using the clonogenic assay. In this assay, for monolayer and 3D cell cultures, Dox consistently inhibited the formation of colonies. Nonetheless, for the preussin exposed groups and the controls, we observed high variability in the number of obtained colonies between assays. We tried various approaches to decrease the obtained variability but could not overcome this inconsistency. We selected the cell seeding density based on the highest number of cells that allowed obtaining isolated colonies without colony superposition, with other authors describing higher concentrations of re-plating for this cell line. Jia et al. (2014) described the usage of this assay similarly to what we described; nonetheless, the number of seeded cells after exposure was 4 times higher but with lower incubation times. Other authors also described the obtention of MDA-MB-231 colonies. Nonetheless, they used a lower cell seeding density, with 300 cells/per well (Franco et al., 2019), while we used 500 cells per well. With the high variability observed, we could not conclude the clonogenic assay on the effects of preussin on long-term survival.

The decrease in cell viability that we observed in the MDA-MB-231 cells exposed to preussin, cultured in a 3D and 2D cell culture model, was accompanied by a reduction in cell proliferation (for the two tested concentrations of 25 and 35 μM), below 50 %. Accordingly, to what was described for cell viability, the decrease in cell proliferation was more accentuated in the cells cultured in a 2D cell culture model. The antiproliferative effects of preussin have been described by other authors. Achenbach et al. (2000) proposed that preussin inhibited cell proliferation at low concentrations but induced cytotoxicity at higher concentrations. Malhão et al. (2019) also described preussin to exhibit antiproliferative proprieties in different BC cell lines cultured in 2D and 3D cell culture models. For MCF-7 and SKBR3, preussin inhibited cell proliferation at concentrations above 25 μM, and only at 50 μM it affected MDA-MB-231 cells cultured in a monolayer (Malhão et al., 2019). As for the 3D cell culture, Malhão et al. (2019) observed that preussin decreased cell proliferation in all cell lines at

50 μM (the lowest tested concentration). Accordingly, the cells exposed to preussin showed a reduced expression of the proliferation marker ki67 in BC cells cultured in a 3D culture model, including the MDA-MB-231 cell line (Malhão et al., 2019).

Priorly, Kasahara et al. (1997) also described preussin to induce cell cycle arrest in the G1 phase in the rat fibroblast cell line 3Y1. Furthermore, Achenbach et al. (2000) explained that preussin reduction of cell proliferation was not caused by inhibition of protein biosynthesis but rather by inhibiting cell cycle progression into the S phase with consequent arrest in the G1 phase through inhibition of cyclin E-CDK2 kinase activity and increase in the expression of the cell cyclin-dependent kinase inhibitors $p27^{KIP-1}$, and decreased cyclin A and E2F-1 (transcription mediator of the CCNE genes) expression, in the HL-60 cells exposed to preussin (Achenbach et al., 2000; Tadesse et al., 2019). In agreement, cyclin E is expressed in the late G1 phase of the cell cycle and activates CDK2, similar to cyclin A, being overexpressed in TNBCs with high recurrence rates (Chen et al., 2018).

The ultrastructural damages observed in mitochondria of cells exposed to preussin, in a concentration-dependent manner (either disorderly and fading of the cristae), may explain not only the decrease in cell viability (since the MTT is in part metabolized by mitochondrial enzymes (Präbst et al., 2017)) but also the decrease in cell proliferation (since mitochondria are described to be involved in the regulation of the cell cycle and cell proliferation (Antico Arciuch et al., 2012)). Nonetheless, further studies should be taken to identify the preussin molecular targets and their specificity towards cyclin E-CDK2 complex, mainly in a TNBC model, such as the MDA-MB-231 cell line.

We also tested the preussin effects on cell migration through the scratch assay. Cell starvation and culture in serum-reduced media were used to inhibit cell growth, which might be a confounding factor in this test. The MDA-MB-231 cell line is described as a TNBC cell line with an invasive phenotype, and it has been described that cell starvation increases the MDA-MB-231 cell aggressiveness and invasion (Ahmadiankia et al., 2019; Ye et al., 2013). Nonetheless, all the tested concentrations of preussin decreased the scratch closure, even at non-lethal doses and at low times of exposure, suggesting a strong effect of preussin in inhibiting cell migration. Further studies of cell invasion and the affected pathways, including cells cultured in a 3D cell culture model, should be performed.

Since TNBC is a subtype of cancer with poor outcomes and is characterized by high rates of invasion and metastasis (Badve et al., 2011; Bauer et al., 2007; Dent et al., 2007; Harris et al., 2006), the development of compounds capable of inhibiting these mechanisms is of great importance.

Our study demonstrated some differences between the 2D and 3D cell culture models. In MDA-MB-231 MCAs, we detected a higher resistance to the effects of preussin, with both inducing a lower reduction in cell viability and proliferation, than in the cells cultured in monolayer. Furthermore, in the unexposed cells, we observed a higher percentage of alive cells in the 2D cell culture model than in cells in 3D cell culture. Consequently, in the 3D cell culture model, we observed a slightly higher number of cells in early apoptosis and a notable difference in cells in late apoptosis/necrosis, compared to the 2D cell culture model. These results may correlate with the oftentimes spotted necrotic-apoptotic core observed in some of the MCAs evaluated through TEM. Besides the necro-apoptotic core, we also observed the presence of lumen-like structures with necrotic and apoptotic cells in the 3D cell cultures. The presence of a necro-apoptotic core in 3D cell culture follows what is described in the literature, mainly in the classically described spheroids (Costa et al., 2016; Habanjar et al., 2021). Even in the less simplistic Malhão et al. (2022) model of cell distribution within the MCAs, it is still possible to observe a higher number of cells in the processes of apoptosis and necrosis, mainly in the center of the MCAs.

We also observed a greater accumulation of lipid droplets in the 3D cultured MDA-MB-231 cells compared to the 2D cultured cells, as described previously (Malhão et al., 2022). These lipidic droplets may also partially explain the higher resistance of the 3D cell cultures to preussin than those cultured in 2D cell culture models. Lipid metabolism of the lipid droplets has been associated with breast cancer malignancy and cell stemness exchanges (Abramczyk et al., 2015). Lipid droplets function as cell organelles with specialized proteins and lipids involved in diverse cell mechanisms, including cell signaling, regulation of inflammatory mediators, and lipid metabolism, and are also involved in membrane exchanges (Abramczyk et al., 2015; Hershey et al., 2019). Lipid droplets have been described to be related to the regulation of cell migration, metastasis, proliferation, and cell survival, linked with multidrug resistance (Gouazé-Andersson et al., 2007; Shyu Jr et al., 2018; Wright et al., 2017). It has been described in the literature that when cultured in different models of culture (2D or 3D), various signaling pathways are activated, and distinct patterns of cell metabolism, differentiation and proliferation rates, viability, cell invasion, transcriptional and apoptosis, as well as the sensitivity to different compounds. In this way, 3D cell culture better mimics the tumor behavior *in vivo* (Białkowska et al., 2020; Duval et al., 2017; Habanjar et al., 2021; Jensen & Teng, 2020; Kapałczyńska et al., 2016; Langhans, 2018).

Overall, the results of this study highlighted the preussin's potential for usage as a scaffold for developing anticancer drugs, including the treatment of TNBC. The major properties of preussin against the TNBC cell line MDA-MB-231, as observed in this study, include anti-

proliferative, cytotoxic (mainly late apoptosis/necrosis), and anti-migratory effects. Additionally, we noticed that preussin had a similar tendency on the MDA-MB-231 cell line in both 2D and 3D cultures and that it did so in a dose-dependent way. Nonetheless, the 3D cell-cultures showed higher resistance to the effects of the drug.

This study also highlighted the value of a refined morphological analysis. The ultrastructural study revealed more numerous pleomorphic multivesicular bodies in MDA-MB-231 cells after preussin treatment, suggesting an increase in autophagic processes. It also allowed observation that preussin induced mitochondrial alterations. Overall, besides corroborating cell death induction, transmission electron microscopy also qualified for unveiling cellular mechanisms caused by the exposure to preussin, otherwise would have been missed. Through ultrastructural analysis, it was possible to observe some morphological differences between the cells cultured in 3D and 2D cell culture models, namely, the presence of high lipid droplet content in cells cultured in 3D culture models. These differences between the culture models may also translate into morphological and physiological differences when comparing *in vitro* and *in vivo* models. These results further corroborate the importance of using cell culture models that better represent the tumor behavior and morphology *in vivo*.

As to future perspectives, it seems relevant to explore the mechanism of action of preussin further, to test its concomitant use with other drugs, or even to test the usage of delivery systems. In this line of thought, additional *in vitro* proxies should be explored to identify some of the molecular targets and signaling pathways affected by exposure to preussin. These items and avenues should include cell cycle arrest, invasion, autophagy, caspases, mitochondrial membrane potential, gene expression, and proteins related to late apoptosis/necrosis, proliferation, and migration, among others.

Wishfully, due to the cytotoxic, anti-proliferative, and anti-migratory properties of preussin, its conjugation with already established TNBC treatment regimens could offer a possibility to mitigate the drug resistance, toxicity, and poor prognosis associated with this aggressive subtype of BC. Conjugating preussin with compounds that may potentiate its effect could allow the reduction of required dosages and potential secondary effects. Depending on the results of further studies, pharmacological combinations could include, for example, drugs involved in autophagy. Furthermore, combining preussin with drug delivery systems such as liposomes, polymeric and inorganic nanoparticles, or antibody-drug conjugates may be a window to decrease the required preussin amount and possible secondary effects.

At last, further studies should also be taken using non-tumoral cell lines, such as human fibroblast cell lines. The results could reveal and help prevent the side effects of preussin in non-tumoral tissues, which is important to validate the use of this fungi-derived compound

in cancer treatment. Whatever the proposals, we cannot forget that the chances of preussin or any anticancer candidate translating into therapies are slim; likely the best reason to try!

Bibliography

Abramczyk, H., Surmacki, J., Kopeć, M., Olejnik, A. K., Lubecka-Pietruszewska, K., & Fabianowska-Majewska, K. (2015). The role of lipid droplets and adipocytes in cancer. Raman imaging of cell cultures: MCF10A, MCF7, and MDA-MB-231 compared to adipocytes in cancerous human breast tissue. The Analyst, 140(7), 2224–2235. https://doi.org/10.1039/C4AN01875C

Achenbach, T. v, Slater, E. P., Brummerhop, H., Bach, T., & Mu, R. (2000). Inhibition of cyclin-dependent kinase activity and induction of apoptosis by preussin in human tumor cells. Antimicrobial Agents and Chemotherapy, 44(10), 2794–2801. https://doi.org/10.1128/aac.44.10.2794-2801.2000

Ahmadiankia, N., Bagheri, M., & Fazli, M. (2019). Differential migration-related gene expression and altered cytokine secretion in response to serum starvation in cultured MDA-MB-231 cells. Asian Biomedicine, 13(4), 123–129. https://doi.org/10.1515/abm-2019-0051

Ahn, S. G., Kim, S. J., Kim, C., & Jeong, J. (2016). Molecular classification of triple-negative breast cancer. Journal of Breast Cancer, 19(3), 223–230. https://doi.org/10.4048/jbc.2016.19.3.223

Alberts, B., Heald, R., Johnson, A., Morgan, D., Raff, M., Roberts, K., & Walter, P. (2022). Molecular Biology of the cell (B. Twitchell, Ed.; 7th ed.). W. W. Norton & Company.

Allison, K. H., Ellis, Ian O., Horii, R., Masuda, S., Penault-Llorca, F., Tsuda, H., & Vicent-Salomon, A. (2019). Epithelial tumors of the Breast. In WHO Classification of Tumors Editorial Board (Ed.), Who classification of tumors: Breast tumors (5th ed., Vol. 2). International Agency for Besearch on Cancer.

Alluri, P., & Newman, L. A. (2014). Basal-like and triple-negative breast cancers. Surgical Oncology Clinics of North America, 23(3), 567–577. https://doi.org/10.1016/j.soc.2014.03.003

Altmann, K. H. (2017). Drugs from the oceans: Marine natural products as leads for drug discovery. Chimia, 71(10), 646–651. https://doi.org/10.2533/chimia.2017.646

Ameen, F., AlNadhari, S., & Al-Homaidan, A. A. (2021). Marine microorganisms as an untapped source of bioactive compounds. Saudi Journal of Biological Sciences, 28(1), 224–231. https://doi.org/10.1016/j.sjbs.2020.09.052

Antoniou, A., Pharoah, P. D. P., Narod, S., Risch, H. A., Eyfjord, J. E., Hopper, J. L., Loman, N., Olsson, H., Johannsson, O., Borg, Å., Pasini, B., Radice, P., Manoukian, S., Eccles, D. M., Tang, N., Olah, E., Anton-Culver, H., Warner, E., Lubinski, J., … Easton, D. F. (2003). Average risks of breast and ovarian cancer associated with BRCA1 or BRCA2 mutations detected in case series unselected for family history: a combined analysis of 22 studies. The American Journal of Human Genetics, 72(5), 1117–1130. https://doi.org/10.1086/375033

Arciuch, V. G. A., Elguero, M. E., Poderoso, J. J., & Carreras, M. C. (2012). Mitochondrial regulation of cell cycle and proliferation. Antioxidants & Redox Signaling, 16(10), 1150–1180. https://doi.org/10.1089/ars.2011.4085

Arévalo-García, E. B. (2014). A concise and efficient synthesis of (+)-preussin. Heterocyclic Communications, 20(1), 47–50. https://doi.org/10.1515/hc-2013-0236

Atanasov, A. G., Zotchev, S. B., Dirsch, V. M., & Supuran, C. T. (2021). Natural products in drug discovery: advances and opportunities. Nature Reviews Drug Discovery, 20(3), 200–216. https://doi.org/10.1038/s41573-020-00114-z

Azqueta, A., & Collins, A. R. (2013). The essential comet assay: a comprehensive guide to measuring DNA damage and repair. Archives of Toxicology, 87(6), 949–968. https://doi.org/10.1007/s00204-013-1070-0

Badve, S., Dabbs, D. J., Schnitt, S. J., Baehner, F. L., Decker, T., Eusebi, V., Fox, S. B., Ichihara, S., Jacquemier, J., Lakhani, S. R., Palacios, J., Rakha, E. A., Richardson, A. L., Schmitt, F. C., Tan, P.-H., Tse, G. M., Weigelt, B., Ellis, I. O., & Reis-Filho, J. S. (2011). Basal-like and triple-negative breast cancers: a critical review with an emphasis on the implications for pathologists and oncologists. Modern Pathology, 24(2), 157–167. https://doi.org/10.1038/modpathol.2010.200

Basler, B., Brandes, S., Spiegel, A., & Bach, T. (2005). Total syntheses of kelsoene and preussin. Topics in Current Chemistry, 243, 1–42. https://doi.org/10.1007/b96880

Bastien, R. R., Rodríguez-Lescure, Á., Ebbert, M. T., Prat, A., Munárriz, B., Rowe, L., Miller, P., Ruiz-Borrego, M., Anderson, D., Lyons, B., Álvarez, I., Dowell, T., Wall, D., Seguí, M. Á., Barley, L., Boucher, K. M., Alba, E., Pappas, L., Davis, C. A., … Martín, M. (2012). PAM50 breast cancer subtyping by RT-qPCR and concordance with standard clinical molecular markers. BMC Medical Genomics, 5. https://doi.org/10.1186/1755-8794-5-44

Bauer, K. R., Brown, M., Cress, R. D., Parise, C. A., & Caggiano, V. (2007). Descriptive analysis of estrogen receptor (ER)-negative, progesterone receptor (PR)-negative, and

HER2-negative invasive breast cancer, the so-called triple-negative phenotype. Cancer, 109(9), 1721–1728. https://doi.org/10.1002/cncr.22618

Beck, A., Goetsch, L., Dumontet, C., & Corvaïa, N. (2017). Strategies and challenges for the next generation of antibody-drug conjugates. Nature Reviews Drug Discovery, 16(5), 315–337. https://doi.org/10.1038/nrd.2016.268

Beier, C., & Schaumann, E. (1997). An epoxide-based enantioselective synthesis of the antifungal antibiotic (+)-preussin. Synthesis, 1997(11), 1296–1300. https://doi.org/10.1055/s-1997-1347

Bertucci, F., Finetti, P., Cervera, N., Esterni, B., Hermitte, F., Viens, P., & Birnbaum, D. (2008). How basal are triple-negative breast cancers? International Journal of Cancer, 123(1), 236–240. https://doi.org/10.1002/ijc.23518

Białkowska, K., Komorowski, P., Bryszewska, M., & Miłowska, K. (2020). Spheroids as a type of three-dimensional cell cultures – examples of methods of preparation and the most important application. International Journal of Molecular Sciences, 21(17), 1–17. https://doi.org/10.3390/ijms21176225

Blayney, D. W., Mohanlal, R., Adamchuk, H., Kirtbaya, D. V., Chen, M., Du, L., Ogenstad, S., Ginn, G., Huang, L., & Zhang, Q. (2022). Efficacy of plinabulin vs pegfilgrastim for prevention of docetaxel-induced neutropenia in patients with solid tumors. JAMA Network Open, 5(1), e2145446. https://doi.org/10.1001/jamanetworkopen.2021.45446

Børresen-Dale, & Anne-Lise. (2003). TP53 and breast cancer. Human Mutation, 21(3), 292–300. https://doi.org/10.1002/humu.10174

Bray, F., & Møller, B. (2006). Predicting the future burden of cancer. Nature Reviews Cancer, 6(1), 63–74. https://doi.org/10.1038/nrc1781

Brinton, L. A., Figueroa, J. D., Awuah, B., Yarney, J., Wiafe, S., Wood, S. N., Ansong, D., Nyarko, K., Wiafe-Addai, B., & Clegg-Lamptey, J. N. (2014). Breast cancer in Sub-Saharan Africa: Opportunities for prevention. Breast Cancer Research and Treatment, 144(3), 467–478. https://doi.org/10.1007/s10549-014-2868-z

Brinton, L. A., Gaudet, M. M., & Gierach, G. L. (2018). Breast cancer. In M. J. Thun, M. S. Linet, J. R. Cerhan, A. H. Christopher, & D. Schottenfeld (Eds.), Schottenfeld and Fraumeni cancer epidemiology and prevention (4th ed., pp. 861–888). Oxford university press.

Brown, M., Tsodikov, A., Bauer, K. R., Parise, C. A., & Caggiano, V. (2008). The role of human epidermal growth factor receptor 2 in the survival of women with estrogen and progesterone receptor-negative, invasive breast cancer: The California Cancer Registry, 1999–2004. Cancer, 112(4), 737–747. https://doi.org/10.1002/cncr.23243

Buchman, M., Csatayová, K., Davies, S. G., Fletcher, A. M., Houlsby, I. T. T., Roberts, P. M., Rowe, S. M., & Thomson, J. E. (2016). Asymmetric Syntheses of (+)-Preussin B, the C(2)-Epimer of (-)-Preussin B, and 3-Deoxy-(+)-preussin B. Journal of Organic Chemistry, 81(12), 4907–4922. https://doi.org/10.1021/acs.joc.6b00362

Burstein, M. D., Tsimelzon, A., Poage, G. M., Covington, K. R., Contreras, A., Fuqua, S. A. W., Savage, M. I., Osborne, C. K., Hilsenbeck, S. G., Chang, J. C., Mills, G. B., Lau, C. C., & Brown, P. H. (2015). Comprehensive genomic analysis identifies novel subtypes and targets of triple-negative breast cancer. Clinical Cancer Research, 21(7), 1688–1698. https://doi.org/10.1158/1078-0432.CCR-14-0432

Buttachon, S., Ramos, A., Inácio, Â., Dethoup, T., Gales, L., Lee, M., Costa, P., Silva, A., Sekeroglu, N., Rocha, E., Pinto, M., Pereira, J., & Kijjoa, A. (2018). Bis-indolyl benzenoids, hydroxypyrrolidine derivatives and other constituents from cultures of the marine sponge-associated fungus *Aspergillus candidus* KUFA0062. Marine Drugs, 16(4), 119. https://doi.org/10.3390/md16040119

Caan, B. J., Sweeney, C., Habel, L. A., Kwan, M. L., Kroenke, C. H., Weltzien, E. K., Quesenberry, C. P., Castillo, A., Factor, R. E., Kushi, L. H., & Bernard, P. S. (2014). Intrinsic subtypes from the PAM50 gene expression assay in a population-based breast cancer survivor cohort: prognostication of short- and long-term outcomes. Cancer Epidemiology, Biomarkers & Prevention, 23(5), 725–734. https://doi.org/10.1158/1055-9965.EPI-13-1017

Cardoso, F., Kyriakides, S., Ohno, S., Penault-Llorca, F., Poortmans, P., Rubio, I. T., Zackrisson, S., & Senkus, E. (2019). Early breast cancer: ESMO clinical practice guidelines for diagnosis, treatment and follow-up. Annals of Oncology, 30(8), 1194–1220. https://doi.org/10.1093/annonc/mdz173

Cheang, M. C. U., Voduc, D., Bajdik, C., Leung, S., McKinney, S., Chia, S. K., Perou, C. M., & Nielsen, T. O. (2008). Basal-like breast cancer defined by five biomarkers has superior prognostic value than triple-negative phenotype. Clinical Cancer Research, 14(5), 1368–1376. https://doi.org/10.1158/1078-0432.CCR-07-1658

Chen, X., Low, K. H., Alexander, A., Jiang, Y., Karakas, C., Hess, K. R., Carey, J. P. W., Bui, T. N., Vijayaraghavan, S., Evans, K. W., Yi, M., Ellis, D. C., Cheung, K. L., Ellis, I. O.,

Fu, S., Meric-Bernstam, F., Hunt, K. K., & Keyomarsi, K. (2018). Cyclin E overexpression sensitizes triple-negative breast cancer to Wee1 kinase inhibition. Clinical Cancer Research, 24(24), 6594–6610. https://doi.org/10.1158/1078-0432.CCR-18-1446

ClinicalTrials.gov. (n.d.). Retrieved September 5, 2022, from https://clinicaltrials.gov/

Coates, A. S., Winer, E. P., Goldhirsch, A., Gelber, R. D., Gnant, M., Piccart-Gebhart, M. J., Thürlimann, B., Senn, H. J., André, F., Baselga, J., Bergh, J., Bonnefoi, H., Burstein, H., Cardoso, F., Castiglione-Gertsch, M., Colleoni, M., Curigliano, G., Davidson, N. E., Leo, A. di, … Xu, B. (2015). Tailoring therapies-improving the management of early breast cancer: St Gallen international expert consensus on the primary therapy of early breast cancer 2015. Annals of Oncology, 26(8), 1533–1546. https://doi.org/10.1093/annonc/mdv221

Cocco, S., Leone, A., Piezzo, M., Caputo, R., di Lauro, V., di Rella, F., Fusco, G., Capozzi, M., Gioia, G. di, Budillon, A., & de Laurentiis, M. (2020). Targeting autophagy in breast cancer. International Journal of Molecular Sciences, 21(21), 7836. https://doi.org/10.3390/ijms21217836

Collins, A. R., Oscoz, A. A., Brunborg, G., Gaivao, I., Giovannelli, L., Kruszewski, M., Smith, C. C., & Stetina, R. (2008). The comet assay: topical issues. Mutagenesis, 23(3), 143–151. https://doi.org/10.1093/mutage/gem051

Cory, G. (2011). Scratch-wound assay. In C. M. Wells & M. Parsons (Eds.), Cell Migration: Developmental Methods and Protocols (2nd ed., pp. 25–30). Human Press. https://doi.org/10.1007/978-1-61779-207-6_2

Costa, E. C., Moreira, A. F., de Melo-Diogo, D., Gaspar, V. M., Carvalho, M. P., & Correia, I. J. (2016). 3D tumor spheroids: an overview on the tools and techniques used for their analysis. Biotechnology Advances, 34(8), 1427–1441. https://doi.org/10.1016/j.biotechadv.2016.11.002

Cragg, G. M., & Pezzuto, J. M. (2016). Natural products as a vital source for the discovery of cancer chemotherapeutic and chemopreventive agents. Medical Principles and Practice, 25(2), 41–59. https://doi.org/10.1159/000443404

Crowley, L. C., Marfell, B. J., Scott, A. P., & Waterhouse, N. J. (2016). Quantitation of apoptosis and necrosis by annexin v binding, propidium iodide uptake, and flow cytometry. Cold Spring Harbor Protocols, 2016(11), 953–957. https://doi.org/10.1101/pdb.prot087288

Cui, Q., Bian, R., Xu, F., Li, Q., Wang, W., & Bian, Q. (2021). New molecular entities and structure–activity relationships of drugs designed by the natural product derivatization

method from 2010 to 2018. In Atta-ur-Rahman (Ed.), Bioactive Natural Products (Vol. 69, pp. 371–415). Elsevier. https://doi.org/10.1016/B978-0-12-819487-4.00016-1

Cybulski, C., Wokołorczyk, D., Jakubowska, A., Huzarski, T., Byrski, T., Gronwald, J., Masojć, B., Dębniak, T., Górski, B., Blecharz, P., Narod, S. A., & Lubiński, J. (2011). Risk of breast cancer in women with a CHEK2 mutation with and without a family history of breast cancer. Journal of Clinical Oncology, 29(28), 3747–3752. https://doi.org/10.1200/JCO.2010.34.0778

Dai, X., Cheng, H., Bai, Z., & Li, J. (2017). Breast cancer cell line classification and its relevance with breast tumor subtyping. Journal of Cancer, 8(16), 3131–3141. https://doi.org/10.7150/jca.18457

de Oliveira Júnior, R. G., Christiane Adrielly, A. F., da Silva Almeida, J. R. G., Grougnet, R., Thiéry, V., & Picot, L. (2018). Sensitization of tumor cells to chemotherapy by natural products: A systematic review of preclinical data and molecular mechanisms. Fitoterapia, 129, 383–400. https://doi.org/10.1016/j.fitote.2018.02.025

Debbab, A., Aly, A. H., & Proksch, P. (2011). Bioactive secondary metabolites from endophytes and associated marine derived fungi. Fungal Diversity, 49, 1–12. https://doi.org/10.1007/s13225-011-0114-0

Deeks, E. D. (2021). Disitamab vedotin: first approval. Drugs, 81(16), 1929–1935. https://doi.org/10.1007/s40265-021-01614-x

Dehelean, C. A., Marcovici, I., Soica, C., Mioc, M., Coricovac, D., Iurciuc, S., Cretu, O. M., & Pinzaru, I. (2021). Plant-derived anticancer compounds as new perspectives in drug discovery and alternative therapy. Molecules, 26(4). https://doi.org/10.3390/molecules26041109

Dent, R., Trudeau, M., Pritchard, K. I., Hanna, W. M., Kahn, H. K., Sawka, C. A., Lickley, L. A., Rawlinson, E., Sun, P., & Narod, S. A. (2007). Triple-negative breast cancer: Clinical features and patterns of recurrence. Clinical Cancer Research, 13(15), 4429–4434. https://doi.org/10.1158/1078-0432.CCR-06-3045

Deshmukh, S. K., Prakash, V., & Ranjan, N. (2018). Marine fungi: A source of potential anticancer compounds. Frontiers in Microbiology, 8, 2536. https://doi.org/10.3389/fmicb.2017.02536

Draper, J. A., & Britton, R. (2010). A concise and stereoselective synthesis of hydroxypyrrolidines: Rapid synthesis of (+)-preussin. Organic Letters, 12(18), 4034–4037. https://doi.org/10.1021/ol101631e

Dubois, C., Dufour, R., Daumar, P., Aubel, C., Szczepaniak, C., Blavignac, C., Mounetou, E., Penault-Llorca, F., & Bamdad, M. (2017). Development and cytotoxic response of two proliferative MDA-MB-231 and non-proliferative SUM1315 three-dimensional cell culture models of triple-negative basal-like breast cancer cell lines. Oncotarget, 8(56), 95316–95331. https://doi.org/10.18632/oncotarget.20517

Duval, K., Grover, H., Han, L. H., Mou, Y., Pegoraro, A. F., Fredberg, J., & Chen, Z. (2017). Modeling physiological events in 2D vs. 3D cell culture. Physiology, 32(4), 266–277. https://doi.org/10.1152/physiol.00036.2016

Dyshlovoy, S. A., & Honecker, F. (2019). Marine compounds and cancer: the first two decades of XXI century. Marine Drugs, 18(1), 20. https://doi.org/10.3390/md18010020

Edmondson, R., Broglie, J. J., Adcock, A. F., & Yang, L. (2014). Three-dimensional cell culture systems and their applications in drug discovery and cell-based biosensors. ASSAY and Drug Development Technologies, 12(4), 207–218. https://doi.org/10.1089/adt.2014.573

el Azreq, M.-A., Naci, D., & Aoudjit, F. (2012). Collagen/β1 integrin signaling up-regulates the ABCC1/MRP-1 transporter in an ERK/MAPK-dependent manner. Molecular Biology of the Cell, 23(17), 3473–3484. https://doi.org/10.1091/mbc.e12-02-0132

Fang, Y., & Eglen, R. M. (2017). Three-dimensional cell cultures in drug discovery and development. SLAS Discovery, 22(5), 456–472. https://doi.org/10.1177/1087057117696795

Ferlay, J., Ervik, M., Lam, F., Colombet, M., Mery, L., Piñeros, M., Znaor, A., Soerjomataram, I., & Bray, F. (2020). Global Cancer Observatory: Cancer Today. Lyon, France: International Agency for Research on Cancer. https://gco.iarc.fr/today

Follo, C., Barbone, D., Richards, W. G., Bueno, R., & Courtney Broaddus, V. (2019). Autophagy in 3D *in vitro* and *ex vivo* cancer models. In: Ktistakis, N., Florey, O. (Eds.), Autophagy: Methods and Protocols (Vol. 1880, pp. 491–510). Springer New York. https://doi.org/10.1007/978-1-4939-8873-0_31

Fontoura, J. C., Viezzer, C., dos Santos, F. G., Ligabue, R. A., Weinlich, R., Puga, R. D., Antonow, D., Severino, P., & Bonorino, C. (2020). Comparison of 2D and 3D cell culture

models for cell growth, gene expression and drug resistance. Materials Science and Engineering: C, 107, 110264. https://doi.org/10.1016/j.msec.2019.110264

Fougner, C., Bergholtz, H., Norum, J. H., & Sørlie, T. (2020). Re-definition of claudin-low as a breast cancer phenotype. Nature Communications, 11(1). https://doi.org/10.1038/s41467-020-15574-5

Franco, M. S., Roque, M. C., & Oliveira, M. C. (2019). Short and long-term effects of the exposure of breast cancer cell lines to different ratios of free or co-encapsulated lipo-somal paclitaxel and doxorubicin. Pharmaceutics, 11(4). https://doi.org/10.3390/pharmaceutics11040178

Freshney, R. I. (2005). Culture of animal cells: a manual of basic technique (5th ed.). John Wiley & Sons, Inc.

Freshney, R. I. (2010). Culture of animal cells: a manual of basic technique (6th ed.). John Wiley & Sons, Inc.

Froehlich, K., Haeger, J. D., Heger, J., Pastuschek, J., Photini, S. M., Yan, Y., Lupp, A., Pfarrer, C., Mrowka, R., Schleuβner, E., Markert, U. R., & Schmidt, A. (2016). Generation of multicellular breast cancer tumor spheroids: comparison of different protocols. Journal of Mammary Gland Biology and Neoplasia, 21(3–4), 89–98. https://doi.org/10.1007/s10911-016-9359-2

Fukuda, T., Sudoh, Y., Tsuchiya, Y., Okuda, T., & Igarashi, Y. (2014). Isolation and biosynthesis of preussin B, a pyrrolidine alkaloid from *Simplicillium lanosoniveum*. Journal of Natural Products, 77(4), 813–817. https://doi.org/10.1021/np400910r

Fusco, N., Sajjadi, E., Venetis, K., Gaudioso, G., Lopez, G., Corti, C., Guerini Rocco, E., Criscitiello, C., Malapelle, U., & Invernizzi, M. (2020). PTEN alterations and their role in cancer management: Are we making headway on precision medicine? Genes, 11(7), 719. https://doi.org/10.3390/genes11070719

Garrido-Castro, A. C., Lin, N. U., & Polyak, K. (2019). Insights into molecular classifications of triple-negative breast cancer: improving patient selection for treatment. Cancer Discovery, 9(2), 176–198. https://doi.org/10.1158/2159-8290.CD-18-1177

Gatti, R., Ataxia-Telangiectasia, P. S., Adam, M. P., Everman, D. B., & Mirzaa, G. M. (1999 (updated 2016)). Ataxia-Telangiectasia. In M. P. Adam, D. B. Everman, G. M. Mirzaa, R. A. Pagon, & S. E. Wallace (Eds.), Gene Reviews: University of Washington. https://www.ncbi.nlm. nih.gov/books/NBK26468

Gauthier, D. T., Cartwright, D. D., Densmore, C. L., Blazer, V. S., & Ottinger, C. A. (2003). Measurement of *in vitro* leucocyte mitogenesis in FISH: ELISA based detection of the thymidine analogue. Fish & Shellfish Immunology, 14(4), 279–288. https://doi.org/10.1006/fsim.2002.0436

Gaynes, R. (2017). The discovery of penicillin – New insights after more than 75 years of clinical use. Emerging Infectious Diseases, 23(5), 849–853. https://doi.org/10.3201/eid2305.161556

Goldhirsch, A., Winer, E. P., Coates, A. S., Gelber, R. D., Piccart-Gebhart, M., Thürlimann, B., Senn, H.-J., Albain, K. S., André, F., Bergh, J., Bonnefoi, H., Bretel-Morales, D., Burstein, H., Cardoso, F., Castiglione-Gertsch, M., Coates, A. S., Colleoni, M., Costa, A., Curigliano, G., … Wood, W. C. (2013). Personalizing the treatment of women with early breast cancer: highlights of the St Gallen international expert consensus on the primary therapy of early breast cancer 2013. Annals of Oncology, 24(9), 2206–2223. https://doi.org/10.1093/annonc/mdt303

Goss Kinzy, T., Harger, J. W., Carr-Schmid, A., Kwon, J., Shastry, M., Justice, M., & Dinman, J. D. (2002). New targets for antivirals: The ribosomal A-site and the factors that interact with it. Virology, 300(1), 60–70. https://doi.org/10.1006/viro.2002.1567

Gouazé-Andersson, V., Yu, J. Y., Kreitenberg, A. J., Bielawska, A., Giuliano, A. E., & Cabot, M. C. (2007). Ceramide and glucosylceramide upregulate expression of the multidrug resistance gene MDR1 in cancer cells. Biochimica et Biophysica Acta (BBA) - Molecular and Cell Biology of Lipids, 1771(12), 1407–1417. https://doi.org/10.1016/j.bbalip.2007.09.005

Gstraunthaler, G., Lindl, T., & van der Valk, J. (2013). A plea to reduce or replace fetal bovine serum in cell culture media. Cytotechnology, 65(5), 791–793. https://doi.org/10.1007/s10616-013-9633-8

Gu, B. bin, Jiao, F. R., Wu, W., Jiao, W. H., Li, L., Sun, F., Wang, S. P., Yang, F., & Lin, H. W. (2018). Preussins with inhibition of IL-6 expression from *Aspergillus flocculosus* 16D-1, a fungus isolated from the marine sponge *Phakellia fusca*. Journal of Natural Products, 81(10), 2275–2281. https://doi.org/10.1021/acs.jnatprod.8b00662

Habanjar, O., Diab-Assaf, M., Caldefie-Chezet, F., & Delort, L. (2021). 3D cell culture systems: tumor application, advantages, and disadvantages. International Journal of Molecular Sciences, 22(22), 12200. https://doi.org/10.3390/ijms222212200

Hammer, D. A. T., Ryan, P. D., Hammer, Ø., & Harper, D. A. T. (2001). PAST: paleontological statistics software package for education and data analysis. Palaeontologia Electronica, 4(1), 9.

Han, Y., Fan, S., Qin, T., Yang, J., Sun, Y., Lu, Y., Mao, J., & Li, L. (2018). Role of autophagy in breast cancer and breast cancer stem cells (Review). International Journal of Oncology. https://doi.org/10.3892/ijo.2018.4270

Harris, L. N., Broadwater, G., Lin, N. U., Miron, A., Schnitt, S. J., Cowan, D., Lara, J., Bleiweiss, I., Berry, D., Ellis, M., Hayes, D. F., Winer, E. P., & Dressler, L. (2006). Molecular subtypes of breast cancer in relation to paclitaxel response and outcomes in women with metastatic disease: results from CALGB 9342. Breast Cancer Research, 8(6), R66. https://doi.org/10.1186/bcr1622

Harvey, A. (2008). Natural products in drug discovery. Drug Discovery Today, 13(19–20), 894–901. https://doi.org/10.1016/j.drudis.2008.07.004

Hausherr, A., Siemeister, G., & Reissig, H. U. (2019). Alkoxyallene-based syntheses of preussin and its analogs and their cytotoxicity. Organic and Biomolecular Chemistry, 17(1), 122–134. https://doi.org/10.1039/c8ob02645a

Heer, E., Harper, A., Escandor, N., Sung, H., McCormack, V., & Fidler-Benaoudia, M. M. (2020). Global burden and trends in premenopausal and postmenopausal breast cancer: a population-based study. The Lancet Global Health, 8(8), e1027–e1037. https://doi.org/10.1016/S2214-109X(20)30215-1

Hershey, B. J., Vazzana, R., Joppi, D. L., & Havas, K. M. (2019). Lipid droplets define a sub-population of breast cancer stem cells. Journal of Clinical Medicine, 9(1), 87. https://doi.org/10.3390/jcm9010087

How, C. W., Ong, Y. S., Low, S. S., Pandey, A., Show, P. L., & Foo, J. B. (2021). How far have we explored fungi to fight cancer? Seminars in Cancer Biology. https://doi.org/10.1016/j.semcancer.2021.03.009

Howlader, N., Altekruse, S. F., Li, C. I., Chen, V. W., Clarke, C. A., Ries, L. A. G., & Cronin, K. A. (2014). US incidence of breast cancer subtypes defined by joint hormone receptor and HER2 status. Journal of the National Cancer Institute, 106(5). https://doi.org/10.1093/jnci/dju055

Hu, Z.-Y., Liu, L., Xie, N., Lu, J., Liu, Z., Tang, Y., Wang, Y., Yang, J., & Ouyang, Q. (2020). Germline PALB2 mutations in cancers and Its distinction from somatic PALB2 mutations in breast cancers. Frontiers in Genetics, 11. https://doi.org/10.3389/fgene.2020.00829

Huang, P. Q., Geng, H., Tian, Y. S., Peng, Q. R., & Xiao, K. J. (2015). The first enantioselective total synthesis of (+)-preussin B and an improved synthesis of (+)-preussin by step-economical methods. Science China Chemistry, 58(3), 478–482. https://doi.org/10.1007/s11426-014-5270-0

Huang, Z., Yu, P., & Tang, J. (2020). Characterization of triple-negative breast cancer MDA-MB-231 cell spheroid model. OncoTargets and Therapy, 13, 5395–5405. https://doi.org/10.2147/OTT.S249756

Hulst, M. B., Grocholski, T., Neefjes, J. J. C., van Wezel, G. P., & Metsä-Ketelä, M. (2022). Anthracyclines: biosynthesis, engineering and clinical applications. Natural Product Reports, 39(4), 814–841. https://doi.org/10.1039/D1NP00059D

Imamura, Y., Mukohara, T., Shimono, Y., Funakoshi, Y., Chayahara, N., Toyoda, M., Kiyota, N., Takao, S., Kono, S., Nakatsura, T., & Minami, H. (2015). Comparison of 2D- and 3D-culture models as drug-testing platforms in breast cancer. Oncology Reports, 33(4), 1837–1843. https://doi.org/10.3892/or.2015.3767

Ivascu, A., & Kubbies, M. (2007). Diversity of cell-mediated adhesions in breast cancer spheroids. International Journal of Oncology, 31(6), 1403–1413. http://www.ncbi.nlm.nih.gov/pubmed/17982667

Ivers, L. P., Cummings, B., Owolabi, F., Welzel, K., Klinger, R., Saitoh, S., O'Connor, D., Fujita, Y., Scholz, D., & Itasaki, N. (2014). Dynamic and influential interaction of cancer cells with normal epithelial cells in 3D culture. Cancer Cell International, 14(1), 108. https://doi.org/10.1186/s12935-014-0108-6

Jakštys, B., Ruzgys, P., Tamošiūnas, M., & Šatkauskas, S. (2015). Different cell viability assays reveal inconsistent results after bleomycin electrotransfer *in vitro*. The Journal of Membrane Biology, 248(5), 857–863. https://doi.org/10.1007/s00232-015-9813-x

Jayme, D., Watanabe, T., & Shimada, T. (1997). Basal medium development for serum-free culture: a historical perspective. Cytotechnology, 23(1/3), 95–101. https://doi.org/10.1023/A:1007967602484

Jensen, C., & Teng, Y. (2020). Is it time to start transitioning from 2D to 3D cell culture? Frontiers in Molecular Biosciences, 7. https://doi.org/10.3389/fmolb.2020.00033

Jia, T., Zhang, L., Duan, Y., Zhang, M., Wang, G., Zhang, J., & Zhao, Z. (2014). The differential susceptibilities of MCF-7 and MDA-MB-231 cells to the cytotoxic effects of curcumin are associated with the PI3K/Akt-SKP2- Cip/Kips pathway. Cancer Cell International, 14(1). https://doi.org/10.1186/s12935-014-0126-4

Jiménez, C. (2018). Marine natural products in medicinal chemistry. ACS Medicinal Chemistry Letters, 9(10), 959–961. https://doi.org/10.1021/acsmedchemlett.8b00368

Jimenez, P., Wilke, D., & Costa-Lotufo, L. (2018). Marine drugs for cancer: surfacing biotechnological innovations from the oceans. Clinics, 73(Suppl 1), 1–7. https://doi.org/10.6061/clinics/2018/e482s

Johnson, J. H., Phillipson, D. W., & Kahle, A. D. (1989). The relative and absolute stereochemistry of the antifungal agent preussin. The Journal of Antibiotics, 42(7), 1184–1185. https://doi.org/10.7164/antibiotics.42.1184

Kanazawa, A., Gillet, S., Delair, P., & Greene, A. E. (1986). Practical Asymmetric Approach to Pyrrolidinones: EfficientSynthesis of (+)-Preussin and (-)-AHPPA. J. I.; Linden, A. J. Org. Chem, 27(2), 4660–4663. https://doi.org/10.1021/jo9801162

Kapałczyńska, M., Kolenda, T., Przybyła, W., Zajączkowska, M., Teresiak, A., Filas, V., Ibbs, M., Bliźniak, R., Łuczewski, Ł., & Lamperska, K. (2016). 2D and 3D cell cultures – a comparison of different types of cancer cell cultures. Archives of Medical Science, 1–10. https://doi.org/10.5114/aoms.2016.63743

Kasahara, K., Yoshida, M., Eishima, J., Takesako, K., Beppu, T., & Horinouchi, S. (1997). Identification of preussin as a selective inhibitor for cell growth of the fission yeast ts mutants defective in Cdc2-regulatory genes. The Journal of Antibiotics, 50(3), 267–269. https://doi.org/10.7164/antibiotics.50.267

Kaurah, P., Huntsman, D. G., Adam, M. P., Everman, D. B., & Mirzaa, G. M. (2002 (updated 2018)). Hereditary Diffuse Gastric Cancer. In M. P. Adam, D. B. Everman, G. M. Mirzaa, R. A. Pagon, & S. E. Wallace (Eds.). Gene Review. University of Washington. https://www.ncbi.nlm.nih.gov/books/NBK1266

Khandare, S. P., Reddy, P. O., & Prasad, K. R. (2020). Addition of lithium anion of (acetylmethylene)triphenylphosphorane to nonracemic sulfinimines: total synthesis of (+)-241D and formal total synthesis of (+)-preussin. Organic Letters, 22(18), 7273–7277. https://doi.org/10.1021/acs.orglett.0c02608

Kieffer, S. R., & Lowndes, N. F. (2022). Immediate-early, early, and late responses to DNA double stranded breaks. Frontiers in Genetics, 13. https://doi.org/10.3389/fgene.2022.793884

Konduri, S., Singh, M., Bobustuc, G., Rovin, R., & Kassam, A. (2020). Epidemiology of male breast cancer. Breast, 54, 8–14. https://doi.org/10.1016/j.breast.2020.08.010

Kornienko, A., Mathieu, V., Rastogi, S. K., Lefranc, F., & Kiss, R. (2013). Therapeutic agents triggering nonapoptotic cancer cell death. Journal of Medicinal Chemistry, 56(12), 4823–4839. https://doi.org/10.1021/jm400136m

Lakhani, S. R., van de Vijver, M. J., Jacquemier, J., Anderson, T. J., Osin, P. P., McGuffog, L., & Easton, D. F. (2002). The pathology of familial breast cancer: predictive value of immunohistochemical markers estrogen receptor, progesterone receptor, HER-2, and P53 in patients with mutations in BRCA1 and BRCA2. Journal of Clinical Oncology, 20(9), 2310–2318. https://doi.org/10.1200/JCO.2002.09.023

Langhans, S. A. (2018). Three-dimensional *in vitro* cell culture models in drug discovery and drug repositioning. Frontiers in Pharmacology, 9(JAN), 1–14. https://doi.org/10.3389/fphar.2018.00006

Large, D. E., Abdelmessih, R. G., Fink, E. A., & Auguste, D. T. (2021). Liposome composition in drug delivery design, synthesis, characterization, and clinical application. Advanced Drug Delivery Reviews, 176, 113851. https://doi.org/10.1016/j.addr.2021.113851

Lee, K. Y., Kim, Y. H., Oh, C. Y., & Ham, W. H. (2000). Facile and efficient total synthesis of (+)-preussin. Organic Letters, 2(25), 4041–4042. https://doi.org/10.1021/ol000289p

Lehmann, B. D., Bauer, J. A., Chen, X., Sanders, M. E., Chakravarthy, A. B., Shyr, Y., & Pietenpol, J. A. (2011). Identification of human triple-negative breast cancer subtypes and preclinical models for selection of targeted therapies. Journal of Clinical Investigation, 121(7), 2750–2767. https://doi.org/10.1172/JCI45014

Lei, S., Zheng, R., Zhang, S., Wang, S., Chen, R., Sun, K., Zeng, H., Zhou, J., & Wei, W. (2021). Global patterns of breast cancer incidence and mortality: A population-based cancer registry data analysis from 2000 to 2020. Cancer Communications, 41(11), 1183–1194. https://doi.org/10.1002/cac2.12207

Lin, S.-R., Chang, C.-H., Hsu, C.-F., Tsai, M.-J., Cheng, H., Leong, M. K., Sung, P.-J., Chen, J.-C., & Weng, C.-F. (2019). Natural compounds as potential adjuvants to cancer therapy: Preclinical evidence. https://doi.org/10.1111/bph.v177.6/issuetoc

Lovitt, C. J., Shelper, T. B., & Avery, V. M. (2018). Doxorubicin resistance in breast cancer cells is mediated by extracellular matrix proteins. BMC Cancer, 18(1), 41. https://doi.org/10.1186/s12885-017-3953-6

Łukasiewicz, S., Czeczelewski, M., Forma, A., Baj, J., Sitarz, R., & Stanisławek, A. (2021). Breast cancer - Epidemiology, risk factors, classification, prognostic markers, and current treatment strategies - An updated review. Cancers, 13(17), 4287. https://doi.org/10.3390/cancers13174287

Lv, D., Hu, Z., Lu, L., Lu, H., & Xu, X. (2017). Three dimensional cell culture: A powerful tool in tumor research and drug discovery (Review). Oncology Letters, 14(6), 6999–7010. https://doi.org/10.3892/ol.2017.7134

Lyons, T. G. (2019). Targeted Therapies for triple-negative breast cancer. Current treatment options in oncology, 20, 82. https://doi.org/10.1007/s11864-019-0682-x

Malhão, F., Macedo, A. C., Costa, C., Rocha, E., & Ramos, A. A. (2021). Fucoxanthin holds potential to become a drug adjuvant in breast cancer treatment: Evidence from 2D and 3D cell cultures. Molecules, 26(14), 4288. https://doi.org/10.3390/molecules26144288

Malhão, F., Macedo, A., Ramos, A., & Rocha, E. (2022). Morphometrical, morphological, and immunocytochemical characterization of a tool for cytotoxicity research: 3D cultures of breast cell lines grown in ultra-low attachment plates. Toxics, 10(8), 415. https://doi.org/10.3390/toxics10080415

Malhão, F., Ramos, A. A., Buttachon, S., Dethoup, T., Kijjoa, A., & Rocha, E. (2019). Cytotoxic and antiproliferative effects of preussin, a hydroxypyrrolidine derivative from the marine sponge-associated fungus *Aspergillus candidus* KUFA 0062, in a panel of breast cancer cell lines and using 2D and 3D cultures. Marine Drugs, 17(448), 1–27. https://doi.org/10.3390/md17080448

Mandujano-Tinoco, E. A., Gallardo-Pérez, J. C., Marín-Hernández, A., Moreno-Sánchez, R., & Rodríguez-Enríquez, S. (2013). Anti-mitochondrial therapy in human breast cancer multi-cellular spheroids. Biochimica et Biophysica Acta (BBA) - Molecular Cell Research, 1833(3), 541–551. https://doi.org/10.1016/j.bbamcr.2012.11.013

Mao, H., Jeong, H., Yang, J., Ha, H. J., & Yang, J. W. (2018). Preparation of chiral contiguous epoxyaziridines and their regioselective ring-opening for drug syntheses. Chemistry - A European Journal, 24(10), 2370–2374. https://doi.org/10.1002/chem.201706161

Mariño, G., Niso-Santano, M., Baehrecke, E. H., & Kroemer, G. (2014). Self-consumption: the interplay of autophagy and apoptosis. Nature Reviews Molecular Cell Biology, 15(2), 81–94. https://doi.org/10.1038/nrm3735

Mathur, S., & Hoskins, C. (2017). Drug development: Lessons from nature. Biomedical Reports, 6(6), 612–614. https://doi.org/10.3892/br.2017.909

Mavaddat, N., Peock, S., Frost, D., Ellis, S., Platte, R., Fineberg, E., Evans, D. G., Izatt, L., Eeles, R. A., Adlard, J., Davidson, R., Eccles, D., Cole, T., Cook, J., Brewer, C., Tischkowitz, M., Douglas, F., Hodgson, S., Walker, L., … Easton, D. F. (2013). Cancer risks for BRCA1 and BRCA2 mutation carriers: results from prospective analysis of EMBRACE. JNCI: Journal of the National Cancer Institute, 105(11), 812–822. https://doi.org/10.1093/jnci/djt095

Mcgarrity, T. J., Amos, C. I., Baker, M. ; J., Adam, M. P., Everman, D. B., & Mirzaa, G. M. (2001 (updated 2016)). Peutz-Jeghers Syndrome. In M. P. Adam, D. B. Everman, G. M. Mirzaa, R. A. Pagon, & S. E. Wallace (Eds.), Gene Reviews. University of Washington. https://www.ncbi.nlm.nih.gov/books/NBK1266

McGrane, P. L., & Livinghouse, T. (1993). Synthetic applications of imidotitanium-alkyne [2+2] cycloadditions. A concise, stereocontrolled total synthesis of the antifungal agent (+)-preussin. Journal of the American Chemical Society, 115(24), 11485–11489. https://doi.org/10.1021/ja00077a053

Meerloo, J. van, Kaspers, G. J. L., & Cloos, J. (2011). Cancer cell culture (I. A. Cree, Ed.; 2nd ed., Vol. 731). Humana Press. https://doi.org/10.1007/978-1-61779-080-5

Mehta, G., Hsiao, A. Y., Ingram, M., Luker, G. D., & Takayama, S. (2012). Opportunities and challenges for use of tumor spheroids as models to test drug delivery and efficacy. Journal of Controlled Release, 164(2), 192–204. https://doi.org/10.1016/j.jconrel.2012.04.045

Miranda, A. da C., Silva, A. M., Glória, L., & Brito, C. (2021). Registo oncológico nacional de todos os tumores na população residente em Portugal, em 2018.

Mitchell, M. J., Billingsley, M. M., Haley, R. M., Wechsler, M. E., Peppas, N. A., & Langer, R. (2021). Engineering precision nanoparticles for drug delivery. Nature Reviews Drug Discovery, 20(2), 101–124. https://doi.org/10.1038/s41573-020-0090-8

Mizushima, N., & Murphy, L. O. (2020). Autophagy assays for biological discovery and therapeutic development. Trends in Biochemical Sciences, 45(12), 1080–1093. https://doi.org/10.1016/j.tibs.2020.07.006

Møller, P., Azqueta, A., Boutet-Robinet, E., Koppen, G., Bonassi, S., Milić, M., Gajski, G., Costa, S., Teixeira, J. P., Costa Pereira, C., Dusinska, M., Godschalk, R., Brunborg, G., Gutzkow, K. B., Giovannelli, L., Cooke, M. S., Richling, E., Laffon, B., Valdiglesias, V., … Langie, S. A. S. (2020). Minimum information for reporting on the comet assay (MIRCA): recommendations for describing comet assay procedures and results. Nature Protocols, 15(12), 3817–3826. https://doi.org/10.1038/s41596-020-0398-1

Muguruma, M., Teraoka, S., Miyahara, K., Ueda, A., Asaoka, M., Okazaki, M., Kawate, T., Kuroda, M., Miyagi, Y., & Ishikawa, T. (2020). Differences in drug sensitivity between two-dimensional and three-dimensional culture systems in triple-negative breast cancer cell lines. Biochemical and Biophysical Research Communications, 533(3), 268–274. https://doi.org/10.1016/j.bbrc.2020.08.075

Napoletano, F., Baron, O., Vandenabeele, P., Mollereau, B., & Fanto, M. (2019). Intersections between regulated cell death and autophagy. Trends in Cell Biology, 29(4), 323–338. https://doi.org/10.1016/j.tcb.2018.12.007

Neve, R. M., Chin, K., Fridlyand, J., Yeh, J., Baehner, F. L., Fevr, T., Clark, L., Bayani, N., Coppe, J.-P., Tong, F., Speed, T., Spellman, P. T., DeVries, S., Lapuk, A., Wang, N. J., Kuo, W.-L., Stilwell, J. L., Pinkel, D., Albertson, D. G., … Gray, J. W. (2006). A collection of breast cancer cell lines for the study of functionally distinct cancer subtypes. Cancer Cell, 10(6), 515–527. https://doi.org/10.1016/j.ccr.2006.10.008

New England Biolabs. (n.d.). Comet assay - modified for detection of oxidized bases using the repair endonucleases FPG, hOGG1 and endonuclease III (Nth) | NEB. Retrieved January 6, 2022, from https://international.neb.com/protocols/0001/01/01/comet-assay-modified-for-detection-of-oxidized-bases-using-the-repair-endonucleases-fpg-hoggi-and-endonuclease-iii-nth

Newman, D. J., & Cragg, G. M. (2020). Natural products as sources of new drugs over the nearly four decades from 01/1981 to 09/2019. Journal of Natural Products, 83(3), 770–803. https://doi.org/10.1021/acs.jnatprod.9b01285

Nigjeh, S. E., Yeap, S. K., Nordin, N., Kamalideghan, B., Ky, H., & Rosli, R. (2018). Citral induced apoptosis in MDA-MB-231 spheroid cells. BMC Complementary and Alternative Medicine, 18(1). https://doi.org/10.1186/s12906-018-2115-y

Niklaus, N. J., Tokarchuk, I., Zbinden, M., Schläfli, A. M., Maycotte, P., & Tschan, M. P. (2021). The multifaceted functions of autophagy in breast cancer development and treatment. Cells, 10(6), 1447. https://doi.org/10.3390/cells10061447

Nunes, A. S., Barros, A. S., Costa, E. C., Moreira, A. F., & Correia, I. J. (2019). 3D tumor spheroids as *in vitro* models to mimic *in vivo* human solid tumors resistance to therapeutic drugs. Biotechnology and Bioengineering, 116(1), 206–226. https://doi.org/10.1002/bit.26845

Odom, R. Y., Dansby, M. Y., Rollins-Hairston, A. M., Jackson, K. M., & Kirlin, W. G. (2009). Phytochemical induction of cell cycle arrest by glutathione oxidation and reversal by N-acetylcysteine in human colon carcinoma cells. Nutrition and Cancer, 61(3), 332–339. https://doi.org/10.1080/01635580802549982

Ohnstad, H. O., Borgen, E., Falk, R. S., Lien, T. G., Aaserud, M., Sveli, M. A. T., Kyte, J. A., Kristensen, V. N., Geitvik, G. A., Schlichting, E., Wist, E. A., Sørlie, T., Russnes, H. G., & Naume, B. (2017). Prognostic value of PAM50 and risk of recurrence score in patients with early-stage breast cancer with long-term follow-up. Breast Cancer Research, 19(1), 120. https://doi.org/10.1186/s13058-017-0911-9

Ojima, I., Lichtenthal, B., Lee, S., Wang, C., & Wang, X. (2016). Taxane anticancer agents: A patent perspective. Expert Opinion on Therapeutic Patents, 26(1), 1–20. https://doi.org/10.1517/13543776.2016.1111872

Okue, M., Watanabe, H., Kasahara, K., Yoshida, M., Horinouchi, S., & Kitahara, T. (2002). Short-step syntheses of all stereoisomers of preussin and their bioactivities. Bioscience, Biotechnology and Biochemistry, 66(5), 1093–1096. https://doi.org/10.1271/bbb.66.1093

Overhand, M., & Hecht, S. M. (1994). A concise synthesis of the antifungal agent (+)-preussin. The Journal of Organic Chemistry, 59(17), 4721–4722. https://doi.org/10.1021/jo00096a007

Ozman, Z., Ozbek Iptec, B., Sahin, E., Guney Eskiler, G., Deveci Ozkan, A., & Kaleli, S. (2021). Regulation of valproic acid induced EMT by AKT/GSK3β/β-catenin signaling pathway in triple negative breast cancer. Molecular Biology Reports, 48(2), 1335–1343. https://doi.org/10.1007/s11033-021-06173-8

Papon, N., Copp, B. R., & Courdavault, V. (2022). Marine drugs: Biology, pipelines, current and future prospects for production. Biotechnology Advances, 54, 107871. https://doi.org/10.1016/j.biotechadv.2021.107871

Park, Y. H., Kim, H. K., & Cho, J. H. (2018). Discordance of the PAM50 intrinsic subtypes compared with IHC-based surrogate in breast cancer patients: Potential implication of genomic alterations of discordance. Annals of Oncology, 29(2), viii674–viii675. https://doi.org/10.1093/annonc/mdy304.015

Parker, J. S., Mullins, M., Cheang, M. C. U., Leung, S., Voduc, D., Vickery, T., Davies, S., Fauron, C., He, X., Hu, Z., Quackenbush, J. F., Stijleman, I. J., Palazzo, J., Marron, J. S., Nobel, A. B., Mardis, E., Nielsen, T. O., Ellis, M. J., Perou, C. M., & Bernard, P. S. (2009). Supervised risk predictor of breast cancer based on intrinsic subtypes. Journal of Clinical Oncology, 27(8), 1160–1167. https://doi.org/10.1200/JCO.2008.18.1370

Patra, J. K., Das, G., Fraceto, L. F., Campos, E. V. R., Rodriguez-Torres, M. del P., Acosta-Torres, L. S., Diaz-Torres, L. A., Grillo, R., Swamy, M. K., Sharma, S., Habtemariam, S., & Shin, H.-S. (2018). Nano based drug delivery systems: recent developments and future prospects. Journal of Nanobiotechnology, 16(1), 71. https://doi.org/10.1186/s12951-018-0392-8

Perou, C. M., Sørlie, T., Eisen, M. B., van de Rijn, M., Jeffrey, S. S., Rees, C. A., Pollack, J. R., Ross, D. T., Johnsen, H., Akslen, L. A., Fluge, Ø., Pergamenschikov, A., Williams, C., Zhu, S. X., Lønning, P. E., Børresen-Dale, A.-L., Brown, P. O., & Botstein, D. (2000). Molecular portraits of human breast tumors. Nature, 406(6797), 747–752. https://doi.org/10.1038/35021093

Präbst Konstantin and Engelhardt, H. and R. S. and H. H. (2017b). Basic colorimetric proliferation assays: MTT, WST, and resazurin. In O. Gilbert Daniel F. and Friedrich (Ed.), Cell Viability Assays: Methods and Protocols (Vol. 1601, pp. 1–17). Springer New York. https://doi.org/10.1007/978-1-4939-6960-9_1

Prat, A., Adamo, B., Cheang, M. C. U., Anders, C. K., Carey, L. A., & Perou, C. M. (2013). Molecular characterization of basal-like and non-basal-like triple-negative breast cancer. The Oncologist, 18(2), 123–133. https://doi.org/10.1634/theoncologist.2012-0397

Prat, A., Chaudhury, A., Solovieff, N., Paré, L., Martinez, D., Chic, N., Martínez-Sáez, O., Brasó-Maristany, F., Lteif, A., Taran, T., Babbar, N., & Su, F. (2021). Correlative biomarker analysis of intrinsic subtypes and efficacy across the MONALEESA Phase III Studies. Journal of Clinical Oncology, 39(13), 1458–1467. https://doi.org/10.1200/JCO.20.02977

Prat, A., Parker, J. S., Karginova, O., Fan, C., Livasy, C., Herschkowitz, J. I., He, X., & Perou, C. M. (2010). Phenotypic and molecular characterization of the claudin-low intrinsic subtype of breast cancer. Breast Cancer Research, 12, R68. https://doi.org/10.1186/bcr2635

Prat, A., Pineda, E., Adamo, B., Galván, P., Fernández, A., Gaba, L., Díez, M., Viladot, M., Arance, A., & Muñoz, M. (2015). Clinical implications of the intrinsic molecular subtypes of breast cancer. The Breast, 24, S26–S35. https://doi.org/10.1016/j.breast.2015.07.008

Press, N. J., Joly, E., & Ertl, P. (2019). Natural product drug delivery: A special challenge? In D. R. Witty & B. Cox (Eds.), Progress in Medicinal Chemistry (Vol. 58, pp. 157–187). Elsevier. https://doi.org/https://doi.org/10.1016/bs.pmch.2019.01.001

Rädler, P. D., Wehde, B. L., Triplett, A. A., Shrestha, H., Shepherd, J. H., Pfefferle, A. D., Rui, H., Cardiff, R. D., Perou, C. M., & Wagner, K. U. (2021). Highly metastatic claudin-low mammary cancers can originate from luminal epithelial cells. Nature Communications, 12(1), 3742. https://doi.org/10.1038/s41467-021-23957-5

Raghavan, S., & Rasheed, M. A. (2003). A novel and stereospecific synthesis of (+)-preussin. Tetrahedron, 59(51), 10307–10312. https://doi.org/10.1016/j.tet.2003.10.032

Rajh, M., Dolinar, K., Miš, K., Pavlin, M., & Pirkmajer, S. (2016). Medium renewal blocks anti-proliferative effects of metformin in cultured MDA-MB-231 breast cancer cells. PLOS ONE, 11(5). https://doi.org/10.1371/journal.pone.0154747

Ramírez-Rendon, D., Passari, A. K., Ruiz-Villafán, B., Rodríguez-Sanoja, R., Sánchez, S., & Demain, A. L. (2022). Impact of novel microbial secondary metabolites on the pharma industry. Applied Microbiology and Biotechnology, 106(5–6), 1855–1878. https://doi.org/10.1007/s00253-022-11821-5

Ramos, A. A., Almeida, T., Lima, B., & Rocha, E. (2019). Cytotoxic activity of the seaweed compound fucosterol, alone and in combination with 5-fluorouracil, in colon cells using 2D and 3D culturing. Journal of Toxicology and Environmental Health - Part A: Current Issues, 82(9), 537–549. https://doi.org/10.1080/15287394.2019.1634378

Reynolds, E. S. (1963). The use of lead citrate at high pH as an electron-opaque stain in electron microscopy. Journal of Cell Biology, 17, 208–212. https://doi.org/10.1083/jcb.17.1.208

Rody, A., Karn, T., Liedtke, C., Pusztai, L., Ruckhaeberle, E., Hanker, L., Gaetje, R., Solbach, C., Ahr, A., Metzler, D., Schmidt, M., Müller, V., Holtrich, U., & Kaufmann, M. (2011). A clinically relevant gene signature in triple negative and basal-like breast cancer. Breast Cancer Research, 13, R97. https://doi.org/10.1186/bcr3035

Rong, H. J., Yao, J. J., Li, J. K., & Qu, J. (2017). Molecular iodine-mediated α-C-H oxidation of pyrrolidines to N,O-acetals: synthesis of (±)-preussin by late-stage 2,5-difunctionalizations of pyrrolidine. Journal of Organic Chemistry, 82(11), 5557–5565. https://doi.org/10.1021/acs.joc.7b00361

Saeed, A. F. U. H., Su, J., & Ouyang, S. (2021). Marine-derived drugs: Recent advances in cancer therapy and immune signaling. Biomedicine and Pharmacotherapy, 134, 111091. https://doi.org/10.1016/j.biopha.2020.111091

Sainz-Cort, A., Müller-Sánchez, C., & Espel, E. (2020). Anti-proliferative and cytotoxic effect of cannabidiol on human cancer cell lines in presence of serum. BMC Research Notes, 13(1), 389. https://doi.org/10.1186/s13104-020-05229-5

Sanchez Sergio and Demain, A. L. (2017). Bioactive Products from Fungi. In M. Puri (Ed.), Food Bioactives: Extraction and Biotechnology Applications (pp. 59–87). Springer International Publishing. https://doi.org/10.1007/978-3-319-51639-4_3

Schwartz, R. E., Liesch, J., Henses, O., Zitano, L., Honeycutt, S., Garrity, G., Fromtling, R. A., Onishi, J., & Monaghan, R. (1988). L-657,398, a novel antifungal agent: Fermentation, isolation, structural elucidation and biological properties. The Journal of Antibiotics, 41(12), 1774–1779. https://doi.org/10.7164/antibiotics.41.1774

Scolamiero, G., Pazzini, C., Bonafè, F., Guarnieri, C., & Muscari, C. (2018). Effects of α-mangostin on viability, growth and cohesion of multicellular spheroids derived from human breast cancer cell lines. International Journal of Medical Sciences, 15(1), 23–30. https://doi.org/10.7150/ijms.22002

Sharma, A., Mishra, T., Thacker, G., Mishra, M., Narender, T., & Trivedi, A. K. (2020). Chebulinic acid inhibits MDA-MB-231 breast cancer metastasis and promotes cell death through down regulation of SOD1 and induction of autophagy. Cell Biology International, 44(12), 2553–2569. https://doi.org/10.1002/cbin.11463

Shin, J.-S., Hong, S.-W., Lee, S.-L., Kim, T.-H., Park, I.-C., An, S.-K., Lee, W.-K., Lim, J.-S., Kim, K.-I., Yang, Y., Lee, S.-S., Jin, D.-H., & Lee, M.-S. (2008). Serum starvation induces G1 arrest through suppression of skp2-CDK2 and CDK4 in SK-OV-3 cells. International Journal of Oncology, 32, 435–439. https://doi.org/10.3892/ijo.32.2.435

Shyu Jr, P., Wong, X. F. A., Crasta, K., & Thibault, G. (2018). Dropping in on lipid droplets: insights into cellular stress and cancer. Bioscience Reports, 38(5), BSR20180764. https://doi.org/10.1042/BSR20180764

Siegel, R. L., Miller, K. D., Fuchs, H. E., & Jemal, A. (2022). Cancer statistics, 2022. CA: A Cancer Journal for Clinicians, 72(1), 7–33. https://doi.org/10.3322/caac.21708

Siegel, R. L., Miller, K. D., & Jemal, A. (2018). Cancer statistics, 2018. CA: A Cancer Journal for Clinicians, 68(1), 7–30. https://doi.org/10.3322/caac.21442

Stepanenko, A. A., & Dmitrenko, V. V. (2015). Pitfalls of the MTT assay: Direct and off-target effects of inhibitors can result in over/underestimation of cell viability. Gene, 574(2), 193–203. https://doi.org/10.1016/j.gene.2015.08.009

Sumantran, V. N. (2011). Cellular chemosensitivity assays: an overview. In I. A. Cree (Ed.), Cancer cell culture: Methods and Protocols (2nd ed., pp. 219–236). Human Press. https://doi.org/10.1007/978-1-61779-080-5_19

Sung, H., Ferlay, J., Siegel, R. L., Laversanne, M., Soerjomataram, I., Jemal, A., & Bray, F. (2021). Global cancer statistics 2020: GLOBOCAN estimates of incidence and mortality worldwide for 36 cancers in 185 countries. CA: A Cancer Journal for Clinicians, 71(3), 209–249. https://doi.org/10.3322/caac.21660

Süntar, I. (2020). Importance of ethnopharmacological studies in drug discovery: role of medicinal plants. Phytochemistry Reviews, 19(5), 1199–1209. https://doi.org/10.1007/s11101-019-09629-9

Tadesse, S., Caldon, E. C., Tilley, W., & Wang, S. (2019). Cyclin-dependent kinase 2 inhibitors in cancer therapy: An update. Journal of Medicinal Chemistry, 62(9), 4233–4251. https://doi.org/10.1021/acs.jmedchem.8b01469

Tang, P., & Tse, G. M. (2016). Immunohistochemical surrogates for molecular classification of breast carcinoma: A 2015 update. Archives of Pathology and Laboratory Medicine, 140(8), 806–814. https://doi.org/10.5858/arpa.2015-0133-RA

The Cancer Genome Atlas Network. (2012). Comprehensive molecular portraits of human breast tumors. Nature, 490(7418), 61–70. https://doi.org/10.1038/nature11412

Thompson, D. (2002). Cancer incidence in BRCA1 mutation carriers. CancerSpectrum Knowledge Environment, 94(18), 1358–1365. https://doi.org/10.1093/jnci/94.18.1358

Torre, L. A., Islami, F., Siegel, R. L., Ward, E. M., & Jemal, A. (2017). Global cancer in women: Burden and trends. Cancer Epidemiology Biomarkers and Prevention, 26(4), 444–457. https://doi.org/10.1158/1055-9965.EPI-16-0858

U.S. Food and Drug Administration (FDA). (2018). The drug development process. https://www.fda.gov/patients/learn-about-drug-and-device-approvals/drug-development-process

van Tonder, A., Joubert, A. M., & Cromarty, A. D. (2015). Limitations of the 3-(4,5-dimethylthiazol-2-yl)-2,5-diphenyl-2H-tetrazolium bromide (MTT) assay when compared to three

commonly used cell enumeration assays. BMC Research Notes, 8(1), 47. https://doi.org/10.1186/s13104-015-1000-8

Varijakzhan, D., Loh, J. Y., Yap, W. S., Yusoff, K., Seboussi, R., Lim, S. H. E., Lai, K. S., & Chong, C. M. (2021). Bioactive compounds from marine sponges: Fundamentals and applications. Marine Drugs, 19(5), 246. https://doi.org/10.3390/md19050246

Veeresa, G., & Datta, A. (1998). Stereoselective synthesis of the antifungal antibiotic (+)-preussin. Tetrahedron, 54(51), 15673–15678. https://doi.org/10.1016/S0040-4020(98)00981-8

Vermes, I., Haanen, C., Steffens-Nakken, H., & Reutellingsperger, C. (1995). A novel assay for apoptosis flow cytometric detection of phosphatidylserine expression on early apoptotic cells using fluorescein labelled Annexin V. Journal of Immunological Methods, 184(1), 39–51. https://doi.org/10.1016/0022-1759(95)00072-I

Vincent-Hubert, F., Arini, A., & Gourlay-Francé, C. (2011). Early genotoxic effects in gill cells and haemocytes of *Dreissena polymorpha* exposed to cadmium, B[a]P and a combination of B[a]P and Cd. Mutation Research/Genetic Toxicology and Environmental Mutagenesis, 723(1), 26–35. https://doi.org/10.1016/j.mrgentox.2011.03.008

Vinci, M., Gowan, S., Boxall, F., Patterson, L., Zimmermann, M., Court, W., Lomas, C., Mendiola, M., Hardisson, D., & Eccles, S. A. (2012). Advances in establishment and analysis of three-dimensional tumor spheroid-based functional assays for target validation and drug evaluation. BMC Biology, 10(1), 29. https://doi.org/10.1186/1741-7007-10-29

Wali, A. F., Majid, S., Rasool, S., Shehada, S. B., Abdulkareem, S. K., Firdous, A., Beigh, S., Shakeel, S., Mushtaq, S., Akbar, I., Madhkali, H., & Rehman, M. U. (2019). Natural products against cancer: Review on phytochemicals from marine sources in preventing cancer. Saudi Pharmaceutical Journal, 27(6), 767–777. https://doi.org/10.1016/j.jsps.2019.04.013

Wang, J., & Xu, B. (2019). Targeted therapeutic options and future perspectives for HER2-positive breast cancer. Signal Transduction and Targeted Therapy, 4, 34. https://doi.org/10.1038/s41392-019-0069-2

Wang, P., Henning, S. M., & Heber, D. (2010). Limitations of MTT and MTS-Based Assays for Measurement of Antiproliferative Activity of Green Tea Polyphenols. PLoS ONE, 5(4), e10202. https://doi.org/10.1371/journal.pone.0010202

Weber-Lassalle, N., Borde, J., Weber-Lassalle, K., Horváth, J., Niederacher, D., Arnold, N., Kaulfuß, S., Ernst, C., Paul, V. G., Honisch, E., Klaschik, K., Volk, A. E., Kubisch, C., Rapp, S., Lichey, N., Altmüller, J., Lepkes, L., Pohl-Rescigno, E., Thiele, H., … Hauke, J. (2019). Germline loss-of-function variants in the BARD1 gene are associated with early-onset familial breast cancer but not ovarian cancer. Breast Cancer Research, 21(1), 55. https://doi.org/10.1186/s13058-019-1137-9

Weigelt, B., Mackay, A., A'hern, R., Natrajan, R., Tan, D. S., Dowsett, M., Ashworth, A., & Reis-Filho, J. S. (2010). Breast cancer molecular profiling with single sample predictors: a retrospective analysis. The Lancet Oncology, 11(4), 339–349. https://doi.org/10.1016/S1470-2045(10)70008-5

White, E. Z., Pennant, N. M., Carter, J. R., Hawsawi, O., Odero-Marah, V., & Hinton, C. v. (2020). Serum deprivation initiates adaptation and survival to oxidative stress in prostate cancer cells. Scientific Reports, 10(1), 12505. https://doi.org/10.1038/s41598-020-68668-x

Wojtyla, C., Bertuccio, P., Wojtyla, A., & la Vecchia, C. (2021). European trends in breast cancer mortality, 1980–2017 and predictions to 2025. European Journal of Cancer, 152, 4–17. https://doi.org/10.1016/j.ejca.2021.04.026

Wright, G. D. (2019). Unlocking the potential of natural products in drug discovery. Microbial Biotechnology, 12(1), 55–57. https://doi.org/10.1111/1751-7915.13351

Wright, H. J., Hou, J., Xu, B., Cortez, M., Potma, E. O., Tromberg, B. J., & Razorenova, O. v. (2017). CDCP1 drives triple-negative breast cancer metastasis through reduction of lipid-droplet abundance and stimulation of fatty acid oxidation. Proceedings of the National Academy of Sciences, 114(32), E6556-E6565. https://doi.org/10.1073/pnas.1703791114

Wu, B., Hussain, M., Zhang, W., Stadler, M., Liu, X., & Xiang, M. (2019). Current insights into fungal species diversity and perspective on naming the environmental DNA sequences of fungi. Mycology, 10(3), 127–140. https://doi.org/10.1080/21501203.2019.1614106

Wu, L., Ye, K., Jiang, S., & Zhou, G. (2021). Marine power on cancer: Drugs, lead compounds, and mechanisms. Marine Drugs, 19(9). https://doi.org/10.3390/md19090488

Yan, G., Elbadawi, M., & Efferth, T. (2020). Multiple cell death modalities and their key features. World Academy of Sciences Journal, 2(2), 39–48. https://doi.org/10.3892/wasj.2020.40

Yang, X., Leslie, G., Doroszuk, A., Schneider, S., Allen, J., Decker, B., Dunning, A. M., Redman, J., Scarth, J., Plaskocinska, I., Luccarini, C., Shah, M., Pooley, K., Dorling, L.,

Lee, A., Adank, M. A., Adlard, J., Aittomäki, K., Andrulis, I. L., … Tischkowitz, M. (2020). Cancer risks associated with germline PALB2 pathogenic variants: An international study of 524 families. Journal of Clinical Oncology, 38(7), 674–685. https://doi.org/10.1200/JCO.19.01907

Yasuhara, S., Zhu, Y., Matsui, T., Tipirneni, N., Yasuhara, Y., Kaneki, M., Rosenzweig, A., & Jeevendra Martyn, J. (2003). Comparison of comet assay, electron microscopy, and flow cytometry for detection of apoptosis. The Journal of Histochemistry & Cytochemistry, 51(7), 873–885. http://www.jhc.org

Ye, Q., Kantonen, S., & Gomez-Cambronero, J. (2013). Serum deprivation confers the MDA-MB-231 breast cancer line with an EGFR/JAK3/PLD2 system that maximizes cancer cell invasion. Journal of Molecular Biology, 425(4), 755–766. https://doi.org/10.1016/j.jmb.2012.11.035

Yersal, O., & Barutca, S. (2014). Biological subtypes of breast cancer: Prognostic and therapeutic implications. World Journal of Clinical Oncology, 5(3), 412–424. https://doi.org/10.5306/wjco.v5.i3.412

Zanoni, M., Piccinini, F., Arienti, C., Zamagni, A., Santi, S., Polico, R., Bevilacqua, A., & Tesei, A. (2016). 3D tumor spheroid models for *in vitro* therapeutic screening: a systematic approach to enhance the biological relevance of data obtained. *Scientific Reports*, *6*(1), 19103. https://doi.org/10.1038/srep19103

Zhao, J., Zhi, Z., Wang, C., Xing, H., Song, G., Yu, X., Zhu, Y., Wang, X., Zhang, X., & Di, Y. (2017). Exogenous lipids promote the growth of breast cancer cells via CD36. Oncology Reports, 38(4), 2105–2115. https://doi.org/10.3892/or.2017.5864